Advances in High Energy Physics

Dark Matter and Dark Energy Cosmologies and Alternative Theories of Gravitation

Lead Guest Editor: Dandala R. K. Reddy
Guest Editors: Sergei D. Odintsov and Tiberiu Harko

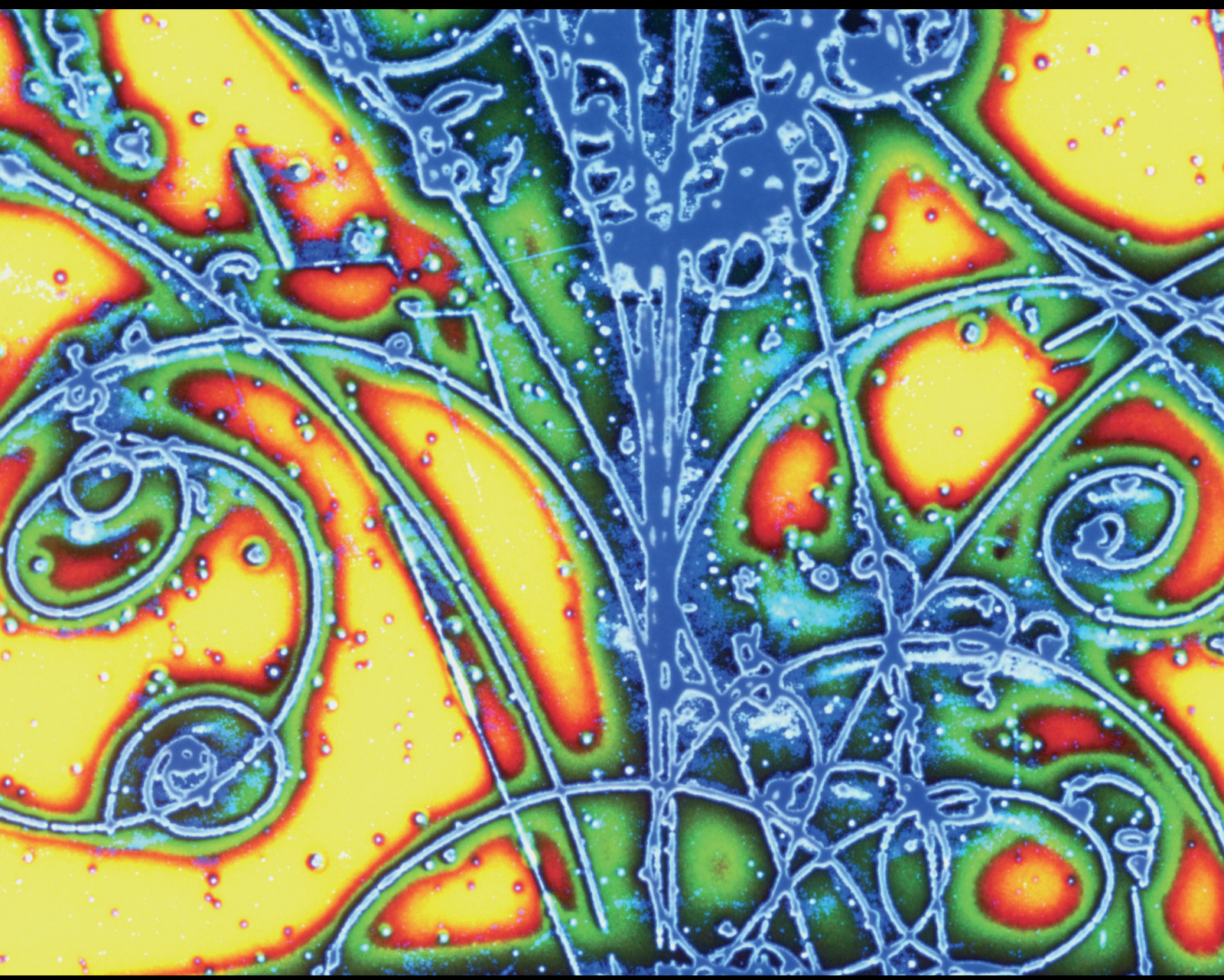

Dark Matter and Dark Energy Cosmologies and Alternative Theories of Gravitation

Advances in High Energy Physics

Dark Matter and Dark Energy Cosmologies and Alternative Theories of Gravitation

Lead Guest Editor: Dandala R. K. Reddy
Guest Editors: Sergei D. Odintsov and Tiberiu Harko

Editorial Board

Contents

Hindawi
Advances in High Energy Physics
Volume 2017, Article ID 8061353, 2 pages
https://doi.org/10.1155/2017/8061353

Editorial

Dark Matter and Dark Energy Cosmologies and Alternative Theories of Gravitation

Dandala R. K. Reddy,[1] Sergei D. Odintsov,[2] and Tiberiu Harko[3]

[1]*Department of Applied Mathematics, Andhra University, Visakhapatnam 530003, India*
[2]*Institucion Catalana de Recerca i Estudis Avancats, Barcelona, Spain*
[3]*Department of Mathematics, University College London, London WC1E 6BT, UK*

Correspondence should be addressed to Dandala R. K. Reddy; reddy_einstein@yahoo.com

Received 22 January 2017; Accepted 22 January 2017; Published 31 May 2017

Presently we are witnessing a period of rapid and intense change in our understanding of the gravitational force, at a rate that is quickly increasing since the important observational discoveries of the late 1990s. With the advent of new observational techniques, we can see the emergence of interesting new cosmological paradigms, from which the CDM seems to fit the best cosmological observations, indicating that the present day Energy Cosmologies Universe is dominated by two mysterious components, dark energy and dark matter, with the former responsible for the accelerated expansion of the Universe, while the latter is required by the strange behavior of the galactic rotation curves. Up to now, no direct detection/observation of the dark matter has been reported, and presently the only evidence for its existence is its gravitational interaction with baryonic matter. Presently, after a long period of intensive observational and experimental results the particle nature of the dark matter is still unknown.

Hence, a large number of astronomical observations strongly suggest that at large scales the force of gravity may not behave according to standard general relativity, as derived from the Hilbert-Einstein action, and that a generalization of the Hilbert-Einstein action, either at the geometric level or at the matter level, may be required for a full understanding of the gravitational interaction.

This special issue is focused on some extensions of the standard theoretical concepts in gravity and cosmology. It includes state-of-the-art research contributions in the following areas: coupled dark energy models, occurring as a q-deformed scalar field, spinor quintom dark energy models with intrinsic spin, in the framework of Einstein-Cartan-Sciama-Kibble theory, black hole solutions in 1 + 1-dimensional Horava-Lifshitz gravity, the study of the dark sector of the Universe by considering the dark energy as an emerging q-deformed bosonic scalar field, which is not only interacting with the dark matter, but also nonminimally coupled to gravity, and the comparison of the galactic rotation curves with the observations in the Bose-Einstein Condensate dark matter model.

In the paper by E. Dil, the q-deformed bosons models having a negative pressure are considered, and it is proposed that the associated scalar fields produced by these deformed bosons represent the dark energy in the Universe. The coupling between q-deformed dark energy and dark matter inhomogeneities in the Friedmann-Robertson-Walker spacetime is also considered.

The spin contribution to the total energy-momentum tensor giving the energy density and the pressure in a spinor quintom dark energy model with intrinsic spin, in the framework of Einstein-Cartan-Sciama-Kibble theory, is obtained in the paper by E. Dil. The equation of state parameter, the Hubble parameter, the deceleration parameter, the state finder parameter, and some distance parameters were obtained in terms of the spinor potential. Choosing some suitable potentials leads to a scenario involving crossing between the quintessence and phantom epochs, respectively, or vice versa. Three quintom scenarios are analyzed, which provides stable expansion phases avoiding Big Rip singularities and yielding matter dominated era through the stabilization of the spinor pressure via the spin contribution.

The article by M. Halilsoy and A. Ovgun is devoted to investigating whether the Banados, Silk, and West type effects, which arise in higher dimensional black holes, are also

present in the 1 + 1-D naked singularity/black hole system. This investigation is performed by using the Horava-Lifshitz gravity theory. In this theoretical framework it is shown that the center-of-mass (CM) energy of the particles grows unbounded in some cases. An interacting dark matter and q-deformed model of dark energy nonminimally coupled to the gravity in the framework of Einsteinian gravity is considered in another paper by E. Dil. The dynamics of the model are investigated, including a phase-space analysis that explicitly shows if the model will give stable attractor solutions, indicating an accelerating expansion of the Universe. Finally, in the paper by M. Dwornik et al., a comparative and comprehensive comparison of both the Bose-Einstein Condensate and the Navarro-Frenk-White dark halo models with galactic rotation curves is performed. Both the advantages and disadvantages of the Bose-Einstein Condensate model over the N avarro-Frenk-White model are pointed out. It is also shown that the weaker performance of the Bose-Einstein Condensate model for the High Surface Brightness type II galaxies is due to the Bose-Einstein Condensate density poles dropping rapidly to zero outside a nearly constant density core.

We hope that this special issue will serve as a reference for initiating and continuing state-of-the-art research in the fundamental fields of modified gravity, dark energy, and dark matter.

Dandala R. K. Reddy
Sergei D. Odintsov
Tiberiu Harko

Hindawi
Advances in High Energy Physics
Volume 2017, Article ID 4025386, 14 pages
https://doi.org/10.1155/2017/4025386

Research Article

Bose-Einstein Condensate Dark Matter Halos Confronted with Galactic Rotation Curves

M. Dwornik, Z. Keresztes, E. Kun, and L. Á. Gergely

Institute of Physics, University of Szeged, Dóm Tér 9, Szeged 6720, Hungary

Correspondence should be addressed to L. Á. Gergely; laszlo.a.gergely@gmail.com

Received 7 October 2016; Revised 15 December 2016; Accepted 25 December 2016; Published 8 February 2017

Academic Editor: Sergei D. Odintsov

We present a comparative confrontation of both the Bose-Einstein Condensate (BEC) and the Navarro-Frenk-White (NFW) dark halo models with galactic rotation curves. We employ 6 High Surface Brightness (HSB), 6 Low Surface Brightness (LSB), and 7 dwarf galaxies with rotation curves falling into two classes. In the first class rotational velocities increase with radius over the observed range. The BEC and NFW models give comparable fits for HSB and LSB galaxies of this type, while for dwarf galaxies the fit is significantly better with the BEC model. In the second class the rotational velocity of HSB and LSB galaxies exhibits long flat plateaus, resulting in better fit with the NFW model for HSB galaxies and comparable fits for LSB galaxies. We conclude that due to its central density cusp avoidance the BEC model fits better dwarf galaxy dark matter distribution. Nevertheless it suffers from sharp cutoff in larger galaxies, where the NFW model performs better. The investigated galaxy sample obeys the Tully-Fisher relation, including the particular characteristics exhibited by dwarf galaxies. In both models the fitting enforces a relation between dark matter parameters: the characteristic density and the corresponding characteristic distance scale with an inverse power.

1. Introduction

The visible part of most galaxies is embedded in a dark matter (DM) halo of yet unknown composition, observable only through its gravitational interaction with the baryonic matter. Assuming the standard ΛCDM cosmological model, the Planck satellite measurements of the cosmic microwave background anisotropy power spectrum support 4.9% baryonic matter, 26.8% DM, and 68.3% dark energy in the Universe [1, 2].

Investigation of mass distribution of spiral galaxies is an essential tool in the research of DM. Beside the stellar disk and central bulge, most of the galaxies harbour a spherically symmetric, massive DM halo, which dominates the dynamics in the outer regions of the stellar disk. Nevertheless there are examples of galaxies which at larger radii are better described by a flattened baryonic mass distribution (global disk model) [3].

Several DM candidates and alternatives have been proposed, the latter assuming Einstein's theory of gravity breaking down on the galactic scale and above ([4–12]). In brane-world and $f(R)$-gravity models, the galactic rotation curves could be explained without DM ([13–16]).

At this moment there are strong experimental constraints for all proposed dark matter candidates. Supersymmetric dark matter has been strongly constrained by LHC [17, 18], sterile neutrinos disruled with 99% confidence level by IceCube [19], Weekly Interacting Massive Particles (WIMPs) severely bounded by the LUX [20], PandaX-II [21], and Xenon100 [22] experiments. Extra dimensional effects as dark matter substitutes have been also contained by LHC [23]. Massive Compact Halo Objects (MACHOs) with masses below 20 solar masses have been shown to give at most 10% of dark matter by microlensing experiments on the Large Magellanic Cloud [24]. There is still hope for larger mass MACHOs as dark matter candidates, revived after the spectacular first direct detection of gravitational waves [25], sourced by black holes of approximately 30 solar masses.

It is well known that hot dark matter (HDM) consisting of light ($m \propto$ eV) particles cannot reproduce the cosmological structure formation, as they imply that the superclusters of galaxies are the first structures to form contradicting CMB

observations, according to which superclusters would form at the present epoch [26]. Warm dark matter ($m \propto$ keV) models seem to be compatible with the astronomical observations on galactic and also cosmological scales [27, 28]. Leading candidates for warm dark matter are the right handed neutrinos, which in contrast with their left handed counterparts do not participate in the weak interaction. The decay of these sterile neutrinos produces high amount of X-rays, which can boost the star formation rate leading to an earlier reionization [29]. The existence of sterile neutrinos was however severely constrained by recent IceCube Neutrino Observatory experiments [30]. Cold dark matter (CDM) also shows remarkably good agreement with observations over kpc scales ([31, 32]). Particular CDM candidates, like neutralinos (which are stable and can be produced thermally in the early Universe) and other WIMPs originating in supersymmetric extensions of the Standard Model were severely constrained by recent LHC results, rendering them into the range $200\,\text{GeV} \lesssim m_n \lesssim 500\,\text{GeV}$ [33]. In a Higgs-portal DM scenario the Higgs boson acts as the mediator particle between DM and Standard Model particles, and it can decay to a pair of DM particles. Very recent constraints established by the ATLAS Collaboration on DM-nucleon scattering cross-section impose upper limits of approximately 60 GeV for each of the scalar, fermion, and vector DM candidates (see Figure 4 of [34]), within the framework of this scenario. While MACHOs of masses less than 10 solar masses (like white dwarfs, neutron stars, brown dwarfs and unassociated planets, and primordial black holes in the astrophysical mass range) were disruled either by Big Bang Nucleosynthesis constraints or microlensing experiments as dominant DM candidates, primordial black holes with intermediate mass could still be viable candidates [35, 36].

Large N-body simulations (e.g., [39]) performed in the framework of the ΛCDM-model (Λ being the cosmological constant) were compatible with CDM halos with central density cusps [40]. They are modeled by the Navarro-Frenk-White (NFW) DM density profile $\rho_{\text{NFW}}(r) = \rho_s/(r/r_s)(1 + r/r_s)^2$, where r_s is a scale radius and ρ_s is a characteristic density. Some observations support such a steep cuspy density profile [41, 42]; nevertheless certain high-resolution rotation curves instead indicate that the distribution of DM in the centres of DM dominated dwarf and Low Surface Brightness (LSB) galaxies is much shallower, exhibiting a core with nearly constant density [43]. In turn, the baryonic matter distribution may also affect the DM density profile. As shown in [44] a dark matter core within an isolated, initially cuspy dark matter halo may form due to strong supernova feedback. By contrast, adiabatic contraction of baryonic gas tends to produce even cuspier dark matter halos [45].

The surface number-density profiles of satellites decline with the projected distance as a power law with the slope $(-2) \div (-1.5)$, while the line-of-sight velocity dispersion declines gradually [46]. These observations support the NFW model on scales of $50 \div 500$ kpc.

In a cosmological setup various scalar field DM models were also discussed ([47, 48] and references therein). A particular scalar field DM model describes light bosons in a dilute gas. The thermal de Broglie wavelength of the particles is $\lambda_T \propto 1/\sqrt{mT}$, which can be large for light bosons ($m <$ eV) and for low temperature. Below a critical temperature (T_c), the bosons' wave packets, which are the order of λ_T overlap, result in correlated particles. Such bosons share the same quantum ground state, behaving as a Bose-Einstein Condensate (BEC), characterized by a single macroscopic wave function. It has been proposed that galactic DM halos could be gigantic BECs [49].

It has been shown that caustics of ring shape appear in rotating BEC models, which have an effect on rotation curves, by causing bumps [50, 51]. Such ring shaped caustics degenerate into the origin in the nonrotating BEC limit, adopted in this paper.

The self-gravitating condensate is described by the Gross-Pitaevskii-Poisson equation system in the mean-field approximation [10, 52–54]. In the Thomas-Fermi approximation, a 2-parameter (mass m and scattering length a) density distribution of the BEC halo is obtained [see (3) below], which is less concentrated towards the centre as compared to the NFW model, relaxing the cuspy halo problem.

In model [55] where a normal dark matter phase with an equation of state $P = \rho c^2 \sigma_{\text{tr}}^2$ condensed into a BEC with self-interaction ($\sigma_{\text{tr}} = 0.0017$ being the one-dimensional velocity dispersion and c the speed of light), the stability of the BEC halo depends on the particle mass and scattering length. For a given mass the stability occurs for larger scattering length and for given scattering length the stability appears at smaller mass. For the following scattering lengths: $a = 10^3$ fm, $a = 10^{-14}$ fm, and $a = 10^{-55}$ fm, the mass of the BEC particle arises as $m > 1$ eV, $m > 2 \times 10^{-6}$ eV, and $m > 4.57 \times 10^{-20}$ eV, respectively. Galactic size stable halos can form with $m > 10^{-24}$ eV (Figure 3 in [56]).

A stable BEC halo can form as a result of gravitational collapse [57]. The model has been tested on kpc scales confronting it with galactic rotation curve observations [10]. It was pointed out by [58] that the effects of BEC DM should be seen in the matter power spectrum if the boson mass is in the range $15\,\text{meV} < m < 35\,\text{meV}$ and $300\,\text{meV} < m < 700\,\text{meV}$ for the scattering lengths $a = 10^6$ fm and $a = 10^{10}$ fm, respectively. In [59] the authors showed that the observed collisional behaviour of DM in Abell 520 cluster can also be recovered within the framework of the BEC model. All of the mentioned BEC particle masses are consistent with the limit $m < 1.87$ eV imposed from galaxy observations and N-body simulation [60]. A discrepancy was however pointed out between the best fit density profile parameters derived from the strong lensing and the galactic rotational curves data. In conclusion the BEC halo should be denser in lens galaxies than in dwarf spheroidals [61].

In this work we critically examine the BEC model as a possible DM candidate against rotation curve data, pointing out both advantages and disadvantages over the NFW model. Previous studies on the compatibility of the BEC model and galactic rotation curves were promising but relied on a less numerous and less diversified set of galaxies than employed here ([62, 63]). The paper has the following structure. The basic properties of the BEC DM model are reviewed in

Section 2. In Section 3 a comparison is made between the theoretical predictions of the BEC model and the observed rotation curve data of three types of galaxies: the High Surface Brightness (HSB), LSB, and dwarf galaxies. The conclusions are presented in Section 4.

2. The Bose-Einstein Condensate Galactic Dark Matter Halo

An ideal, dilute Bose gas at very low temperature forms a Bose-Einstein Condensate in which all particles are in the same ground state. In the thermodynamic limit, the critical temperature for the condensation is $T_c = 2\pi\hbar^2(n/\zeta)^{3/2}/mk_B$ [64]. Here n and m are the number density and the mass of the bosons, respectively, and $\zeta = 2.612$ is a constant, while $\hbar$ and k_B denote the reduced Planck and Boltzmann constants, respectively. Atoms can be regarded as quantum-mechanical wave packets of the order of their thermal de Broglie wavelength $\lambda_T = \sqrt{2\pi\hbar^2/(mk_BT)}$. The condition for the condensation $T < T_c$ can be reformulated as $l < \lambda_T/\zeta^{-1/3}$, where l is the average distance between pairs of bosons, and it occurs when the temperature, hence the momentum of the bosons, decreases and as a consequence their de Broglie wavelengths overlap. The thermodynamic limit is only approximately realized, the finite size giving corrections to the critical temperature [65–68]. A dilute, nonideal Bose gas also displays BEC; on the other hand, the condensate fraction is smaller than unity at zero temperature and the critical temperature is also modified [69–72]. Experimentally, BEC (which could be formed by bosonic atoms but also form fermionic Cooper pairs) has been realized first in ^{87}Rb [73–75], then in ^{23}Na [76, 77], and in ^{7}Li [78].

In a dilute gas, only two-particle interactions dominate. The repulsive, two-body interparticle potential is approximated as $V_{\text{self}} = \lambda\delta(\mathbf{r} - \mathbf{r}')$, with a self-coupling constant $\lambda = 4\pi\hbar^2 a/m$, where a is the scattering length. Then in the mean-field approximation (in case when we neglect the contribution of the excited states) the BEC is described by the Gross-Pitaevskii equation [52–54]:

$$i\hbar\frac{\partial}{\partial t}\psi(\mathbf{r},t) = \left[-\frac{\hbar^2}{2m}\Delta + V_{\text{self grav}}(\mathbf{r}) + \lambda\rho(\mathbf{r},t)\right]\psi(\mathbf{r},t), \tag{1}$$

where $\psi(\mathbf{r},t)$ is the wave function of the condensate and Δ is the 3-dimensional Laplacian. The probability density $\rho(\mathbf{r},t) = |\psi(\mathbf{r},t)|^2$ is normalized to

$$n_0(t) = \int d\mathbf{r}\rho(\mathbf{r},t), \tag{2}$$

where $n_0(t)$ is the number of particles in the ground state and $\rho(\mathbf{r},t)$ is the number density of the condensate. The potential $V_{\text{self grav}}(\mathbf{r})/m$ is the Newtonian gravitational potential produced by the Bose-Einstein Condensate.

Stationary solutions of the Gross-Pitaevskii equation can be found in a simple way by using the Madelung representation of complex wave functions [79, 80], then deriving the Madelung hydrodynamic equations [79]. Madelung's equations can be interpreted as the continuity and Euler equations of fluid mechanics, with quantum corrections included. However, the quantum correction potential in the generalized Euler equation contributes significantly only close to the boundary of the system [81]. In the Thomas-Fermi approximation the quantum correction potential is neglected compared to the self-interaction term. This approximation becomes more accurate as the particle number increases [82].

Assuming a spherically symmetric distribution of the condensate the following solution was found [10, 81]:

$$\rho_{\text{BEC}}(r) = \rho_{\text{BEC}}^{(c)}\frac{\sin kr}{kr}, \tag{3}$$

where $\rho_{\text{BEC}} = m\rho(r)$ and

$$k = \sqrt{\frac{Gm^3}{\hbar^2 a}}. \tag{4}$$

The central density $\rho_{\text{BEC}}^{(c)} \equiv \rho_{\text{BEC}}(0)$ is determined from normalization condition (2) as

$$\rho_{\text{BEC}}^{(c)} = \frac{n_0 mk^3}{4\pi^2}. \tag{5}$$

The Thomas-Fermi approximation remains valid for $n_0 \gg 1/ka$ [81].

The BEC galactic DM halo's size is defined by $\rho(R_{\text{BEC}}) = 0$, giving $k = \pi/R_{\text{BEC}}$, that is,

$$R_{\text{BEC}} = \pi\sqrt{\frac{\hbar^2 a}{Gm^3}}. \tag{6}$$

The mass profile of the BEC halo is then given as

$$m_{\text{BEC}}(r) = 4\pi\int_0^r \rho_{\text{BEC}}(r)\, r^2 dr = \frac{4\pi\rho_{\text{BEC}}^{(c)}}{k^2} r\left(\frac{\sin kr}{kr} - \cos kr\right). \tag{7}$$

The BEC halo contributes to the velocity profile of the particles which are moving on circular orbit as dictated by the Newtonian gravitational force [10]. This can be taken into account by the following equation:

$$v^2(r) = \frac{4\pi G\rho_{\text{BEC}}^{(c)}}{k^2}\left(\frac{\sin kr}{kr} - \cos kr\right), \tag{8}$$

which needs to be added to the baryonic contribution, respectively.

3. Confronting the Model with Rotation Curve Data

The validity of our model was tested by confronting the rotation curve data of a sample of 6 HSB, 6 LSB, and 7 dwarf galaxies, with both the NFW DM and the BEC density

profiles. For reasons to become obvious during our analysis, we split both the HSB and LSB data sets into two groups (type I. and II.), based on the shapes of the curves. In the first group the rotational velocities increase over the whole observed range, while in the second set the rotation curves exhibit long flat regions.

The commonly used NFW model has the mass density profile

$$\rho_{\mathrm{NFW}}(r) = \frac{\rho_s}{(r/r_s)\left(1 + r/r_s\right)^2}, \tag{9}$$

where ρ_s and r_s are a characteristic density and distance scale, to be determined from the fit.

The mass within a sphere with radius $r = yr_s$ is then given as

$$m_{\mathrm{NFW}}(r) = 4\pi\rho_s r_s^3 \left[\ln\left(1 + y\right) - \frac{y}{1 + y}\right], \tag{10}$$

where y is a positive dimensionless radial coordinate.

3.1. HSB Galaxies. In this subsection we will follow the method described in [15]. In HSB galaxy the baryonic component was decomposed into a thin stellar disk and a spherically symmetric bulge. It was assumed that the mass distribution of bulge component follows the deprojected luminosity distribution with a factor known as the mass-to-light ratio. The bulge parameters were estimated from a Sérsic $r^{1/n}$ bulge model, which was obtained by the fitting of the optical I-band galaxy light profiles.

Each galaxy's spheroidal bulge component has a surface brightness profile which is described by a generalized Sérsic function [83];

$$I_b(r) = I_{0,b} \exp\left[-\left(\frac{r}{r_0}\right)^{1/n}\right], \tag{11}$$

wherein $I_{0,b}$ is the central surface brightness of the bulge, r_0 is the characteristic radius of the bulge, and the magnitude-radius curve's shape parameter is denoted by n.

The mass-to-light ratio for the Sun is $\gamma_\odot = 5133\,\mathrm{kg\,W^{-1}}$. The mass-to-light ratio of the bulge σ will be given in units of $\gamma_\odot$ (solar units). We will also give the mass in units of the solar mass $M_\odot = 1.98892 \times 10^{30}$ kg. We assume that the radial distribution of visible mass follows the radial distribution of light derived from the bulge-disk decomposition. Accordingly the mass of the bulge inside the projected radius r can be derived from the surface brightness observed within this radius:

$$m_b(r) = \sigma \frac{\mathcal{N}(D)}{F_\odot} 2\pi \int_0^r I_b(r)\, r\, dr, \tag{12}$$

where $F_\odot(D)$ is the apparent flux density of the Sun at a distance D Mpc, $F_\odot(D) = 2.635 \times 10^{6-0.4 f_\odot}$ mJy, with $f_\odot = 4.08 + 5\lg(D/1\ \mathrm{Mpc}) + 25$ mag, and

$$\mathcal{N}(D) = 4.4684 \times 10^{-35} D^{-2}\,\mathrm{m^{-2}\,arcsec^2}. \tag{13}$$

The rotational velocity related to the bulge is

$$v_b^2(r) = \frac{G m_b(r)}{r}, \tag{14}$$

where G is the gravitational constant.

In case of a spiral galaxy, the radial surface brightness profile of the disk decreases exponentially as a function of the radius [84];

$$I_d(r) = I_{0,d}^{\mathrm{HSB}} \exp\left(-\frac{r}{h^{\mathrm{HSB}}}\right), \tag{15}$$

where $I_{0,d}^{\mathrm{HSB}}$ is the central surface brightness of the disk and h^{HSB} is a characteristic disk length scale. The disk contributes to the circular velocity as follows ([84]):

$$v_d^2(x) = \frac{G M_D^{\mathrm{HSB}}}{2h^{\mathrm{HSB}}} x^2 \left(I_0 K_0 - I_1 K_1\right), \tag{16}$$

where $x = r/h^{\mathrm{HSB}}$ and I_n and K_n are the modified Bessel functions evaluated at $x/2$, while M_D^{HSB} is the total mass of the disk.

Accordingly in HSB galaxy the rotational velocity adds up as

$$v_{\mathrm{tg}}^2(x) = v_b^2(x) + v_d^2(x) + v_{\mathrm{DM}}^2(x). \tag{17}$$

In order to validate the BEC+baryonic model, we confront it with rotation curve data of 6 well-tested galaxies (which were already employed in [15] for testing a brane-world model). The data was obtained from a sample given in [37] and meets the following criteria: (i) it has to be among the best accuracies obtained from the sample and (ii) the bulge has to be spherically symmetric. As a check we also fitted the NFW + baryonic model with the same data set. The respective rotation curves are plotted for both models on Figures 1 and 2. The small humps on both figures are due to the baryonic component. From the available photometric data the best fitting values were derived for the baryonic model parameters $I_{0,b}$, n, r_0, r_b, and $I_{0,d}^{\mathrm{HSB}}$ h^{HSB}. By fitting BEC and NFW models to the investigated rotation curve data, the parameters for these models (as well as the corresponding baryonic parameters) were calculated. The parameter values are indicated in Tables 1 and 2.

Both the BEC and NFW DM models give comparable χ^2_{min} values (within 1σ confidence level) for HSB I galaxies. In case of galaxies with extended flat regions (HSB II), the NFW DM model fits better the rotation curves; nevertheless BEC model gives rotational curves which fall outside the 1σ confidence level.

3.2. LSB Galaxies. The surface brightness of LSB galaxies is substantially fainter than the brightness of the sky at night. They belong to an early stage class of galaxies [85]. LSB galaxies were found to be metal poor, which indicates a lower star formation rate than what is generally found in HSB galaxies [86]. Wide spectrum of colors can be measured in case of LSB galaxies ranging from red to blue [87] and they are diverse as regards morphologies and other properties.

Table 1: The distances (D) and the photometric parameters of the 6 HSB galaxy sample as determined by the fit with available photometric data [37]. Bulge parameters: the central surface brightness ($I_{0,b}$), the shape parameter (n), the characteristic radius (r_0), and radius of the bulge (r_b). Disk parameters: central surface brightness ($I_{0,d}^{\mathrm{HSB}}$) and length scale (h^{HSB}) of the disk.

Galaxy	D	$I_{0,b}$	n	r_0	r_b	$I_{0,d}^{\mathrm{HSB}}$	h^{HSB}
	Mpc	mJy/arcsec^2		kpc	kpc	mJy/arcsec^2	kpc
ESO215G39	61.29	0.1171	0.6609	0.78	2.58	0.0339	4.11
ESO322G77	38.19	0.1949	0.7552	0.33	1.37	0.0744	2.20
ESO509G80	92.86	0.2090	0.7621	1.10	4.69	0.0176	11.03
ESO323G25	59.76	0.1113	0.4626	0.43	0.99	0.0825	3.47
ESO383G02	85.40	0.6479	0.7408	0.42	1.94	0.5118	3.82
ESO446G01	98.34	0.2093	0.8427	1.28	6.33	0.0357	5.25

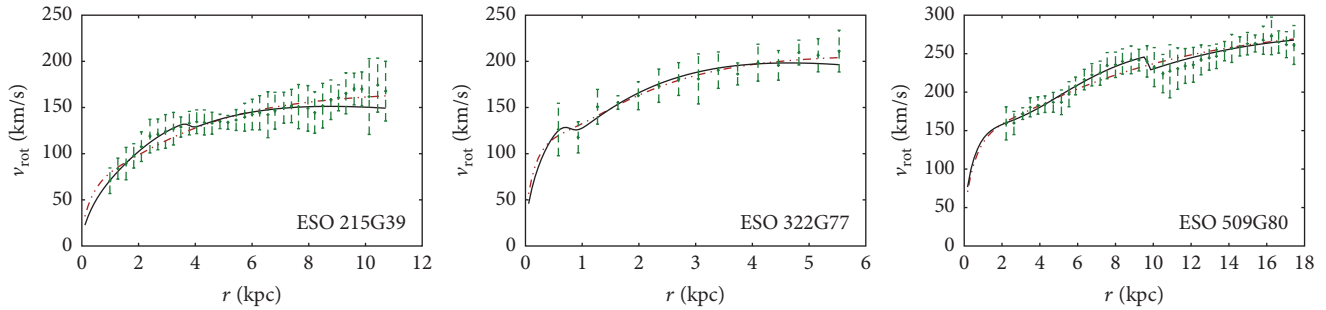

Figure 1: Best fit curves for the HSB I. galaxy sample where the solid black lines hold for the baryonic matter + BEC model, while the dashed red lines refer to the baryonic matter + NFW model.

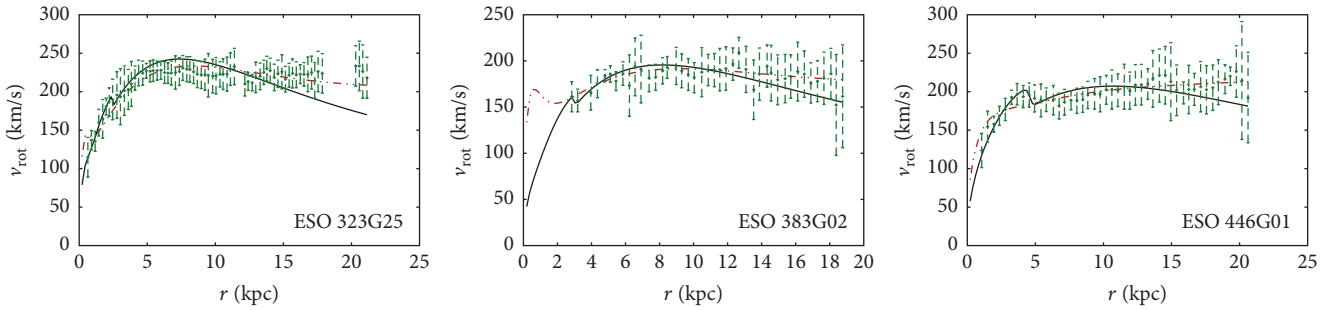

Figure 2: Best fit curves for the HSB II. galaxy sample. The solid black lines hold for the baryonic matter + BEC model, while the dashed red lines hold for the baryonic matter + NFW model. The BEC model does not describe well the extended flat regions.

Most of the LSB galaxies that were observed are dwarf galaxies; however there is also a significant number of large spirals among LSB galaxies [88].

According to our model the LSB galaxy is made up of two main components, one being a thin stellar + gas disk and the other one being a CDM component which is assumed to be a BEC. We use the same model for the disk component as in the case of the HSB galaxies. The surface brightness profile can be described by the following equation [84]:

$$I_d(r) = I_{0,d}^{\mathrm{LSB}} \exp\left(-\frac{r}{h^{\mathrm{LSB}}}\right), \tag{18}$$

where $I_{0,d}^{\mathrm{LSB}}$ is the central surface brightness and h^{LSB} is the disk length scale. The contribution of the disk to the circular velocity can be expressed as

$$v_d^2(r) = \frac{GM_D^{\mathrm{LSB}}}{2h^{\mathrm{LSB}}} q^2 \left(I_0K_0 - I_1K_1\right), \tag{19}$$

where $q = r/h^{\mathrm{LSB}}$ and M_D^{LSB} are the total mass of the disk while the modified Bessel functions I_n and K_n are evaluated at $q/2$.

Consequently, for an arbitrary projected radius r the rotational velocity can be calculated based on the combined model resulting in the following equation:

$$v_{\mathrm{tg}}^2(r) = v_d^2(r) + v_{\mathrm{DM}}^2. \tag{20}$$

A preliminary check confirmed that the BEC + baryonic model represents a better fit than the purely BEC model.

We confronted the BEC model with 6 LSB galaxies chosen from a larger sample [38]. The applied data were obtained from both HI and $H\alpha$ measurements. From a χ^2-test the parameters in both the BEC + baryonic and NFW + baryonic models were identified: these are shown in Table 3. The best fit rotation curves are represented on Figures 3 and 4.

Table 2: The best fit parameters and the minimum values ($\chi^2_{\min}$) of the χ^2 statistics for the HSB I and II galaxies (the first and last three galaxies, respectively). Columns 2–5 give the BEC model parameters (radius R_{BEC} and central density $\rho^{(c)}_{\mathrm{BEC}}$ of the BEC halo) and the corresponding baryonic parameters (mass-to-light ratio σ (BEC) of the bulge and total mass of the disk M_D^{HSB} (BEC)). Columns 7–10 give the NFW model parameters (scale radius r_s and characteristic density ρ_s of the halo) and the corresponding baryonic parameters (mass-to-light ratio σ (NFW) of the bulge and total mass of the disk M_D^{HSB} (NFW)). The 1σ confidence levels are shown in the last column (these are the same for both models). For HSB I galaxies the two models give similar $\chi^2_{\min}$ values (within 1σ confidence level); however in case of HSB II galaxies with extended flat regions, the NFW model fits better the rotation curves. The $\chi^2_{\min}$ values in the case of BEC model are outside the 1σ confidence level for HSB II galaxies.

Galaxy	σ (BEC) $\odot$	M_D^{HSB} (BEC) $10^{10}\,\mathrm{M}_\odot$	R_{BEC} kpc	$\rho^{(c)}_{\mathrm{BEC}}$ $10^{-21}\,\mathrm{kg/m^3}$	$\chi^2_{\min}$ (BEC)	σ (NFW) $\odot$	M_D^{HSB} (NFW) $10^{10}\,\mathrm{M}_\odot$	r_s kpc	ρ_s $10^{-24}\,\mathrm{kg/m^3}$	$\chi^2_{\min}$ (NWF)	1σ
ESO215G39	0.3	5.61	3.8	2.0	23.07	0.6	3.84	187	14.7	22.22	34.18
ESO322G77	1.6	5.1	0.8	89.0	9.15	2.5	3.79	709	8	7.69	11.53
ESO509G80	1.4	48.74	9.7	1.2	12.52	0.9	11	22	800	33.48	36.3
ESO323G25	2.5	12.18	2.5	11.8	222.74	6	9.43	436	6	80.55	66.74
ESO383G02	0.13	8.77	3.0	5.7	48.83	1.7	6.32	459	4.2	23.3	47.9
ESO446G01	0.6	12.77	4.6	5.9	86.02	1.4	6.7	786	4.1	43.37	44.74

Table 3: The best fit BEC and NFW parameters of the LSB I and II type galaxies (the first and last three galaxies, respectively). D is taken from [38]. The rest of the parameters are rotation curve fits. For LSB I galaxies the BEC DM model gives significantly better fitting velocity curves (within 1σ confidence level) than the NFW model. However the velocity curves are outside the 1σ confidence level for LSB II galaxies.

Galaxy	D Mpc	h^{LSB} kpc	M_D^{LSB} (BEC) $10^9\,\mathrm{M}_\odot$	$\rho_{\mathrm{BEC}}^{(c)}$ $10^{-21}\,\mathrm{kg/m^3}$	R_{BEC} kpc	χ^2_{min} (BEC)	M_D^{LSB} (NFW) $10^9\,\mathrm{M}_\odot$	ρ_s $10^{-24}\,\mathrm{kg/m^3}$	r_s kpc	χ^2_{min} (NFW)	1σ
DDO 189	12.6	1.9	2.71	0.38	8.3	0.519	2.16	16	70	1.09	7.03
NGC 4455	6.8	2.3	0.231	1.44	5.5	9.29	0.11	25.04	66	5.39	18.11
UGC 10310	15.6	5.2	0.443	0.98	7.8	2.66	0.9	14.9	88	5.76	13.74
NGC 2366	3.4	1.5	2.43	0.22	5.3	110.73	2.5	0.2	1000	116.93	26.72
NGC 5023	4.8	0.8	0.894	2.45	5.6	53.2	0.0449	457	13	143.08	32.05
NGC 3274	6.7	0.5	1.1	1.69	6.4	269.8	0.252	2373	4	148.44	20.27

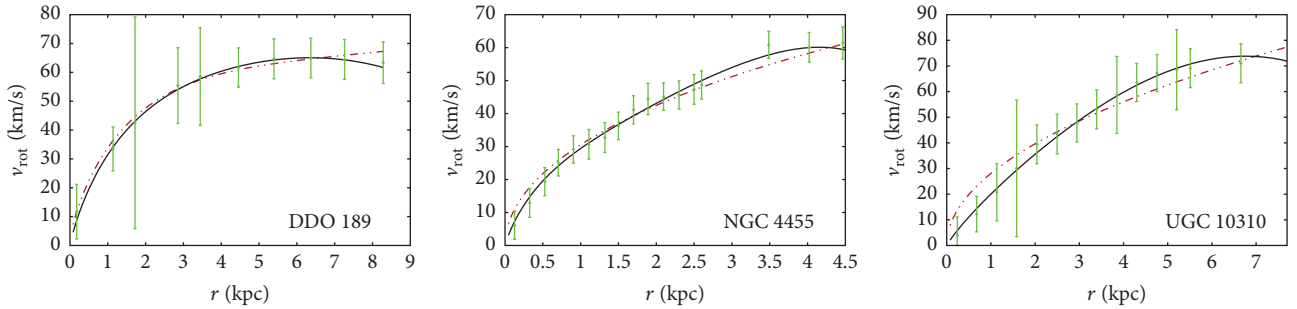

Figure 3: Best fit curves for the LSB I. galaxy sample. The solid black lines indicate the baryonic matter + BEC model, while the dashed red lines indicate the baryonic matter + NFW model.

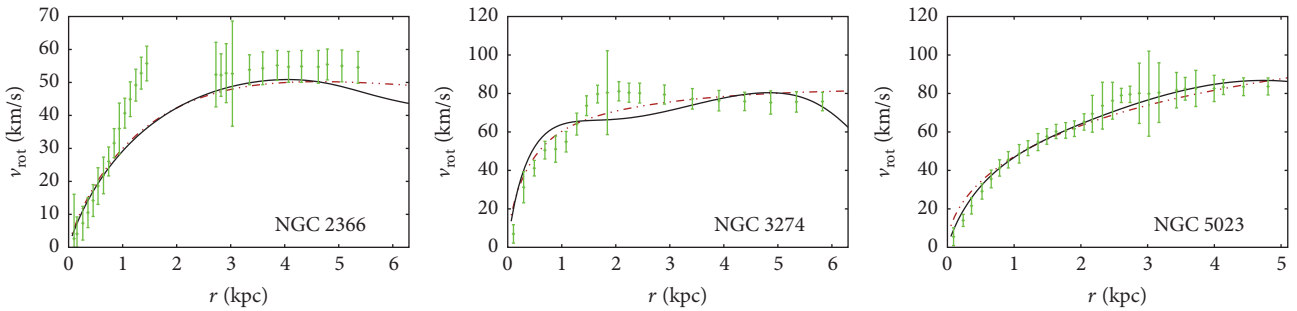

Figure 4: Best fit curves for the LSB II. galaxy sample. The solid black lines refer to the baryonic matter + BEC model, while the dashed red lines to the baryonic matter + NFW model. As for HSB galaxies, the BEC model fails to explain the extended flat regions of the rotation curves.

For the LSB I galaxies the BEC DM model gives significantly better fitting velocity curves (all within the 1σ confidence level) compared to the NFW model (which in two cases out of the three gives fits falling outside 1σ). For LSB II galaxies the quality of the fits is comparable, but in both models they are beyond the 1σ confidence level.

3.3. Dwarf Galaxies. Approximately 85% of the explored galaxies in the Local Volume [89] are dwarf galaxies. The dwarfs are defined by having an absolute magnitude which is fainter than $M_B \sim -16$ mag. On the other hand they are larger than globular clusters [90].

Although little is known about their formation, it is generally accepted that dwarfs are formed at the centres of subhalos. Dwarf galaxies can be categorised in five groups according to their optical appearance. The five groups being dwarf ellipticals, dwarf irregulars, dwarf spheroidals, blue compact dwarfs, and dwarf spirals. The dwarfs falling in the last group represent the very small ends of spirals [91]. Dwarf spheroidals are old systems and among the most DM dominated galaxies in the Universe.

The central velocity dispersion of most dwarf galaxies is in the range $6 \div 25$ km/s [92]. In a typical dwarf galaxy, assuming dynamical equilibrium, the mass derived from the observed velocity dispersion is substantially greater than the observed total visible mass. This implies that the mass-to-light ratio is very high compared to other types of galaxies; hence they can greatly contribute to the understanding of DM distribution on small scales. Dwarf galaxies allow for proving or falsifying different alternative gravity theories [93].

We decided to use 7 dwarf galaxies for testing the BEC model. We have selected the sample dwarf galaxies such as to ensure that sufficient high-resolution rotation curve data would be available for our study. We fitted both the BEC + baryonic and the NFW + baryonic models, respectively, with similar baryonic components as for the LSB galaxies. As the length scales of the stellar disks were not available for the selected sample, they were calculated by χ^2 minimization, too.

A preliminary check showed that the addition of the BEC dark matter halo to the baryonic model improved (giving lower $\chi^2_{\min}$ values) on the fit in all cases. By contrast, the NFW model was unable to improve on the purely baryonic fit in four out of seven cases. We note that since the data does not contain the error margins, the $\chi^2_{\min}$ values are relatively high (beyond the 1σ confidence level in most cases). The best fit BEC and NFW parameters are shown in Table 4 and the corresponding rotation curves are represented on Figure 5. The inclusion of the BEC DM model gives significantly (in some cases one order of magnitude in the value of χ^2) better fits compared to the case of NFW model. This is due to the cusp avoidance in the central density profile of the BEC model and the fact that dwarf galaxies do not exhibit extended flat regions in their rotation curves.

4. Discussions and Final Remarks

We have performed a χ^2-test of the BEC and NFW DM models, with the rotation curves of 6 HSB, 6 LSB, and 7 dwarf

Table 4: The best rotation curve data fit BEC + baryonic and NFW + baryonic parameters for the dwarf galaxy sample.

Galaxy	h^{dwarf} (BEC) kpc	M_D^{dwarf} (BEC) $10^9\ M_\odot$	$\rho_{\text{BEC}}^{(c)}$ 10^{-21} kg/m^3	R_{BEC} kpc	χ^2_{min} (BEC)	h^{dwarf} (NFW) kpc	M_D^{dwarf} (NFW) $10^9\ M_\odot$	ρ_s 10^{-24} kg/m^3	r_s kpc	χ^2_{min} (NFW)	1σ
IC 2574	1.2	0.1122	0.4	13	68.47	7.9	28.44	0	0	714.73	44.74
HoI	0.2	0.0107	3.6	1.9	95.26	0.9	0.533	0	0	241.30	20.27
HoII	1.2	0.4431	0.2	7.69	33.33	1.7	0.642	4	92	43.86	26.72
DDO 39	1.3	1.1235	0.7	10.01	69.39	4.3	7.21	43	35	69.82	17.02
DDO 53	0.2	0.0061	1.8	2.5	20.05	1.6	0.976	1	24	51.53	10.42
DDO 154	3.1	3.3502	0.2	5.8	1.48	3.2	4.52	0	0	9.40	9.30
M81dwB nor	0.9	1.023	3.7	0.7	6.19	0.7	0.705	0	0	8.4	10.42

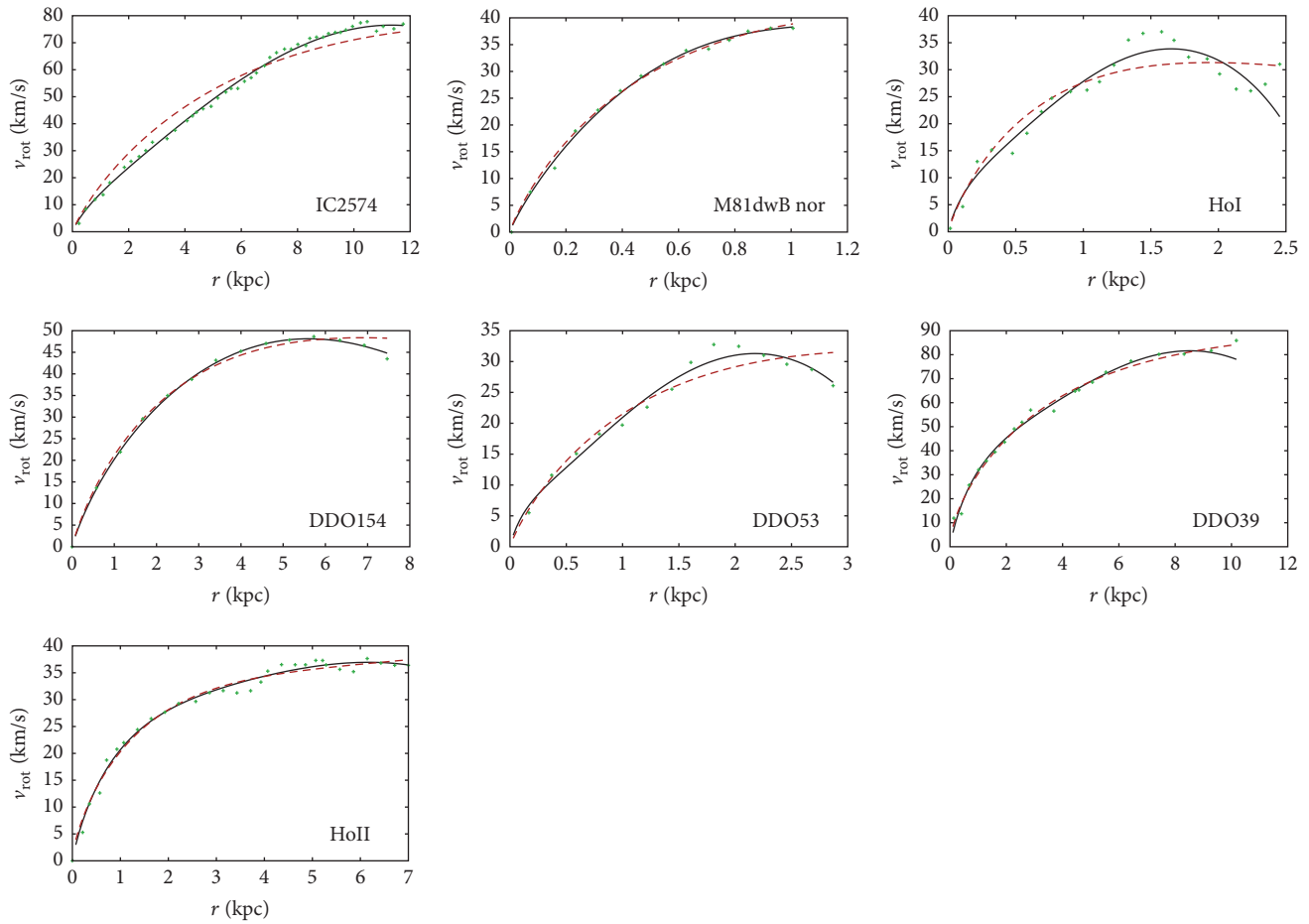

FIGURE 5: The best fit curves for the dwarf galaxy sample. The BEC + baryonic model (solid black curves) give a better fit in all cases than the NFW + baryonic model (dashed red lines). In both cases the fit was performed with the same baryonic model.

galaxy samples. For improved accuracy we also included realistic baryonic models in every case. For the HSB galaxy sample, both the rotation curve and the surface photometry data were available. Most of the rotation curves were smooth, symmetric, and uniform in quality.

The circular velocity of the investigated galaxies was decomposed into its baryonic and DM contribution: $v^2_{\text{model}}(r) = v^2_{\text{baryonic}} + v^2_{\text{DM}}$. For the BEC model the DM contribution to the rotational velocity can be described as (8). Then the rotation curves are fitted with the parameters of the baryonic and DM halo models (BEC and NFW) using χ^2 minimization method.

The analysis of the *HSB I galaxies* showed a remarkably good agreement for both DM models with observations. The BEC and NFW models show similar fits. However, the rotation curves of the HSB II type galaxies are significantly better described by the NFW model.

It was previously known that for *LSB galaxies and without including the baryonic sector*, the BEC model gave a better fit than the NFW model [62]. We additionally found that including the baryonic component improves on the fit of [62]. Our detailed analysis showed a significantly better performance of the BEC model for LSB type I galaxies, while comparable fits for LSB type II galaxies were obtained. These latter fits were however outside the 2σ confidence level.

The unsatisfactory large distance behaviour of the BEC model for both the HSB and LSB galaxies of type II originates in the sharp cutoff of the BEC DM distribution and clearly indicates that it would be desirable to modify the BEC model on larger scale, also to comply with the behaviour of the universal rotation curves (URCs) at larger radii [94].

From the above analysis of HSB and LSB galaxies it is also obvious that (while on large distances the BEC model suffers from problems due to the sharp cutoff) close to the core it works overall better than the NFW model. This is also supported by our fit of both the BEC + baryonic and NFW + baryonic DM models with rotation curve data of a sample of 7 dwarf galaxies. Since dwarf galaxies are DM dominated, they allow for the best comparison between the various models. The results can be seen in Figure 5. We also note that the NFW DM improved over the pure baryonic fit in four cases out of seven, while including the BEC component improved over the fit with the baryonic component in all cases.

The BEC parameters were determined for all cases. The parameters $\rho^{(c)}_{\text{BEC}}$, R_{BEC} are given in Tables 2, 3, and 4. The averages of the radii R_{DM} of the BEC halos for the HSB, LSB,

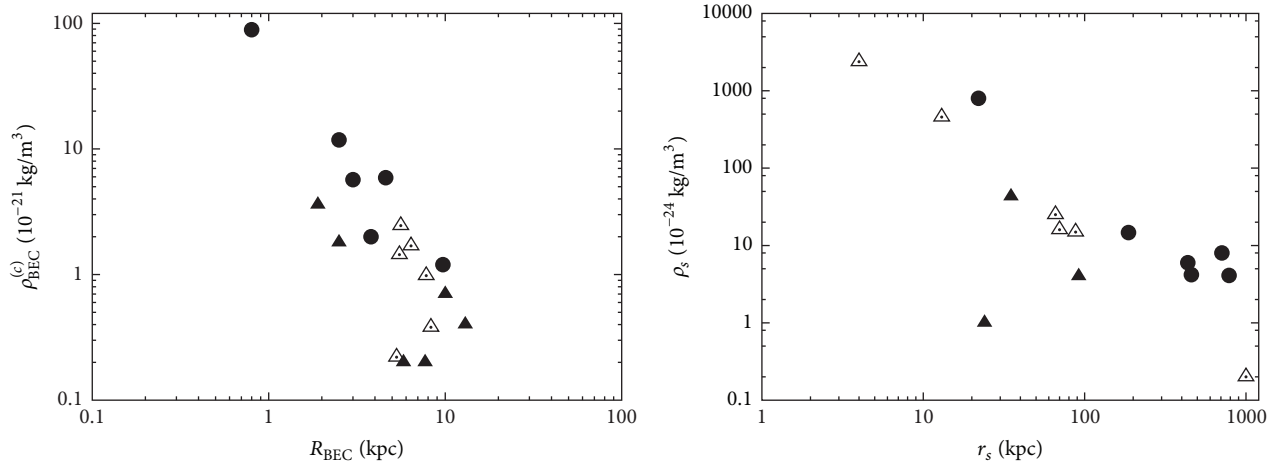

FIGURE 6: The density parameter $\rho^{(c)}_{\rm BEC}$ of the BEC model is shown as function of $R_{\rm BEC}$ in (a), and the density parameter ρ_s of the NFW model is shown as function of r_s in (b). The HSB, LSB, and dwarf galaxies are represented by filled circles, empty triangles, and filled triangles, respectively.

and dwarf galaxies are $\langle R^{\rm HSB}_{\rm BEC}\rangle \approx 4.06\,$kpc, $\langle R^{\rm LSB}_{\rm DM}\rangle \approx 6.48\,$kpc, and $\langle R^{\rm dwarf}_{\rm DM}\rangle \approx 5.94\,$kpc, respectively. The scatter however is large; there are no universal BEC parameters which globally fit all the galaxies, not even at 3σ confidence level. The closer to this goal were the HSB galaxies, where 3 out of 6 had overlapping 3σ domains. Nonetheless the given values of $R_{\rm DM}$ are consistent within the order of magnitude with the halo radii of 59 other galaxies determined from weak lensing [95].

We represent the density parameter $\rho^{(c)}_{\rm BEC}$ of the BEC model as function of $R_{\rm BEC}$ in Figure 6(a) and the density parameter ρ_s of the NFW model as function of r_s in Figure 6(b) (four dwarf galaxies are absent, as the NFW halo does not improve the fit over the pure baryonic case). The fitting enforces a relation between the dark matter parameters: the characteristic density scales with an inverse power with the corresponding characteristic distance.

We verify the Tully-Fisher relation for the investigated galaxy sample and present the results on Figure 7. Apparent B magnitudes and galaxy distances were collected from the NASA/IPAC extragalactic database [96] and were corrected for extinction based on Landolt standard fields to calculate the absolute magnitudes. It is known that the Tully-Fisher relation holds for spiral and lenticular galaxies with the same slope (e.g., [97]). A larger slope and scatter characterize the Tully-Fisher relation for the dwarf galaxies (e.g., [97, 98]). The investigated sample exactly exhibits these features.

There is a relation among the mass m of the BEC particle, its coherent scattering length a, and the radius of the DM halo $R_{\rm DM}$ [10]:

$$m = \left(\frac{\pi^2\hbar^2 a}{G R^2_{\rm BEC}}\right)^{1/3} \approx 6.73\times 10^{-2}\,[a\,({\rm fm})]^{1/3}\,[R_{\rm BEC}\,({\rm kpc})]^{-2/3}\,{\rm eV}. \quad (21)$$

Axions have been proposed as the Peccei-Quinn solution to the strong CP problem [99] and they are among the best dark matter candidates. Being bosons, they may also form BEC. The Axion Dark Matter Experiment has already established limits on the dark matter axions [100, 101].

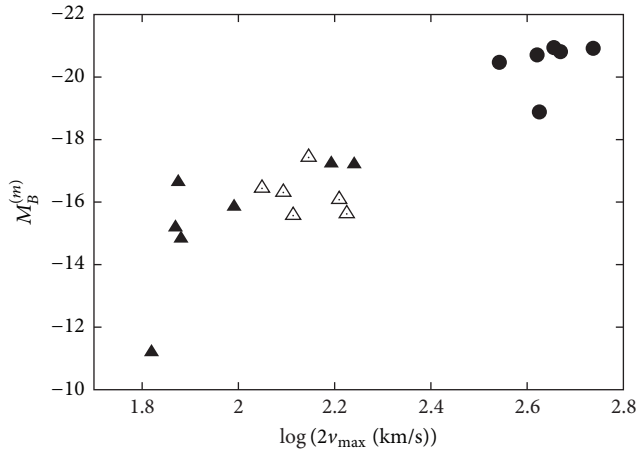

FIGURE 7: The baryonic Tully-Fisher relation of our galaxy sample. Absolute B magnitudes are presented as function of the logarithm of the maximal rotational velocity. The HSB, LSB, and dwarf galaxies are represented by filled circles, empty triangles, and filled triangles, respectively.

Assuming the BEC is formed of axions with mass of 10^{-6} eV, the scattering lengths for the three types of galaxies emerge as $a_{\rm HSB} \approx 5.4\times 10^{-14}\,$fm, $a_{\rm LSB} \approx 1.37\times 10^{-13}\,$fm, and $a_{\rm dwarf} \approx 1.15\times 10^{-13}\,$fm. These values are consistent with the results of [95], which are based on a statistical analysis of 61 DM dominated galaxies. The total energy of the BEC halo is negative with these scattering lengths and particle mass, meaning the halo is stable (see Figure 3 of [56]).

Competing Interests

The authors declare that they have no competing interests.

Acknowledgments

In the earlier stages of this work M. Dwornik, Z. Keresztes, and L. Á. Gergely were supported by the European Union and the State of Hungary, cofinanced by the European Social Fund in the framework of TÁMOP 4.2.4. A/2-11-/1-2012-0001 "National Excellence Program". L. Á. Gergely was also supported by the Japan Society for the Promotion of Science.

References

[1] P. A. R. Ade, N. Aghanim, C. Armitage-Caplan et al., "Planck 2013 results. I. Overview of products and scientific results," *Astronomy & Astrophysics*, vol. 571, article 1, 2014.

[2] M. Francis, "First Planck results: the Universe is still weird and interesting," *Arstechnica*, 2013.

[3] J. Ja locha, L. Bratek, M. Kutschera, and P. Skindzier, "Global disc models for galaxies NGC 1365, 6946, 7793 and UGC 6446," *Monthly Notices of the Royal Astronomical Society*, vol. 406, no. 4, pp. 2805–2816, 2010.

[4] M. Milgrom, "A modification of the Newtonian dynamics as a possible alternative to the hidden mass hypothesis," *The Astrophysical Journal*, vol. 270, pp. 365–370, 1983.

[5] R. H. Sanders, "Anti-gravity and galaxy rotation curves," *Astronomy & Astrophysics*, vol. 136, no. 2, pp. L21–L23, 1984.

[6] J. Moffat and I. Sokolov, "Galaxy dynamics predictions in the nonsymmetric gravitational theory," *Physics Letters B*, vol. 378, no. 1–4, pp. 59–67, 1996.

[7] P. D. Mannheim, "Are galactic rotation curves really flat?" *Astrophysical Journal*, vol. 479, no. 2, pp. 659–664, 1997.

[8] M. D. Roberts, "Galactic metrics," *General Relativity and Gravitation*, vol. 36, no. 11, pp. 2423–2431, 2004.

[9] C. G. Böhmer and T. Harko, "On Einstein clusters as galactic dark matter haloes," *Monthly Notices of the Royal Astronomical Society*, vol. 379, no. 1, pp. 393–398, 2007.

[10] C. G. Böhmer and T. Harko, "Can dark matter be a Bose-Einstein condensate?" *Journal of Cosmology and Astroparticle Physics*, vol. 2007, no. 6, 2007.

[11] O. Bertolami, C. G. Böhmer, T. Harko, and F. S. Lobo, "Extra force in ***f(R)*** modified theories of gravity," *Physical Review D. Particles, Fields, Gravitation, and Cosmology*, vol. 75, no. 10, Article ID 104016, 2007.

[12] C. G. Böhmer, T. Harko, and F. S. N. Lobo, "Dark matter as a geometric effect in f (R) gravity," *Astroparticle Physics*, vol. 29, no. 6, pp. 386–392, 2008.

[13] M. K. Mak and T. Harko, "Can the galactic rotation curves be explained in brane world models?" *Physical Review D*, vol. 70, no. 2, Article ID 024010, 2004.

[14] F. Rahaman, M. Kalam, A. DeBenedictis, A. A. Usmani, and R. Saibal, "Galactic rotation curves and brane world models," *Monthly Notices of the Royal Astronomical Society*, vol. 389, no. 1, pp. 27–33, 2008.

[15] L. Á. Gergely, T. Harko, M. Dwornik, G. Kupi, and Z. Keresztes, "Galactic rotation curves in brane world models," *Monthly Notices of the Royal Astronomical Society*, vol. 415, no. 4, pp. 3275–3290, 2011.

[16] A. Stabile and S. Capozziello, "Galaxy rotation curves in $f(R,\phi)$ gravity," *Physical Review D*, vol. 87, no. 6, Article ID 064002, 2013.

[17] E. Conover, "Physicists narrow in on electrical short in Large Hadron Collider," *Science*, 2015.

[18] N. Arkani-Hamed et al., *SUSY Bet: Arkani-Hamed and Panel Discussion*, Current Themes in High Energy Physics and Cosmology, Copenhagen, Denmark, 2016.

[19] M. G. Aartsen, K. Abraham, M. Ackermann et al., "Searches for sterile neutrinos with the IceCube detector," *Physical Review Letters*, vol. 117, no. 7, Article ID 071801, 9 pages, 2016.

[20] D. S. Akerib, H. M. Araujo, X. Bai et al., "First results from the LUX dark matter experiment at the sanford underground research facility," *Physical Review Letters*, vol. 112, no. 9, Article ID 091303, 2013.

[21] PandaX-II Collaboration, "Dark matter results from First 98.7-day data of pandaX-II experiment," *Physical Review Letters*, vol. 117, Article ID 121303, 2016.

[22] E. Aprile, J. Aalbers, F. Agostini et al., "XENON100 dark matter results from a combination of 477 live days," *Physical Review D*, vol. 94, no. 12, Article ID 122001, 2016.

[23] D. Choudhury and K. Ghosh, "Bounds on universal extra dimension from LHC run I and II data," *Physics Letters B*, vol. 763, pp. 155–160, 2016.

[24] C. Alcock, R. A. Allsman, D. R. Alves et al., "The MACHO project: microlensing results from 5.7 years of large magellanic cloud observations," *Astrophysical Journal*, vol. 542, no. 1, pp. 281–307, 2000.

[25] B. P. Abbott, R. Abbott, T. D. Abbott et al., "Observation of gravitational waves from a binary black hole merger," *Physical Review Letters*, vol. 116, no. 6, Article ID 061102, 2016.

[26] D. O. Caldwell, *Current Aspects of Neutrino Physics*, Springer, Berlin, Heidelberg, 2001.

[27] H. J. de Vega and N. G. Sanchez, "Warm dark matter in the galaxies: theoretical and observational progresses. Highlights and conclusions of the chalonge meudon workshop 2011," https://arxiv.org/abs/1109.3187.

[28] H. Wei, Z.-C. Chen, and J. Liu, "Cosmological constraints on variable warm dark matter," *Physics Letters B*, vol. 720, no. 4-5, pp. 271–276, 2013.

[29] P. L. Biermann and A. Kusenko, "Relic keV sterile neutrinos and reionization," *Physical Review Letters*, vol. 96, no. 9, Article ID 091301, 2006.

[30] M. G. Aartsen, M. Ackermann, J. Adams et al., "Searches for sterile neutrinos with the icecube detector," *Physical Review Letters*, vol. 117, no. 7, Article ID 071801, 2016.

[31] T. Padmanabhan, "Cosmological constant—the weight of the vacuum," *Physics Reports. A Review Section of Physics Letters*, vol. 380, no. 5-6, pp. 235–320, 2003.

[32] P. J. Peebles and B. Ratra, "The cosmological constant and dark energy," *Reviews of Modern Physics*, vol. 75, no. 2, pp. 559–606, 2003.

[33] A. Fowlie, K. Kowalska, L. Roszkowski, E. M. Sessolo, and Y.-L. S. Tsai, "Dark matter and collider signatures of the MSSM," *Physical Review D*, vol. 88, no. 5, Article ID 055012, 2013.

[34] G. Aad, T. Abajyan, B. Abbott et al., "Search for invisible decays of a higgs boson produced in association with a Z boson in ATLAS," *Physical Review Letters*, vol. 112, no. 20, Article ID 201802, 19 pages, 2014.

[35] P. H. Frampton, "Angular momentum of dark matter black holes," https://arxiv.org/abs/1608.05009.

[36] M. Sasaki, T. Suyama, T. Tanaka, and S. Yokoyama, "Primordial black hole scenario for the gravitational-wave event GW150914," *Physical Review Letters*, vol. 117, no. 6, Article ID 061101, 2016.

[37] P. Palunas and T. B. Williams, "Maximum disk mass models for spiral galaxies," *Astronomical Journal*, vol. 120, no. 6, pp. 2884–2903, 2000.

[38] W. J. G. de Blok and A. Bosma, "High-resolution rotation curves of low surface brightness galaxies," *Astronomy and Astrophysics*, vol. 385, no. 3, pp. 816–846, 2002.

[39] V. Springel, S. D. M. White, A. Jenkins et al., "Simulations of the formation, evolution and clustering of galaxies and quasars," *Nature*, vol. 435, no. 7042, pp. 629–636, 2005.

[40] J. F. Navarro, C. S. Frenk, and S. D. M. White, "The structure of cold dark matter halos," *Astrophysical Journal*, vol. 462, no. 2, pp. 563–575, 1996.

[41] O. Valenzuela, G. Rhee, A. Klypin et al., "Is there evidence for flat cores in the halos of dwarf galaxies? The case of NGC 3109 and NGC 6822," *Astrophysical Journal*, vol. 657, no. 2 I, pp. 773–789, 2007.

[42] J. R. Jardel, K. Gebhardt, M. H. Fabricius, N. Drory, and M. J. Williams, "Measuring dark matter profiles non-parametrically in dwarf spheroidals: an application to Draco," *Astrophysical Journal*, vol. 763, no. 2, article 91, 2013.

[43] A. Burkert, "The structure of dark matter halos. Observation versus theory," in *Dark Matter in Astro- and Particle Physics: (DARK '96): Heidelberg, Germany, 16–20 September 1996*, H. V. Klapdor-Kleingrothaus and Y. Ramachers, Eds., p. 35, World Scientific, Singapore, 1997.

[44] R. Teyssier, A. Pontzen, Y. Dubois, and J. I. Read, "Cusp-core transformations in dwarf galaxies: observational predictions," *Monthly Notices of the Royal Astronomical Society*, vol. 429, no. 4, pp. 3068–3078, 2013.

[45] S. Inoue and T. R. Saitoh, "Cores and revived cusps of dark matter haloes in disc galaxy formation through clump clusters," *Monthly Notices of the Royal Astronomical Society*, vol. 418, no. 4, pp. 2527–2531, 2011.

[46] A. Klypin and F. Prada, "Testing gravity with motion of satellites around galaxies: Newtonian gravity against modified Newtonian dynamics," *Astrophysical Journal*, vol. 690, no. 2, pp. 1488–1496, 2009.

[47] L. Á. Gergely and S. Tsujikawa, "Effective field theory of modified gravity with two scalar fields: dark energy and dark matter," *Physical Review D*, vol. 89, no. 6, Article ID 064059, 2014.

[48] I. Rodríguez-Montoya, J. Magaña, T. Matos, and A. Pérez-Lorenzana, "Ultra light bosonic dark matter and cosmic microwave background," *Astrophysical Journal*, vol. 721, no. 2, pp. 1509–1514, 2010.

[49] S.-J. Sin, "Late-time phase transition and the galactic halo as a Bose liquid," *Physical Review D*, vol. 50, no. 6, article 3650, 1994.

[50] P. Sikivie, "Caustic rings of dark matter," *Physics Letters B*, vol. 432, no. 1-2, pp. 139–144, 1998.

[51] P. Sikivie, "Caustic ring singularity," *Physical Review D—Particles, Fields, Gravitation and Cosmology*, vol. 60, no. 6, pp. 1–16, 1999.

[52] E. P. Gross, "Structure of a quantized vortex in boson systems," *Nuovo Cimento*, vol. 20, no. 3, pp. 454–477, 1961.

[53] E. P. Gross, "Hydrodynamics of a superfluid condensate," *Journal of Mathematical Physics*, vol. 4, no. 2, p. 195, 1963.

[54] L. P. Pitaevskii, "Vortex lines in an imperfect bose gas," *Zhurnal Éksperimental'noĭ i Teoreticheskoĭ Fiziki*, vol. 40, no. 2, p. 646, 1961.

[55] T. Harko, "Cosmological dynamics of dark matter Bose-Einstein condensation," *Physical Review D*, vol. 83, no. 12, Article ID 123515, 2011.

[56] J. C. C. De Souza and M. O. C. Pires, "Discussion on the energy content of the galactic dark matter Bose-Einstein condensate halo in the Thomas-Fermi approximation," *Journal of Cosmology and Astroparticle Physics*, vol. 2014, no. 3, article no. 010, 2014.

[57] T. Harko, "Gravitational collapse of Bose-Einstein condensate dark matter halos," *Physical Review D—Particles, Fields, Gravitation and Cosmology*, vol. 89, no. 8, Article ID 084040, 2014.

[58] H. Velten and E. Wamba, "Power spectrum for the Bose-Einstein condensate dark matter," *Physics Letters, Section B: Nuclear, Elementary Particle and High-Energy Physics*, vol. 709, no. 1-2, pp. 1–5, 2012.

[59] J. W. Lee, S. Lim, and D. Choi, "BEC dark matter can explain collisions of galaxy clusters," https://arxiv.org/abs/0805.3827.

[60] D. Boyanovsky, H. J. De Vega, and N. G. Sanchez, "Constraints on dark matter particles from theory, galaxy observations, and N-body simulations," *Physical Review D*, vol. 77, no. 4, Article ID 043518, 2008.

[61] A. X. González-Morales, A. Diez-Tejedor, L. A. Ureña-López, and O. Valenzuela, "Hints on halo evolution in scalar field dark matter models with galaxy observations," *Physical Review D*, vol. 87, no. 2, 2013.

[62] V. H. Robles and T. Matos, "Flat central density profile and constant dark matter surface density in galaxies from scalar field dark matter," *Monthly Notices of the Royal Astronomical Society*, vol. 422, no. 1, pp. 282–289, 2012.

[63] M. Dwornik, Z. Keresztes, and L. Á. Gergely, "Rotation curves in bose-einstein condensate dark matter halos," in *Recent Development in Dark Matter Research*, N. Kinjo and A. Nakajima, Eds., pp. 195–219, Nova Science, 2014.

[64] L. P. Pitaevskii and S. Stringari, *Bose-Einstein Condensation*, Oxford University Press, New York, NY, USA, 2003.

[65] S. Grossmann and M. Holthaus, "On Bose-Einstein condensation in harmonic traps," *Physics Letters A*, vol. 208, no. 3, pp. 188–192, 1995.

[66] W. Ketterle and N. J. van Druten, "Two-step condensation of the ideal bose gas in highly anisotropic traps," *Physical Review A*, vol. 54, p. 656, 1996.

[67] K. Kirsten and D. J. Toms, "Bose-Einstein condensation of atomic gases in a general harmonic-oscillator confining potential trap," *Physical Review A—Atomic, Molecular, and Optical Physics*, vol. 54, no. 5, article 4188, 1996.

[68] H. Haugerud, T. Haugset, and F. Ravndal, "A more accurate analysis of Bose-Einstein condensation in harmonic traps," *Physics Letters, Section A: General, Atomic and Solid State Physics*, vol. 225, no. 1-3, pp. 18–22, 1997.

[69] S. Giorgini, L. P. Pitaevskii, and S. Stringari, "Theory of ultracold atomic Fermi gases," *Reviews of Modern Physics*, vol. 80, no. 4, 2008.

[70] K. Glaum, A. Pelster, H. Kleinert, and T. Pfau, "Critical temperature of weakly interacting dipolar condensates," *Physical Review Letters*, vol. 98, no. 8, Article ID 080407, 2007.

[71] M. Schütte and A. Pelster, "Critical temperature of a bose-einstein condensate with 1/r interactions," in *Proceedings of the 9th International Conference on Path Integrals: New Trends and Perspectives (PI '07)*, W. Janke and A. Pelster, Eds., pp. 417–420, World Scientific, Dresden, Germany, September 2007.

[72] F. Dalfovo, S. Giorgini, L. P. Pitaevskii, and S. Stringari, "Theory of Bose-Einstein condensation in trapped gases," *Reviews of Modern Physics*, vol. 71, no. 3, pp. 463–512, 1999.

[73] M. H. Anderson, J. R. Ensher, M. R. Matthews, C. E. Wieman, and E. A. Cornell, "Observation of Bose-Einstein condensation in a dilute atomic vapor," *Science*, vol. 269, no. 5221, pp. 198–201, 1995.

[74] D. J. Han, R. H. Wynar, P. Courteille, and D. J. Heinzen, "Bose-Einstein condensation of large numbers of atoms in a magnetic time-averaged orbiting potential trap," *Physical Review A—Atomic, Molecular, and Optical Physics*, vol. 57, no. 6, pp. R4114–R4117, 1998.

[75] U. Ernst, A. Marte, F. Schreck, J. Schuster, and G. Rempe, "Bose-Einstein condensation in a pure Ioffe-Pritchard field configuration," *Europhysics Letters*, vol. 41, no. 1, pp. 1–6, 1998.

[76] K. B. Davis, M.-O. Mewes, M. R. Andrews et al., "Bose-Einstein condensation in a gas of sodium atoms," *Physical Review Letters*, vol. 75, no. 22, article 3969, 1995.

[77] L. V. Hau, B. D. Busch, C. Liu, Z. Dutton, M. M. Burns, and J. A. Golovchenko, "Near-resonant spatial images of confined Bose-Einstein condensates in a 4-Dee magnetic bottle," *Physical Review A*, vol. 58, no. 1, pp. R54–R57, 1998.

[78] C. C. Bradley, C. A. Sackett, J. J. Tollett, and R. G. Hulet, "Evidence of Bose-Einstein condensation in an atomic gas with attractive interactions," *Physical Review Letters*, vol. 75, no. 9, pp. 1687–1690, 1995.

[79] E. Madelung, "Quantum theory in hydrodynamic form," *Zeitschrift für Physik*, vol. 40, pp. 322–326, 1926.

[80] S. Sonego, "Interpretation of the hydrodynamical formalism of quantum mechanics," *Foundations of Physics. An International Journal Devoted to the Conceptual Bases and Fundamental Theories of Modern Physics, Biophysics, and Cosmology*, vol. 21, no. 10, pp. 1135–1181, 1991.

[81] X. Z. Wang, "Cold Bose stars: self-gravitating Bose-Einstein condensates," *Physical Review D*, vol. 64, no. 12, Article ID 124009, 2001.

[82] E. H. Lieb, R. Seiringer, and J. Yngvason, "A rigorous derivation of the Gross-Pitaevskii energy functional," *Physical Review A*, vol. 61, no. 4, Article ID 043602, 2000.

[83] J. L. Sérsic, *Atlas de Galaxias Australes*, Observatorio Astronomico, Cordoba, Argentina, 1968.

[84] K. C. Freeman, "On the disks of spiral and so galaxies," *The Astrophysical Journal*, vol. 160, p. 811, 1970.

[85] C. Impey and G. Bothun, "Low surface brightness galaxies," *Annual Review of Astronomy and Astrophysics*, vol. 35, no. 1, pp. 267–307, 1997.

[86] S. S. Mcgaugh, "Oxygen abundances in low surface brightness disk galaxies," *Astrophysical Journal*, vol. 426, no. 1, pp. 135–149, 1994.

[87] K. O'Neil, G. D. Bothun, J. Schombert, M. E. Cornell, and C. D. Impey, "A wide field ccd survey for low surface brightness galaxies. II. Color distributions, stellar populations, and missing baryons," *Astronomical Journal*, vol. 114, no. 6, p. 2448, 1997.

[88] M. Beijersbergen, W. J. G. De Blok, and J. M. Van Der Hulst, "Surface photometry of bulge dominated low surface brightness galaxies," *Astronomy and Astrophysics*, vol. 351, no. 3, pp. 903–919, 1999.

[89] I. D. Karachentsev, V. E. Karachentseva, W. K. Huchtmeier, and D. I. Makarov, "A catalog of neighboring galaxies," *Astronomical Journal*, vol. 127, no. 4, pp. 2031–2068, 2004.

[90] G. A. Tammann, "Dwarf galaxies in the past," in *Dwarf Galaxies, ESO Conference and Workshop Proc No. 49*, p. 3, 1994.

[91] L. D. Matthews and J. S. Gallagher III, "B and V CCD photometry of southern, extreme late-type spiral galaxies," *Astronomical Journal*, vol. 114, no. 5, pp. 1899–1919, 1997.

[92] M. Mateo, "Dwarf galaxies of the local group," *Annual Review of Astronomy and Astrophysics*, vol. 36, no. 1, pp. 435–506, 1998.

[93] S. Capozziello, V. F. Cardone, and A. Troisi, "Low surface brightness galaxy rotation curves in the low energy limit of R^n gravity: no need for dark matter?" *Monthly Notices of the Royal Astronomical Society*, vol. 375, no. 4, pp. 1423–1440, 2007.

[94] M. Persic, P. Salucci, and F. Stel, "The universal rotation curve of spiral galaxies—I. The dark matter connection," *Monthly Notices of the Royal Astronomical Society*, vol. 281, no. 1, pp. 27–47, 1996.

[95] M. O. C. Pires and J. C. C. De Souza, "Galactic cold dark matter as a Bose-Einstein condensate of WISPs," *Journal of Cosmology and Astroparticle Physics*, vol. 2012, no. 11, article 024, 2012.

[96] G. Helou, B. F. Madore, M. Schmitz, M. D. Bicay, X. Wu, and J. Bennett, "The NASA/IPAC extragalactic database," in *Databases & On-Line Data in Astronomy*, vol. 171 of *Astrophysics and Space Science Library*, pp. 89–106, Springer Netherlands, 1991.

[97] S. S. Mcgaugh, J. M. Schombert, G. D. Bothun, and W. J. G. De Blok, "The baryonic tully-fisher relation," *Astrophysical Journal*, vol. 533, no. 2, pp. L99–L102, 2000.

[98] S. S. McGaugh and J. Olf, "Local group dwarf spheroidals: correlated deviations from the Baryonic Tully-Fisher Relation," *Astrophysical Journal*, vol. 722, no. 1, pp. 248–261, 2010.

[99] R. D. Peccei and H. R. Quinn, "CP conservation in the presence of pseudoparticles," *Physical Review Letters*, vol. 38, no. 25, pp. 1440–1443, 1977.

[100] S. J. Asztalos, G. Caosi, C. Hagmann et al., "The Axion Dark Matter eXperiment," in *Proceedings of the 31st International Symposium on Physics in Collision*, Vancouver, Canada, August 2011.

[101] L. J. Rosenberg, "Dark-matter QCD-axion searches," *Proceedings of the National Academy of Sciences of the United States of America*, vol. 112, no. 40, pp. 12278–12281, 2015.

Hindawi
Advances in High Energy Physics
Volume 2017, Article ID 4383617, 7 pages
https://doi.org/10.1155/2017/4383617

Research Article

Particle Collision Near 1 + 1-Dimensional Horava-Lifshitz Black Hole and Naked Singularity

M. Halilsoy and A. Ovgun

Physics Department, Eastern Mediterranean University, Gazimagusa, Northern Cyprus, Mersin 10, Turkey

Correspondence should be addressed to A. Ovgun; ali.ovgun@emu.edu.tr

Received 5 October 2016; Revised 29 November 2016; Accepted 27 December 2016; Published 16 January 2017

Academic Editor: Tiberiu Harko

The unbounded center-of-mass (CM) energy of oppositely moving colliding particles near horizon emerges also in 1 + 1-dimensional Horava-Lifshitz gravity. This theory has imprints of renormalizable quantum gravity characteristics in accordance with the method of simple power counting. Surprisingly the result obtained is not valid for a 1-dimensional Compton-like process between an outgoing photon and an infalling massless/massive particle. It is possible to achieve unbounded CM energy due to collision between infalling photons and particles. The source of outgoing particles may be attributed to an explosive process just outside the horizon for a black hole and the naturally repulsive character for the case of a naked singularity. It is found that absence of angular momenta in 1 + 1-dimension does not yield unbounded energy for collisions in the vicinity of naked singularities.

1. Introduction

It is known that in spacetime dimensions less than four gravity has no life of its own unless supplemented by external sources. With that addition we can have lower dimensional gravity and we can talk of black holes, wormholes, geodesics, lensing effect, and so on in analogy with the higher dimensions. One effect that attracted much interest in recent times is the process of particle collisions near the horizon of black holes due to Bañados et al. [1] which came to be known as the BSW effect. This problem arose as a result of imitating the rather expensive venture of high energy particle collisions in laboratory. From curiosity the natural question arises: is there a natural laboratory (a particle accelerator) in our cosmos that we may extract information/energy in a cheaper way? This automatically drew attention to the strong gravity regions such as near horizon of black holes. Rotating black holes host greater energy reservoir due to their angular momenta and attention naturally focused therein first [2, 3]. In case the metric is static and diagonal, there are reasons to consider the collision process in the vicinity of a naked singularity as well.

We note from physical grounds that outgoing particles from the event horizon of a black hole cannot occur. Hawking radiation particles/photons emerge too weak to compare with infalling particles. Thus collision of two particles can only be argued if both are infalling toward the horizon of a black hole. Such a process, however, yields no BSW effect in the nonrotating metrics, which is our main interest in this study. In order to have an unbounded CM energy in a collision process both particles must be taken in the same coordinate frame and in opposite directions. This is possible in the vicinity of a naked singularity whose repulsive effect compels particles/photons to make collisions with an infalling particle/photon. From the outset we state that such a collision taking place near the naked singularity in the absence of angular momenta does not yield an unbounded CM energy. To extend our study to cover also collisions near black holes we assume that some unspecified process, such as disintegration decay process of some particles, yields outgoing particles photons while the partners fall into the hole. For a thorough analysis of all these problems covering the ergosphere region of a Kerr black hole, Penrose process, particle collisions, and so on one must consult [4].

In general one considers the radial geodesics and upon energy-momentum conservation in the center-of-mass (CM) frame the near horizon limit is checked whether the energy is bounded/unbounded. Our aim in this study is to consider black hole solutions in 1 + 1-dimensional Horava-Lifshitz

(HL) gravity [5] and check the BSW effect in such reduced dimensional theory. Let us remark that at the Planck scale in higher dimensions the spherical part $r^2 d\Omega^2_{D-2}$ of the line element is less effective compared to the time and radial components. For this reason 1+1-dimension becomes significant at the Planck scale. For a number of reasons HL gravity is promising as a candidate for a renormalizable quantum gravity physics which has been yearned for a long time [6]. The key idea in HL- gravity is the inhomogeneous scaling properties of time and space coordinates which violate the Lorentz invariance. Arnowitt-Deser-Misner (ADM) splitting of space and time [7] constitutes its geometrical background. BSW effect in lower/higher dimensions has been worked out by many authors [8–44]. Following the similar idea we consider black hole solutions and naked singularities in 1 + 1-dimension and search for the same effect in this lower dimension. It should be added that with 1 + 1-dimensional HL theory the simplest nontrivial solution is the solution describing an accelerated particle in the flat space of Rindler frame. This justifies also the meaning of the vector field (a_i) as the acceleration in the HL gravity. The role of Rindler acceleration in 3 + 1-dimension as a possible source of flat rotation curves and geodesics motion has been discussed recently [45]. It is our belief that the results in lower dimensions are informative for higher dimensions and as a toy model can play the role as precursors in this regard. Even a Compton-like process can be considered at the toy level between a massless photon outgoing from a naked singularity and a particle falling into the naked singularity. The diverging CM energy results in the case of photon-particle collision in 1 + 1-dimension under specific conditions.

Organization of the paper is as follows. In Section 2, we review in brief the 1 + 1-D HL theory with a large class of black hole and naked singularity solutions. CM energy of colliding particles near horizon and naked singularity is considered in Section 3. Section 4 proceeds with applications to particular examples. The case of particle-photon collision is studied separately in Section 5. The paper ends with our conclusion in Section 6.

2. 1 + 1-D HL Black Hole/Naked Singularity

HL formalism in 3 + 1-D makes use of the ADM splitting of time and space components as follows:

$$ds^2 = -N^2 dt^2 + g_{ij}\left(dx^i + N^i dt\right)\left(dx^j + N^j dt\right), \quad (1)$$

where $N(t)$ and N^i are the lapse and shift functions, respectively. The action of this theory is

$$S = \frac{M_{Pl}^2}{2}\int d^3x\, dt\, \sqrt{g}\left(K_{ij}K^{ij} + \lambda K^2 + V(\phi)\right), \quad (2)$$

where K_{ij} is the extrinsic curvature tensor with trace K and Planck mass M_{Pl}. $V(\phi)$ stands for the potential function of a scalar field ϕ, and λ is a constant ($\lambda > 1$). Reduction from 3 + 1-D to 1 + 1-D results in the action [5]:

$$S = \int dt\, dx\left(-\frac{1}{2}\eta N^2 a_1^2 + \alpha N^2 \phi'^2 - V(\phi)\right) \quad (3)$$

where η = constant and α = constant will be chosen to be unity and $a_1 = (\ln N)'$. Let us comment that a "prime" denotes d/dx. We note that also the first term in S is inherited from the geometric part of the action while the other two terms are from the scalar field source. For simplicity we have set also $M_{Pl} = 1$.

It has been shown in [5] that by variational principle a general class of solutions is obtained as follows:

$$N(x)^2 = 2C_2 + \frac{A}{\eta}x^2 - 2C_1 x + \frac{B}{\eta x} + \frac{C}{3\eta x^2} \quad (4)$$

in which C_2, A, C_1, B, and C are integration constants. Reference [5] must be consulted for the physical content of these constants.

The line element is

$$ds^2 = -N(x)^2 dt^2 + \frac{dx^2}{N(x)^2} \quad (5)$$

with the scalar field

$$\phi(x) = \ln\sqrt{2C_2 + \frac{A}{\eta}x^2 - 2C_1 x + \frac{B}{\eta x} + \frac{C}{3\eta x^2}}. \quad (6)$$

Note that the associated potential is

$$V(\phi(x)) = A + \frac{B}{x^3} + \frac{C}{x^4} \quad (7)$$

and the Ricci scalar is calculated as

$$R = -\frac{2}{\eta}\left(A + \frac{B}{x^3} + \frac{C}{x^4}\right). \quad (8)$$

There is naked singularity when $A = C_1 = 0$ and $C_2 = B = C = \eta = 1$, so that there is no horizon for

$$N(x)^2 = 2 + \frac{1}{x} + \frac{1}{3x^2}. \quad (9)$$

Another black hole solution reported by Bazeia et al. [5] is found by taking $C_1 \neq 0, C_2 \neq 0, B \neq 0$, and $A = C = 0$.

$$N(x)^2 = 2C_2 - 2C_1 x + \frac{B}{\eta x}. \quad (10)$$

This solution develops the following horizons:

$$x_h^{\pm} = \frac{C_2}{2C_1} \pm \sqrt{\Delta}, \quad \Delta = \frac{C_2^2}{4C_1^2} + \frac{B}{2\eta C_1}. \quad (11)$$

As $\Delta = 0$ they degenerate; that is, $x_h^+ = x_h^-$.

The Hawking temperature is given in terms of the outer (x_h^+) horizon as follows:

$$T_H = \left.\frac{\left(N(x)^2\right)'}{4\pi}\right|_{x=x_h^+}. \quad (12)$$

For the special case $C_2 = 0$, $C_1 = -M$, and $B = -2M$ the horizons are independent of the mass M:

$$x_h^{\pm} = \pm\frac{1}{\sqrt{\eta}} \quad (\eta > 0). \tag{13}$$

The temperature is then given simply by

$$T_H = \frac{M}{\pi}. \tag{14}$$

This is a typical relation between the Hawking temperature and the mass of black holes in 1 + 1-dimension [46].

In the case of $C_2 = 1/2$, $B = -2M$, $\eta = 1$, and $A = C = C_1 = 0$ it gives a Schwarzschild-like solution;

$$N(x)^2 = 1 - \frac{2M}{x}. \tag{15}$$

On the other hand, the choice of the parameters, for $C_2 = 1/2$, $B = -2M$, $C = 3Q^2$, $\eta = 1$, and $A = C_1 = 0$, gives a Reissner–Nordstrom-like solution.

$$N(x)^2 = 1 - \frac{2M}{x} + \frac{Q^2}{x^2}. \tag{16}$$

As in the general relativity we can make particular choice of the parameters so that we end up with a naked singularity instead of a black hole. The choice $Q^2 > M^2$ in (16), for instance, transforms the HL- black hole into a naked singularity at $x = 0$. Similarly $M < 0$ turns (15) into a naked singular metric at $x = 0$.

3. CM Energy of Particle Collision near the Horizon of the 1 + 1-D HL Black Hole

Here we will derive the equations of motion of an˜uncharged massive test particle by using the method of geodesic Lagrangian. Such equations can be derived from the Lagrangian equation,

$$\mathscr{L} = \frac{1}{2}\left[-N(x)^2\left(\frac{dt}{d\tau}\right)^2 + \frac{1}{N(x)^2}\left(\frac{dx}{d\tau}\right)^2\right], \tag{17}$$

in which τ is the proper time for time-like geodesics (or massive particles). The canonical momenta are

$$p_t = \frac{d\mathscr{L}}{d\dot{t}} = -N(x)^2\,\dot{t}, \tag{18}$$

$$p_x = \frac{d\mathscr{L}}{d\dot{x}} = \frac{\dot{x}}{N(x)^2} \tag{19}$$

The 1 + 1-D HL black hole has only one killing vector ∂_t. The associated conserved quantity will be labeled by E. From (18), E is related to $N(x)^2$ as

$$-N(x)^2\,\dot{t} = -E. \tag{20}$$

Hence,

$$\dot{t} = \frac{E}{N(x)^2}. \tag{21}$$

The two velocities of the particles are given by $u^\mu = dx^\mu/d\tau$. We have already obtained u^t in the above derivation. To find $u^x = \dot{x}$, the normalization condition for time-like particles, $u^\mu u_\mu = -1$ [1, 47], can be used as

$$g_{tt}\left(u^t\right)^2 + g_{xx}\left(u^x\right)^2 = -1. \tag{22}$$

By substituting u^t to (22), one obtains u^x as

$$\left(u^x\right)^2 = E^2 - N(x)^2 \tag{23}$$

for which an effective potential V_{eff} can be defined by

$$\left(u^x\right)^2 + V_{\text{eff}} = E^2. \tag{24}$$

Now, the two velocities can be written as

$$u^t = \dot{t} = \frac{E}{N(x)^2}, \qquad u^x = \dot{x} = \sqrt{E^2 - N(x)^2}. \tag{25}$$

We proceed now to present the CM energy of two particles with two velocities u_1^μ and u_2^μ. We will assume that both have rest mass $m_0 = 1$. The CM energy is given by

$$E_{\text{cm}} = \sqrt{2}\sqrt{\left(1 - g_{\mu\nu}u_1^\mu u_2^\nu\right)}. \tag{26}$$

So

$$\frac{E_{\text{cm}}^2}{2} = 1 + \frac{E_1E_2}{N(x)^2} - \frac{\kappa\sqrt{E_1^2 - N(x)^2}\sqrt{E_2^2 - N(x)^2}}{N(x)^2}, \tag{27}$$

where $\kappa = \pm 1$ corresponds to particles moving in the same/opposite direction with respect to each other. We wish to stress that our concern is for the case $\kappa = \pm 1$ since no physical particle is ejected from the black hole. Note that E_1 and E_2 are the energy constants corresponding to each particle. In case the second term under the square root is too small than the first one,

$$\sqrt{E^2 - N(x)^2} \approx \left(E - \frac{N(x)^2}{2E^2} + \cdots\right) \tag{28}$$

so that the higher order terms can be neglected and CM energy of two particles can be written as [23]

$$\frac{E_{\text{cm}}^2}{2} \approx 1 + (1-\kappa)\frac{E_1E_2}{N(x)^2} + \frac{\kappa}{2}\left(\frac{E_2}{E_1} + \frac{E_1}{E_2}\right). \tag{29}$$

The case with $\kappa = +1$ is obvious, in which the CM energy becomes

$$\frac{E_{\text{cm}}^2}{2} \approx 1 + \frac{\left(E_2^2 + E_1^2\right)}{2E_1E_2}, \tag{30}$$

where the CM energy is independent of metric function, and it gives always a finite energy. On the other hand $\kappa = -1$ gives

$$\frac{E_{\text{cm}}^2}{2} \approx 1 + \frac{2E_1E_2}{N(x)^2} - \frac{\left(E_2^2 + E_1^2\right)}{2E_1E_2} \tag{31}$$

in which it gives unbounded CM energy near the horizon of the HL black holes provided an outgoing particle mechanism from the horizon is established. Otherwise the yield of two ingoing particles collision remains finite.

4. Some Examples

4.1. Schwarzschild-Like Solution. In the case of $C_2 = 1/2$, $B = -2M$, $\eta = 1$, and $A = C = C_1 = 0$ it gives Schwarzschild-like solution, where

$$V(\phi(x)) = -\frac{2M}{x^3}, \qquad N(x)^2 = 1 - \frac{2M}{x}. \tag{32}$$

For the CM energy on the horizon, we have to compute the limiting value of (27) as $x \to x_h = 2M$, where the horizon of the black hole is. Setting $\kappa = -1$ as it is, the CM energy near the event horizon for 1 + 1 D Schwarzschild BH is

$$E^2_{\mathrm{cm}}(x \longrightarrow x_h) = \infty. \tag{33}$$

This result for 4-D Schwarzschild Black hole is already calculated by Baushev [24]. Hence, the condition of $\kappa = -1$, when the location of particle 1 approaches the horizon and on the other hand the particle 2 runs outward from the horizon due to some unspecified physical process, yet yields $E^2_{\mathrm{cm}} \to \infty$ so there is BSW effect for 1 + 1 Schwarzschild-like solution when the condition $\kappa = -1$ is satisfied.

4.2. Reissner-Nordstrom-Like Solution. On the other hand, the choice of the parameters, for $C_2 = 1/2$, $B = -2M$, $C = 3Q^2$, $\eta = 1$, and $A = C_1 = 0$ gives the Reissner–Nordstrom-like solution.

$$N(x)^2 = 1 - \frac{2M}{x} + \frac{Q^2}{x^2}, \tag{34}$$

$$V(\phi(x)) = -\frac{2M}{x^3} + \frac{3Q^2}{x^4} \tag{35}$$

So the CM energy is calculated by using the limiting value of (31)

$$E^2_{\mathrm{cm}}\left(x \longrightarrow x_{h=M+\sqrt{(M^2-Q^2)}}\right) = \infty. \tag{36}$$

So there is a BSW effect.

4.3. The Extremal Case of the Reissner-Nordstrom-Like Black Hole. For the extremal case we have with $M = Q$, from (34),

$$N(x)^2 = \left(1 - \frac{M}{x}\right)^2 \tag{37}$$

so that it also gives the same answer from (31) as

$$E^2_{\mathrm{cm}}(x \longrightarrow x_h) = \infty. \tag{38}$$

4.4. Specific New Black Hole Case. The new 3-parameter black hole solution given by Bazeia et al. [5] is chosen as

$$N(x)^2 = 2C_2 - 2C_1 x + \frac{B}{\eta x} \tag{39}$$

with the potential

$$V(\phi(x)) = \frac{B}{x^3}. \tag{40}$$

For the special case $C_2 = 0$, $C_1 = -M$, and $B = -2M$ we have

$$N(x)^2 = 2Mx - \frac{2M}{\eta x} \tag{41}$$

with suitable potential which is

$$V(\phi(x)) = -\frac{2M}{x^3}. \tag{42}$$

The CM energy of two colliding particles is calculated by taking the limiting values of (31)

$$E^2_{\mathrm{cm}}(x \longrightarrow x_h) = \infty. \tag{43}$$

Hence the BSW effect arises here as well.

4.5. Near Horizon Coordinates. We have explored the region near the horizon by replacing r by a coordinate ρ. The proper distance from the horizon ρ [48] is given as follows:

$$\rho = \int \sqrt{g_{xx}(x')}\, dx' = \int_{x_h}^{x} \frac{1}{N(x')}\, dx'. \tag{44}$$

The first example is the Schwarzschild-like solution which is

$$N(x)^2 = 1 - \frac{2M}{x} \tag{45}$$

so that proper distance is calculated as

$$\rho = \int_{x_h}^{x} \left(1 - \frac{2M}{x}\right)^{-1/2} dx' = \sqrt{x(x-2M)} + 2MG \sinh^{-1}\left(\sqrt{\frac{x}{2M} - 1}\right). \tag{46}$$

The new metric is

$$ds^2 = -\left(1 - \frac{2M}{x(\widetilde{\rho})}\right) dt^2 + d\widetilde{\rho}^2, \tag{47}$$

where $\widetilde{\rho} \simeq 2\sqrt{2M(x-2M)}$ so that it gives approximately

$$ds^2 \simeq -\frac{\rho^2}{(4M)^2} dt^2 + d\rho^2 \tag{48}$$

which is once more the Rindler-type line element. Let us note that this Rindler-type line element is valid within the near horizon limit approximation. For practical purposes there are advantages in adapting such an approximation which conforms with the equivalence principle [48]. The CM energy of two colliding particles is given by

$$\frac{E^2_{\mathrm{cm}}}{2m_0^2} = 1 + \frac{(4M)^2\left(E_1E_2 - \kappa\sqrt{E_1^2 - \rho^4/(4M)^4}\sqrt{E_2^2 - \rho^4/(4M)^4}\right)}{\rho^2} \tag{49}$$

so that there is BSW effect for $\kappa = -1$ when $\rho \to 0$.

5. Particle Collision near the Naked Singularity

There is a naked singularity for our 1 + 1-D HL model at the location of $x = 0$, with $Q^2 > M^2$ in (16). In addition $M < 0$ turns (15) into a naked singular metric at $x = 0$. There is also naked singularity when we choose metric function as follows:

$$N(x)^2 = 2 + \frac{1}{x} + \frac{1}{3x^2} = \frac{6x^2 + 3x + 1}{3x^2}. \tag{50}$$

As it is given in (27), CM energy of the collision of two particles generally is (for $N(x) \to \infty$).

$$\frac{E_{\text{cm}}^2}{2} \approx 1 - \kappa + \frac{1}{2N(x)^2}\left[2E_1E_2 + \kappa\left(E_1^2 + E_2^2\right)\right]. \tag{51}$$

For the case $\kappa = \pm 1$, when x goes to zero, the CM energy remains finite for radially moving particles.

$$\left.\frac{E_{\text{c.m.}}^2}{2}\right|_{x=0} \longrightarrow 1 - \kappa. \tag{52}$$

This suggests that although one of the particle is boosted by the naked singularity, there is not any unlimited collisional energy near such singularity. Note that Compton-like processes were considered first in [4], where rotational effect of Kerr black hole played a significant role. Our case here is entirely free of rotational effects.

6. Photon versus an Infalling Particle

A massless photon can naturally scatter an infalling particle or vice versa. This phenomenon is analogous to a Compton scattering taking place in 1 + 1-dimension. Null-geodesics for a photon can be described simply by

$$\begin{aligned} \frac{dt}{d\lambda} &= \frac{E_1}{N^2} \\ \frac{dx}{d\lambda} &= \pm\sqrt{E_1^2 - N^2}, \end{aligned} \tag{53}$$

where λ is an affine parameter and E_1 stands for the photon energy. Defining $E_1 = \hbar\omega_0$, where ω_0 is the frequency (with the choice $\hbar = 1$) we can parametrize energy of the photon by ω_0 alone. The CM energy of a photon and the infalling particle can be taken now as

$$E_{\text{cm}}^2 = -\left(p^\mu + k^\mu\right)^2 \tag{54}$$

in which $p^\mu = mu^\mu$ and k^μ refer to the particle and photon, 2 momenta, respectively. This amounts to

$$E_{\text{cm}}^2 = m^2 - 2mg_{\mu\nu}u^\mu k^\nu, \tag{55}$$

where we have for the particle

$$p^\mu = m\left(\frac{E_2}{N^2}, \sqrt{E_2^2 - N^2}\right) \tag{56}$$

and for the photon

$$k^\mu = \left(\frac{E_1}{N^2}, -E_1\right). \tag{57}$$

One obtains

$$E_{\text{cm}}^2 = m^2 + \frac{2mE_1}{N^2}\left(E_2 + \kappa\sqrt{E_2^2 - N^2}\right). \tag{58}$$

In the near horizon limit this reduces to

$$E_{\text{cm}}^2 = m^2 + \frac{2mE_1}{N^2}\left(E_2 + \kappa E_2 - \frac{N^2}{2E_2}\right). \tag{59}$$

Note that for $\kappa = -1$ we have E_{cm}^2 given by

$$E_{\text{cm}}^2 = m^2\left(1 - \frac{E_1}{mE_2}\right) \tag{60}$$

which is finite between the collision of a photon and an infalling particle and therefore is not of interest. As a matter of fact the occurrence of outgoing photon from the event horizon cannot be justified unless an explosive/decay process is assumed to take place. As a result for $\kappa = +1$ from (59) we obtain an unbounded E_{cm}^2 between the collision of infalling photon and particle. Let us add that "inverse" Compton process in the ergosphere of Kerr black hole was considered in [4] where the photon's energy showed increment due to rotational and curvature effects. The energy, however, attained an upper bound which was finite. Our result obtained here being entirely radial on the other hand can hardly be compared with those of [4].

7. Conclusion

Our aim was to investigate whether the BSW type effect which arises in higher dimensional black holes applies also to the 1 + 1-D naked singularity/black hole. The theory we adapted is not general relativity but instead the recently popular HL gravity. We employed the class of 5-parameter black hole/naked singularity solutions found recently [5]. The class has particular limits of flat Rindler, Schwarzschild, and Reissner-Nordstrom-like solutions. For each case we have calculated the center-of-mass (CM) energy of the particles and shown that the energy can grow unbounded for some cases. In other words the strong gravity near the event horizon affects the collision process with unlimited source to turn it into a natural accelerator. The model we use applies also to the case of a photon/particle collision with different characteristics. It is observed that the CM energy of the infalling particles from the rest at infinity will remain finite in the CM frame at the event horizon of a black hole. Contrariwise, unlimited CM energy will be attained between the collision of the outgoing particles from the event horizon region and infalling particles. It is also possible to achieve the infinite energy between an infalling photon and an infalling massive particle. However, we found finite CM energy between an outgoing photon and infalling particle. Finally, we must admit that absence of rotational effects in 1 + 1-D restricts the problem to the level of a toy model in which particles move on pure radial geodesics yielding finite CM energy in the vicinity of a naked singularity.

Disclosure

This work was presented as a poster at Karl Schwarzschild Meeting 20–24 July 2015 Frankfurt Institute for Advanced Studies.

Competing Interests

The authors declare that they have no competing interests.

References

[1] M. Bañados, J. Silk, and S. M. West, "Kerr black holes as particle accelerators to arbitrarily high energy," *Physical Review Letters*, vol. 103, no. 11, Article ID 111102, 2009.

[2] T. Jacobson and J. P. Sotiriou, "Spinning black holes as particle accelerators," *Physical Review Letters*, vol. 104, no. 2, Article ID 021101, 3 pages, 2010.

[3] K. Lake, "Particle accelerators inside spinning black holes," *Physical Review Letters*, vol. 104, Article ID 211102, 2010.

[4] T. Piran and J. Shaham, "Upper bounds on collisional penrose processes near rotating black-hole horizons," *Physical Review D*, vol. 16, no. 6, pp. 1615–1635, 1977.

[5] D. Bazeia, F. A. Brito, and F. G. Costa, "Two-dimensional Horava-Lifshitz black hole solutions," *Physical Review D. Particles, Fields, Gravitation, and Cosmology*, vol. 91, no. 4, Article ID 044026, 2015.

[6] P. Horava, "Quantum gravity at a Lifshitz point," *Physical Review D*, vol. 79, no. 8, Article ID 084008, 2009.

[7] R. Arnowitt, S. Deser, and C. W. Misner, "Republication of: the dynamics of general relativity," *General Relativity and Gravitation*, vol. 40, no. 9, pp. 1997–2027, 2008.

[8] E. Berti, V. Cardoso, L. Gualtieri, F. Pretorius, and U. Sperhake, "Comment on "kerr black holes as particle accelerators to arbitrarily high energy"," *Physical Review Letters*, vol. 103, no. 23, Article ID 239001, 2009.

[9] M. Bañados, B. Hassanain, J. Silk, and S. M. West, "Emergent flux from particle collisions near a Kerr black hole," *Physical Review D*, vol. 83, no. 2, Article ID 023004, 2011.

[10] T. Jacobson and T. P. Sotiriou, "Spinning black holes as particle accelerators," *Physical Review Letters*, vol. 104, no. 2, Article ID 021101, 2010.

[11] O. B. Zaslavskii, "Acceleration of particles by nonrotating charged black holes," *JETP Letters*, vol. 92, no. 9, pp. 571–574, 2011.

[12] S. W. Wei, Y. X. Liu, H. T. Li, and F. W. Chen, "Particle collisions on stringy black hole background," *Journal of High Energy Physics*, vol. 2010, no. 12, article 066, 2010.

[13] O. B. Zaslavskii, "Energy extraction from extremal charged black holes due to the Banados-Silk-West effect," *Physical Review D*, vol. 86, Article ID 124039, 2012.

[14] H. Saadat, "The centre-of-mass energy of two colliding particles in STU black holes," *Canadian Journal of Physics*, vol. 92, no. 12, pp. 1562–1564, 2014.

[15] N. Tsukamoto and C. Bambi, "High energy collision of two particles in wormhole spacetimes," *Physical Review D. Particles, Fields, Gravitation, and Cosmology*, vol. 91, no. 8, Article ID 084013, 2015.

[16] S. G. Ghosh, P. Sheoran, and M. Amir, "Rotating Ayón-Beato-García black hole as a particle accelerator," *Physical Review D*, vol. 90, no. 10, Article ID 103006, 2014.

[17] A. Galajinsky, "Particle collisions on near horizon extremal Kerr background," *Physical Review D*, vol. 88, no. 2, Article ID 027505, 2013.

[18] V. P. Frolov, "Weakly magnetized black holes as particle accelerators," *Physical Review D*, vol. 85, no. 2, Article ID 024020, 2012.

[19] A. M. Al Zahrani, V. P. Frolov, and A. A. Shoom, "Critical escape velocity for a charged particle moving around a weakly magnetized Schwarzschild black hole," *Physical Review D*, vol. 87, no. 8, Article ID 084043, 2013.

[20] J. Sadeghi and B. Pourhassan, "Particle acceleration in Horava-Lifshitz black holes," *The European Physical Journal C*, vol. 72, no. 4, article 1984, 2012.

[21] J. Sadeghi, B. Pourhassan, and H. Farahani, "Rotating charged hairy black hole in (2+1) dimensions and particle acceleration," *Communications in Theoretical Physics*, vol. 62, no. 3, pp. 358–362, 2014.

[22] C. Liu, S. Chen, C. Ding, and J. Jing, "Particle acceleration on the background of the Kerr–Taub–NUT spacetime," *Physics Letters. B*, vol. 701, no. 3, pp. 285–290, 2011.

[23] M. Patil and P. S. Joshi, "Ultrahigh energy particle collisions in a regular spacetime without black holes or naked singularities," *Physical Review D*, vol. 86, no. 4, Article ID 044040, 2012.

[24] A. N. Baushev, "Dark matter annihilation in the gravitational field of a black hole," *International Journal of Modern Physics D*, vol. 18, no. 8, pp. 1195–1203, 2009.

[25] M. Patil and P. S. Joshi, "Particle acceleration by Majumdar–Papapetrou di-hole," *General Relativity and Gravitation*, vol. 46, no. 10, 2014.

[26] J. D. Schnittman, "Revised upper limit to energy extraction from a kerr black hole," *Physical Review Letters*, vol. 113, no. 26, Article ID 261102, 2014.

[27] M. Patil and P. S. Joshi, "Naked singularities as particle accelerators," *Physical Review D*, vol. 82, no. 10, Article ID 104049, 2010.

[28] M. Patil, P. S. Joshi, and D. Malafarina, "Naked singularities as particle accelerators. II," *Physical Review D*, vol. 83, no. 6, Article ID 064007, 2011.

[29] A. Grib and Y. Pavlov, "On particle collisions in the gravitational field of the Kerr black hole," *Astroparticle Physics*, vol. 34, no. 7, pp. 581–586, 2011.

[30] M. Sharif and N. Haider, "Study of center of mass energy by particles collision in some black holes," *Astrophysics and Space Science*, vol. 346, no. 1, pp. 111–117, 2013.

[31] I. Hussain, M. Jamil, and B. Majeed, "A slowly rotating black hole in horava-lifshitz gravity and a 3+1 dimensional topological black hole: motion of particles and BSW mechanism," *International Journal of Theoretical Physics*, vol. 54, no. 5, pp. 1567–1577, 2015.

[32] S. Hussain, I. Hussain, and M. Jamil, "Dynamics of a charged particle around a slowly rotating Kerr black hole immersed in magnetic field," *The European Physical Journal C*, vol. 74, no. 12, 2014.

[33] M. Amir and S. G. Ghosh, "Rotating Hayward's regular black hole as particle accelerator," *Journal of High Energy Physics*, vol. 2015, no. 7, article 015, 2015.

[34] B. Pourhassan and U. Debnath, "Particle acceleration in rotating modified hayward and bardeen black holes," https://arxiv.org/abs/1506.03443.

[35] A. A. Grib and Y. V. Pavlov, "Are black holes totally black?" *Gravitation and Cosmology*, vol. 21, no. 1, pp. 13–18, 2015.

[36] A. A. Grib and Y. V. Pavlov, "High energy physics in the vicinity of rotating black holes," *Theoretical and Mathematical Physics*, vol. 185, no. 1, pp. 1425–1432, 2015.

[37] C. Ding, C. Liu, and Q. Quo, "Spacetime noncommutative effect on black hole as particle accelerators," *International Journal of Modern Physics D*, vol. 22, no. 04, Article ID 1350013, 2013.

[38] J. Yang, Y.-L. Li, Y. Li, S.-W. Wei, and Y.-X. Liu, "Particle collisions in the lower dimensional rotating black hole spacetime with the cosmological constant," *Advances in High Energy Physics*, vol. 2014, Article ID 204016, 7 pages, 2014.

[39] H. Nemoto, U. Miyamoto, T. Harada, and T. Kokubu, "Escape of superheavy and highly energetic particles produced by particle collisions near maximally charged black holes," *Physical Review D*, vol. 87, no. 12, Article ID 127502, 2013.

[40] C. Zhong and S. Gao, "Particle collisions near the cosmological horizon of a Reissner-Nordström-de Sitter black hole," *JETP Letters*, vol. 94, no. 8, pp. 589–592, 2011.

[41] C. Liu, S. Chen, and J. Jing, "Collision of two general geodesic particles around a kerr—newman black hole," *Chinese Physics Letters*, vol. 30, no. 10, Article ID 100401, 2013.

[42] Y. Zhu, S. Wu, Y. Liu, and Y. Jiang, "General stationary charged black holes as charged particle accelerators," *Physical Review D*, vol. 84, no. 4, Article ID 043006, 2011.

[43] U. Miyamoto, H. Nemoto, and M. Shimano, "Particle creation by naked singularities in higher dimensions," *Physical Review D*, vol. 83, no. 8, Article ID 084054, 2011.

[44] Y. Li, J. Yang, Y.-L. Li, S.-W. Wei, and Y.-X. Liu, "Particle acceleration in Kerr-(anti-)de Sitter black hole backgrounds," *Classical and Quantum Gravity*, vol. 28, no. 22, Article ID 225006, 2011.

[45] M. Halilsoy, O. Gurtug, and S. H. Mazharimousavi, "Rindler modified Schwarzschild geodesics," *General Relativity and Gravitation*, vol. 45, no. 11, pp. 2363–2381, 2013.

[46] S. W. Hawking, "Black holes and thermodynamics," *Physical Review D*, vol. 13, no. 2, pp. 191–197, 1976.

[47] C. W. Misner, K. S. Thorne, and J. A. Wheeler, *Gravitation*, W.H. Freeman & Co., San Francisco, Calif, USA, 1972.

[48] L. Susskind and J. Lindesay, *An Introduction to Black Holes, Information and the String Theory Revolution: The Holographic Universe*, World Scientific, Hackensack, NJ, USA, 2005.

Hindawi Publishing Corporation
Advances in High Energy Physics
Volume 2016, Article ID 7380372, 17 pages
http://dx.doi.org/10.1155/2016/7380372

Research Article

Interacting Dark Matter and q-Deformed Dark Energy Nonminimally Coupled to Gravity

Emre Dil

Department of Physics, Sinop University, Korucuk, 57000 Sinop, Turkey

Correspondence should be addressed to Emre Dil; emredil@sakarya.edu.tr

Received 5 October 2016; Revised 10 November 2016; Accepted 17 November 2016

Academic Editor: Sergei D. Odintsov

In this paper, we propose a new approach to study the dark sector of the universe by considering the dark energy as an emerging q-deformed bosonic scalar field which is not only interacting with the dark matter, but also nonminimally coupled to gravity, in the framework of standard Einsteinian gravity. In order to analyze the dynamic of the system, we first give the quantum field theoretical description of the q-deformed scalar field dark energy and then construct the action and the dynamical structure of this interacting and nonminimally coupled dark sector. As a second issue, we perform the phase-space analysis of the model to check the reliability of our proposal by searching the stable attractor solutions implying the late-time accelerating expansion phase of the universe.

1. Introduction

The dark energy is accepted as the effect of causing the late-time accelerated expansion of universe which is experienced by the astrophysical observations such as Supernova Ia [1, 2], large-scale structure [3, 4], the baryon acoustic oscillations [5], and cosmic microwave background radiation [6–9]. According to the standard model of cosmological data 70% of the content of the universe consists of dark energy. Moreover, the remaining 25% of the content is an unknown form of matter having a mass but in nonbaryonic form that is called dark matter and the other 5% of the energy content of the universe belongs to ordinary baryonic matter [10]. While the dark energy spread all over the intergalactic media of the universe and produces a gravitational repulsion by its negative pressure to drive the accelerating expansion of the universe, the dark matter is distributed over the inner galactic media inhomogeneously and it contributes to the total gravitational attraction of the galactic structure and fixes the estimated motion of galaxies and galactic rotation curves [11, 12].

Miscellaneous dark models have been proposed to explain a better mechanism for the accelerated expansion of the universe. These models include interactions between dark energy, dark matter, and the gravitational field. The coupling between dark energy and dark matter seems possible due to the equivalence of order of the magnitudes in the present time [13–22]. On the other hand, there are also models in which the dark energy nonminimally couples to gravity in order to provide quantum corrections and renormalizability of the scalar field in the curved spacetime. Also the crossing of the dark energy from the quintessence phase to phantom phase, known as the Quintom scenario, can be possible in the models where the dark energy interacts with the gravity. If the dark energy minimally couples to gravity, the equation of state parameter of the dark energy cannot cross the cosmological constant boundary $\omega = 1$ in the Friedmann-Robertson-Walker (FRW) geometry; therefore it is possible to emerge the Quintom scenario in the model where the dark energy nonminimally couples to gravity [23–37].

The constitution of the dark energy can be alternatively the cosmological constant Λ with a constant energy density filling the space homogeneously [38–41]. As the varying energy density dark energy models, instead of the cosmological constant, quintessence, phantom, and tachyon fields can be considered. However, all these different dark energy models are the same in terms of the nondeformed field constituting the dark energy. There is no reason to prevent us from assuming that the dark energy is a deformed scalar field, having a negative pressure, too, as expected from the dark energy. Therefore, we propose that the dark energy considered in

this study is formed of the deformed scalar field whose field equations are defined by the deformed oscillator algebras.

The quantum algebra and quantum group structure were firstly introduced by Kulish et al. [42–44], during the investigations of integrable systems in quantum field theory and statistical mechanics. Quantum groups and deformed boson algebras are closely related terms. It is known that the deformation of the standard boson algebra is first proposed by Arik-Coon [45]. Later on, Macfarlane and Biedenharn have realized the deformation of boson algebra in a different manner from Arik-Coon [46, 47]. The relation between quantum groups and the deformed oscillator algebras can be constructed obviously with this study by expressing the deformed boson operators in terms of the $su_q(2)$ Lie algebra operators. Therefore, the construction of the relation between quantum groups and deformed algebras leads the deformed algebras of great interest with many different applications. The deformed version of Bardeen-Cooper-Schrieffer (BCS) many-body formalism in nuclear force, deformed creation, and annihilation operators are used to study the quantum occupation probabilities [48]. As another study, in Nambu-Jona-Lasinio (NJL) model, the deformed fermion operators are used instead of standard fermion operators and this leads to an increase in the NJL four-fermion coupling force and the quark condensation related to the dynamical mass [49]. The statistical mechanical studies of the deformed boson and fermion systems have been familiar in recent years [50–60]. Moreover, the investigations on the internal structure of composite particles involve the deformed fermions or bosons as the building block of the composite structures [61, 62]. There are also applications of the deformed particles in black hole physics [63–66]. The range of the deformed boson and fermion applications diverses from atomic-molecular physics to solid state physics in a widespread manner [67–72].

The ideas on considering the dark energy as the deformed scalar field have become common in the literature [73–76]. In this study, we then take into account the deformed bosons as the scalar field dark energy interacting with the dark matter and also nonminimally coupled to gravity. In order to confirm our proposal that the dark energy can be considered as a deformed scalar field, we firstly introduce the dynamics of the interacting and nonminimally coupled dark energy, dark matter, and gravity model in a spatially flat FRW background and then perform the phase-space analysis to check whether it will provide the late-time stable attractor solutions implying the accelerated expansion phase of the universe.

2. Dynamics of the Model

The field equations of the scalar field dark energy are considered to be defined by the q-deformed boson fields in our model. Constructing a q-deformed quantum field theory after the idea of q-deformation of the single particle quantum mechanics [45–47] has naturally been nonsurprising [77–79]. The bosonic part of the deformed particle fields corresponds to the deformed scalar field and the fermionic counterpart corresponds to the deformed vector field. In this study, we consider the q-deformed bosonic scalar field as the q-deformed dark energy under consideration. In our model, the q-deformed dark energy interacts with the dark matter and also nonminimally couples to gravity.

Early Universe scenarios can be well understood by studying the quantum field theory in curved spacetime. The behavior of the classical scalar field near the initial singularity can be translated to the quantum field regime by constructing the coherent states in quantum mechanics for any mode of the scalar field. It is now impossible to determine the quantum state of the scalar field near the initial singularity by an observer, at the present universe. In order to overcome the undeterministic nature, Hawking proposes to take the random superposition of all possible states in that spacetime. It has been realized by Berger with taking random superposition of coherent states. Also the particle creation in an expanding universe with a nonquantized gravitational metric has been investigated by Parker. It has been stated by Goodison and Toms that if the field quanta obey the Bose or Fermi statistics, when considering the evolution of the scalar field in an expanding universe, then the particle creation does not occur in the vacuum state. Their result gives signification to the possibility of the existence of the deformed statistics in coherent or squeezed states in the Early Universe [79–84].

Motivated by this significant possibility, we propose that the dark energy consists of a q-deformed scalar field whose particles obey the q-deformed algebras. Therefore, we now define the q-deformed scalar field constructing the dark energy in our model. The field operator of the q-deformed scalar field dark energy can be given as [79]

$$\phi_q(x) = \int \frac{d^3k}{(2\pi)^{3/2}} \frac{1}{(2w_k)^{1/2}} \left[a_q(k)\, e^{ikx} + a_q^*(k)\, e^{-ikx}\right]. \quad (1)$$

The following commutation relations for the deformed annihilation operator $a_q(k)$ and creations operator $a_q^*(k)$ in q-bosonic Fock space are given by [45]

$$\begin{aligned} a_q(k)\, a_q^*\left(k'\right) - q^2 a_q^*\left(k'\right) a_q(k) &= \delta\left(k - k'\right), \\ a_q(k)\, a_q\left(k'\right) - q^2 a_q\left(k'\right) a_q(k) &= 0, \end{aligned} \quad (2)$$

where q is a real deformation parameter in interval $0 < q < \infty$ and $[\widehat{N}(k)] = a_q^*(k)a_q(k)$ is the deformed number operator of kth mode whose eigenvalue spectrum is given as

$$[N(k)] = \frac{1 - q^{2N(k)}}{1 - q^2}. \quad (3)$$

Here $\widehat{N}(k) = a_s^*(k)a_s(k)$ is the standard nondeformed number operator. By using (2) in (1), we can obtain the commutation relations and planewave expansion of the q-deformed scalar field $\phi_q(x)$, as follows:

$$\phi_q(x)\, \phi_q^*\left(x'\right) - q^2 \phi_q^*\left(x'\right) \phi_q(x) = i\Delta\left(x - x'\right), \quad (4)$$

where

$$\Delta\left(x - x'\right) = \frac{-1}{(2\pi)^3} \int \frac{d^3k}{w_k} \sin w_k \left(x - x_0\right). \quad (5)$$

The metric of the spatially flat FRW spacetime in which the q-oscillator algebra represents the q-deformed scalar field dark energy is defined by

$$ds^2 = -dt^2 + a^2(t)\left[dr^2 + r^2 d\theta^2 + r^2 \sin^2\theta d\phi^2\right], \quad (6)$$

and for a FRW metric

$$w_k^2 = g\left(\sum_i \frac{k_i^2}{a^2} + m\right), \quad (7)$$

where $g = \det g_{\mu\nu}$. Also the relation between deformed and standard annihilation operators a_q and a_s [85] is given as

$$a_q = a_s \sqrt{\frac{\left[\widehat{N}\right]}{\widehat{N}}}, \quad (8)$$

which is used to obtain the relation between deformed and standard bosonic scalar fields by using (3) in (8) and (1):

$$\phi_q = \phi \sqrt{\frac{1 - q^{2\widehat{N}}}{(1-q^2)\,\widehat{N}}}. \quad (9)$$

Here we have used the Hermiticity of the number operator $\widehat{N}$.

Now the Friedmann equations will be derived for our interacting dark matter and nonminimally coupled q-deformed dark energy model in a FRW spacetime by using the scale factor $a(t)$ in Einstein's equations. In order to obtain these equations, we relate the scale factor to the energy-momentum tensor of the objects in the model under consideration. We use the fluid description of the objects in our model by considering energy and matter as a perfect fluid, which are dark energy and matter in our model. An isotropic fluid in one coordinate frame leads to an isotropic metric in another frame coinciding with the frame of the fluid. This means that the fluid is at rest in commoving coordinates. Then the four velocities of the fluid are given as [52]

$$U^\mu = (1, 0, 0, 0), \quad (10)$$

and the energy-momentum tensor follows as

$$T_{\mu\nu} = (\rho + p) U_\mu U_\nu + p g_{\mu\nu} = \begin{pmatrix} \rho & 0 & 0 & 0 \\ 0 & & & \\ 0 & & g_{ij} p & \\ 0 & & & \end{pmatrix}. \quad (11)$$

A more suitable form can be obtained by raising one, such that

$$T^\mu_\nu = \mathrm{diag}(-\rho, p, p, p). \quad (12)$$

Since we have two constituents, q-deformed dark energy and the dark matter in our model, the total energy density and the pressure are given by

$$\begin{aligned} \rho_{\mathrm{tot}} &= \rho_q + \rho_m, \\ p_{\mathrm{tot}} &= p_q + p_m, \end{aligned} \quad (13)$$

where ρ_q and p_q are the energy density and the pressure of the q-deformed dark energy and ρ_m and p_m are the energy density and the pressure of the dark matter, respectively. The equation of state of the energy-momentum carrying cosmological fluid component under consideration in the FRW universe is given by $p = \omega\rho$ which relates the pressure and the energy density and ω is called the equation of state parameter. We then express the total equation of state parameter, such that

$$\omega_{\mathrm{tot}} = \frac{p_{\mathrm{tot}}}{\rho_{\mathrm{tot}}} = \omega_q \Omega_q + \omega_m \Omega_m, \quad (14)$$

where $\Omega_q = \rho_q/\rho_{\mathrm{tot}}$ and $\Omega_m = \rho_m/\rho_{\mathrm{tot}}$ are the density parameters for the q-deformed dark energy and the dark matter, respectively. Then the total density parameter is defined as

$$\Omega_{\mathrm{tot}} = \Omega_q + \Omega_m = \frac{\kappa^2 \rho_{\mathrm{tot}}}{3H^2} = 1. \quad (15)$$

We now turn to Einstein's equations of the form $R_{\mu\nu} = \kappa^2(T_{\mu\nu} - (1/2) g_{\mu\nu} T)$. Then, by using the components of the Ricci tensor for a FRW spacetime (6) and the energy-momentum tensor in (12), we rewrite Einstein's equations, for $\mu\nu = 00$ and $\mu\nu = ij$, as follows:

$$-3\frac{\ddot{a}}{a} = \frac{\kappa^2}{2}(\rho + 3p), \quad (16)$$

$$\frac{\ddot{a}}{a} + 2\left(\frac{\dot{a}}{a}\right)^2 = \frac{\kappa^2}{2}(\rho - p), \quad (17)$$

respectively. Here dot also represents the derivative with respect to cosmic time t. Using (16) and (17) gives the Friedmann equations for the FRW metric as

$$\begin{aligned} H^2 &= \frac{\kappa^2}{3}\left(\rho_q + \rho_m\right), \\ \dot{H} &= -\frac{\kappa^2}{2}\left(\rho_q + p_q + \rho_m + p_m\right), \end{aligned} \quad (18)$$

where $H = \dot{a}/a$ is the Hubble parameter. From the conservation of energy, we can obtain the continuity equations for the q-deformed dark energy and the dark matter constituents in the form of evolution equations, such as

$$\dot{\rho}_q + 3H\left(\rho_q + p_q\right) = -Q, \quad (19)$$

$$\dot{\rho}_m + 3H\left(\rho_m + p_m\right) = Q, \quad (20)$$

where Q is an interaction current between the q-deformed dark energy and the dark matter which transfers the energy and momentum from the dark matter to dark energy and vice versa. Q vanishes for the models having no interaction between the dark energy and the dark matter.

Now we will define the Dirac-Born-Infeld type action integral of the interacting dark matter and q-deformed dark energy nonminimally coupled to gravity in the framework of Eisteinian general relativity [86–88]. After that we will obtain the energy-momentum tensor $T_{\mu\nu}$ for the q-deformed dark

energy and the dark matter in order to get the energy density ρ and pressure p of these dark objects explicitly. Then the action is given as

$$S = \int d^4x\sqrt{-g}\left[\frac{R}{2\kappa^2} - \frac{1}{2}g^{\mu\nu}\partial_\mu\phi_q\partial_\nu\phi_q - V - \xi f\left(\phi_q\right)R + L_m\right], \tag{21}$$

where ξ is a dimensionless coupling constant between q-deformed dark energy and the gravity, so $\xi f(\phi_q)R$ denotes the explicit nonminimal coupling between energy and the gravity. Also $L_q = -(1/2)g^{\mu\nu}\partial_\mu\phi_q\partial_\nu\phi_q - V - \xi f(\phi_q)R$ and L_m are the Lagrangian densities of the q-deformed dark energy and the dark matter, respectively. Then the energy-momentum tensors of the dark energy constituent of our model can be calculated, as follows [89]:

$$\begin{aligned} T^q_{\mu\nu} &= -2\frac{\partial L_q}{\partial g^{\mu\nu}} + g_{\mu\nu}L_q \\ &= \partial_\mu\phi_q\partial_\nu\phi_q + 2\xi f\left(\phi_q\right)\frac{\partial R}{\partial g^{\mu\nu}} \\ &\quad - \frac{1}{2}g_{\mu\nu}\left[g^{\alpha\beta}\partial_\alpha\phi_q\partial_\beta\phi_q + 2V\right] - g_{\mu\nu}\xi f\left(\phi_q\right)R. \end{aligned} \tag{22}$$

In order to find the derivative of the Ricci scalar with respect to the metric tensor, we use the variation of the contraction of the Ricci tensor identity $\delta R = R_{\mu\nu}\delta g^{\mu\nu} + g^{\mu\nu}\delta R_{\mu\nu}$. This leads us to finding the variation of the contraction of the Riemann tensor identity, as follows: $\delta R_{\mu\nu} = \delta R^\rho_{\mu\rho\nu} = \nabla_\rho(\delta\Gamma^\rho_{\nu\mu}) - \nabla_\nu(\delta\Gamma^\rho_{\rho\mu})$. Here ∇_μ represents the covariant derivative and $\Gamma^\rho_{\nu\mu}$ represents the Christoffel connection. By using the metric compatibility and the tensor nature of $\delta\Gamma^\rho_{\nu\mu}$, we finally obtain

$$\frac{\delta R}{\delta g^{\mu\nu}} = R_{\mu\nu} + g_{\mu\nu}\Box - \nabla_\mu\nabla_\nu, \tag{23}$$

where $\Box = g^{\alpha\beta}\nabla_\alpha\nabla_\beta$ is the covariant d'Alembertian. Using (23) in (22) gives

$$\begin{aligned} T^q_{\mu\nu} &= \partial_\mu\phi_q\partial_\nu\phi_q - \frac{1}{2}g_{\mu\nu}\left[g^{\alpha\beta}\partial_\alpha\phi_q\partial_\beta\phi_q\right] - g_{\mu\nu}V \\ &\quad + 2\xi\left[R_{\mu\nu} - \frac{1}{2}g_{\mu\nu}R\right]f\left(\phi_q\right) + 2\xi\Box f\left(\phi_q\right) \\ &\quad - 2\xi\nabla_\mu\nabla_\nu f\left(\phi_q\right). \end{aligned} \tag{24}$$

Then the $\mu\nu = 0,0$ component of the energy-momentum tensor leads to the energy density ρ_q:

$$\rho_q = T^q_{00} = \frac{1}{2}\dot\phi_q^2 + V + 6\xi H^2 f\left(\phi_q\right) + 6\xi H f'\left(\phi_q\right)\dot\phi_q, \tag{25}$$

where prime refers to derivative with respect to the field ϕ_q and we use $\Box = -\partial_0^2 - 3H\partial_0$, because of the homogeneity and the isotropy for ϕ_q in space. Also $R_{00} = -3\ddot a/a$ and $R = 6[\ddot a/a + \dot a^2/a^2]$ is used for the FRW geometry. The $\mu\nu = i,i$ components of $T^q_{\mu\nu}$ also give the pressure p_q as

$$\begin{aligned} p_q &= g^{ii}T^q_{ii} = \frac{1}{2}\dot\phi_q^2 - V - 2\xi\left[2\dot H f\left(\phi_q\right) + 3H^2 f\left(\phi_q\right)\right. \\ &\quad \left. + f''\left(\phi_q\right)\dot\phi_q^2 + f'\left(\phi_q\right)\ddot\phi_q + 2Hf'\left(\phi_q\right)\dot\phi_q\right], \end{aligned} \tag{26}$$

where we use $(\nabla_i\nabla_i)f(\phi_q) = (\partial_i\nabla_i - \Gamma^\lambda_{ii}\nabla_\lambda)f(\phi_q) = -\Gamma^0_{11}\partial_0 f(\phi_q)$ with $\Gamma^0_{11} = \dot a a$ for the FRW spacetime. We can now obtain the equation of motion for the q-deformed dark energy by inserting (25) and (26) into the evolution equation (19), such that

$$\ddot\phi_q + 3H\dot\phi_q + \frac{\partial V}{\partial\phi_q} + \xi R f'\left(\phi_q\right) = -\frac{Q}{\dot\phi_q}. \tag{27}$$

The usual assumption in the literature is to consider the coupling function as $f(\phi_q) = \phi_q^2/2$ [90] and the potential as $V = V_0e^{-\kappa\lambda\phi_q}$ [91–93]. In order to find the energy density, pressure, and equation of motion in terms of the deformation parameter q, we use the above coupling function and potential with the rearrangement of equation (9) as $\phi_q = \Delta(q)\phi$ in the equations (25)–(27) and obtain

$$\begin{aligned} \rho_q &= \frac{1}{2}\Delta^2\dot\phi^2 + e^{-\kappa\lambda\Delta\phi} + 3\xi H^2\Delta^2\phi^2 + 6\xi H\Delta^2\phi\dot\phi \\ &\quad + \frac{1}{2}\dot\Delta^2\phi^2 + \Delta\dot\Delta\phi\dot\phi + 6\xi H\Delta\dot\Delta\phi^2, \end{aligned} \tag{28}$$

$$\begin{aligned} p_q &= \frac{1}{2}\Delta^2\dot\phi^2 - e^{-\kappa\lambda\Delta\phi} \\ &\quad - 2\xi\Delta^2\left[\dot H\phi^2 + \frac{3}{2}H^2\phi^2 + \dot\phi^2 + \phi\ddot\phi + 2H\phi\dot\phi\right] \\ &\quad + (1-8\xi)\Delta\dot\Delta\phi\dot\phi + \left(\frac{1}{2} - 2\xi\right)\Delta^2\phi^2 - 2\xi\Delta\ddot\Delta\phi^2 \\ &\quad - 4\xi H\phi\dot\phi\Delta\dot\Delta\phi^2, \end{aligned} \tag{29}$$

$$\begin{aligned} &\Delta\ddot\phi + 3\Delta H\dot\phi - \kappa\lambda e^{-\kappa\lambda\Delta\phi} + \xi\Delta R\phi + 2\dot\Delta\dot\phi + \ddot\Delta\phi \\ &\quad + 3H\dot\Delta\phi = -\beta\kappa\rho_m. \end{aligned} \tag{30}$$

Here we consider that the particles in each mode can vary by creation or annihilation in time for $\Delta = \sqrt{(1-q^{2N})/(1-q^2)}N$; therefore its time derivatives are nonvanishing. On the other hand, the common interaction current in the literature $Q = \beta\kappa\rho_m\dot\phi_q$ is used here [17].

Now the phase-space analysis for our interacting dark matter and nonminimally coupled q-deformed dark energy model will be performed, whether the late-time stable attractor solutions can be obtained, in order to confirm our model.

3. Phase-Space and Stability Analysis

The cosmological properties of the proposed q-deformed dark energy model can be investigated by performing the

phase-space analysis. Therefore, we first transform the equations of the dynamical system into its autonomous form by introducing the auxiliary variables [15, 94–98], such as

$$\begin{aligned} x &= \frac{\kappa\Delta\dot{\phi}}{\sqrt{6}H} = \Delta x_s, \\ y &= \frac{\kappa\sqrt{e^{-\kappa\lambda\Delta\phi}}}{\sqrt{3}H} = \sqrt{e^{-\kappa\lambda\phi(\Delta-1)}}\, y_s, \\ z &= \frac{\kappa\dot{\Delta\phi}}{\sqrt{6}H}, \quad z_s = 0 \\ u &= \kappa\Delta\phi = \Delta u_s, \end{aligned} \tag{31}$$

where x_s, y_s, z_s, and u_s are the standard form of the auxiliary variables in $q \to 1$ limit. We now write the density parameters for the dark matter and q-deformed scalar field dark energy in the autonomous system by using (28) with (36):

$$\Omega_m = \frac{\kappa^2\rho_m}{3H^2}, \tag{32}$$

$$\begin{aligned} \Omega_q &= \frac{\kappa^2\rho_q}{3H^2} \\ &= x^2 + y^2 + \xi u^2 + 2\sqrt{6}\xi xu + z^2 + 2xz \\ &\quad + 2\sqrt{6}\xi zu. \end{aligned} \tag{33}$$

Then the total density parameter reads

$$\begin{aligned} \Omega_{\text{tot}} &= \frac{\kappa^2\rho_{\text{tot}}}{3H^2} \\ &= x^2 + y^2 + \xi u^2 + 2\sqrt{6}\xi xu + z^2 + 2xz \\ &\quad + 2\sqrt{6}\xi zu + \Omega_m = 1. \end{aligned} \tag{34}$$

We should also obtain the $\kappa^2 p_q/3H^2$ in the autonomous form to write the equation of state parameters, such that

$$\begin{aligned} \frac{\kappa^2 p_q}{3H^2} &= (1-4\xi)\, x^2 - y^2 + \left(\frac{2}{3}\xi + 4\xi^2\right) su^2 \\ &\quad + \left(8\xi^2 - \xi\right) u^2 + \frac{2\sqrt{6}}{3}\xi xu + (1-4\xi)\, z^2 \\ &\quad + 2\,(1-4\xi)\, xz + \frac{2\sqrt{6}}{3}\xi zu + 2\xi\beta u\Omega_m \\ &\quad - 2\xi\lambda y^2 u, \end{aligned} \tag{35}$$

where $s = -\dot{H}/H^2$. Using (33) and (35), we find the equation of state parameter for the dark energy as

$$\begin{aligned} \omega_q = \frac{p_q}{\rho_q} &= \Bigg[(1-4\xi)\, x^2 - y^2 + \left(\frac{2}{3}\xi + 4\xi^2\right) su^2 \\ &\quad + \left(8\xi^2 - \xi\right) u^2 + \frac{2\sqrt{6}}{3}\xi xu + (1-4\xi)\, z^2 \\ &\quad + 2\,(1-4\xi)\, xz + \frac{2\sqrt{6}}{3}\xi zu + 2\xi\beta u\Omega_m - 2\xi\lambda y^2 u\Bigg] \\ &\quad \cdot \left[x^2 + y^2 + \xi u^2 + 2\sqrt{6}\xi xu + z^2 + 2xz \right. \\ &\quad \left. + 2\sqrt{6}\xi zu\right]^{-1}. \end{aligned} \tag{36}$$

Also from (33) and (36), the total equation of state parameter can be obtained as

$$\begin{aligned} \omega_{\text{tot}} &= \omega_q\Omega_q + \omega_m\Omega_m \\ &= (1-4\xi)\, x^2 - y^2 + \left(\frac{2}{3}\xi + 4\xi^2\right) su^2 \\ &\quad + \left(8\xi^2 - \xi\right) u^2 + \frac{2\sqrt{6}}{3}\xi xu + (1-4\xi)\, z^2 \\ &\quad + 2\,(1-4\xi)\, xz + \frac{2\sqrt{6}}{3}\xi zu + 2\xi\beta u\Omega_m \\ &\quad - 2\xi\lambda y^2 u + (\gamma - 1)\,\Omega_m, \end{aligned} \tag{37}$$

where $\gamma = 1 + \omega_m$ is defined to be the barotropic index. We need to give the junk parameter s in the autonomous form, such that

$$\begin{aligned} s = -\frac{\dot{H}}{H^2} = \frac{3}{2}\left(1 + \omega_{\text{tot}}\right) &= \frac{3}{2}\Bigg[1 + (1-4\xi)\, x^2 - y^2 \\ &\quad + \left(\frac{2}{3}\xi + 4\xi^2\right) su^2 + \left(8\xi^2 - \xi\right) u^2 + \frac{2\sqrt{6}}{3}\xi xu \\ &\quad + (1-4\xi)\, z^2 + 2\,(1-4\xi)\, xz + \frac{2\sqrt{6}}{3}\xi zu \\ &\quad + 2\xi\beta u\Omega_m - 2\xi\lambda y^2 u + (\gamma - 1)\,\Omega_m\Bigg]. \end{aligned} \tag{38}$$

Pulling s from the right-hand side of (38) to the left-hand side gives

$$\begin{aligned} s &= \Bigg[1 + (1-4\xi)\, x^2 - y^2 + \left(8\xi^2 - \xi\right) u^2 + \frac{2\sqrt{6}}{3}\xi xu \\ &\quad + (1-4\xi)\, z^2 + 2\,(1-4\xi)\, xz + \frac{2\sqrt{6}}{3}\xi zu \\ &\quad + 2\xi\beta u\Omega_m - 2\xi\lambda y^2 u + (\gamma - 1)\,\Omega_m\Bigg]\left[\frac{2}{3} - \frac{2}{3}\xi u^2 \right. \\ &\quad \left. - 4\xi^2 u^2\right]^{-1}. \end{aligned} \tag{39}$$

Table 1: Critical points and existence conditions.

Label	$x+z$	y	u	ω_{tot}	q_D	Existence
A	0	1	0	-1	-1	$\lambda = 0, \Omega_m = 0$
B	0	-1	0	-1	-1	$\lambda = 0, \Omega_m = 0$
C	0	$\sqrt{(4\xi/\lambda)\left(-2/\lambda + \sqrt{4/\lambda^2 + 1/\xi}\right)}$	$\left(-2/\lambda + \sqrt{4/\lambda^2 + 1/\xi}\right)$	-1	-1	$\lambda \neq 0, \Omega_m = 0$
D	0	$-\sqrt{(4\xi/\lambda)\left(-2/\lambda + \sqrt{4/\lambda^2 + 1/\xi}\right)}$	$\left(-2/\lambda + \sqrt{4/\lambda^2 + 1/\xi}\right)$	-1	-1	$\lambda \neq 0, \Omega_m = 0$

While s is a junk parameter alone, it gains physical meaning in the deceleration parameter q_D, such that

$$q_D = -1 + s = -1 + \left[1 + (1-4\xi)\,x^2 - y^2 + \left(8\xi^2 - \xi\right)u^2 + \frac{2\sqrt{6}}{3}\xi xu + (1-4\xi)\,z^2 + 2\,(1-4\xi)\,xz + \frac{2\sqrt{6}}{3}\xi zu + 2\xi\beta u\Omega_m - 2\xi\lambda y^2 u + (\gamma - 1)\,\Omega_m\right]\left[\frac{2}{3} - \frac{2}{3}\xi u^2 - 4\xi^2 u^2\right]^{-1}. \tag{40}$$

Now we convert the Friedmann equations (18), the continuity equation (20), and the equation of motion (30) into the autonomous system by using the auxiliary variables in (31) and their derivatives with respect to $N = \ln a$. For any quantity F, this derivative has the relation with the time derivative as $\dot{F} = H(dF/dN) = HF'$. Then we will obtain $X' = f(X)$, where X is the column vector including the auxiliary variables and $f(X)$ is the column vector of the autonomous equations. We then find the critical points X_c of X, by setting $X' = 0$. We then expand $X' = f(X)$ around $X = X_c + U$, where U is the column vector of perturbations of the auxiliary variables, such as δx, δy, δz, and δu for each constituent in our model. Thus, we expand the perturbation equations up to the first order for each critical point as $U' = MU$, where M is the matrix of perturbation equations. The eigenvalues of perturbation matrix M determine the type and stability of each critical point [99–108]. Then the autonomous form of the cosmological system is

$$x' = -3x - 3z + sx - z' + sz + \sqrt{6}\xi su - 2\sqrt{6}\xi u + \frac{\sqrt{6}}{2}\lambda y^2 - \frac{\sqrt{6}}{2}\beta\Omega_m, \tag{41}$$

$$y' = sy - \frac{\sqrt{6}}{2}\lambda yx - \frac{\sqrt{6}}{2}\lambda yz, \tag{42}$$

$$z' = -3x - 3z + sx - x' + sz + \sqrt{6}\xi su - 2\sqrt{6}\xi u + \frac{\sqrt{6}}{2}\lambda y^2 - \frac{\sqrt{6}}{2}\beta\Omega_m, \tag{43}$$

$$u' = \sqrt{6}x + \sqrt{6}z. \tag{44}$$

Here (41) and (43) in fact give the same autonomous equations, which means that the variables x and z do not form an orthonormal basis in the phase-space. However, $+z$, y, and u form a complete orthonormal set for the phase-space. Therefore, we set (41) and (43) in a single autonomous equation as

$$x' + z' = -3x - 3z + sx + sz + \sqrt{6}\xi su - 2\sqrt{6}\xi u + \frac{\sqrt{6}}{2}\lambda y^2 - \frac{\sqrt{6}}{2}\beta\Omega_m. \tag{45}$$

The autonomous equation system (42), (44), and (45) represents three invariant submanifolds $+z = 0$, $y = 0$, and $u = 0$ which, by definition, cannot be intersected by any orbit. This means that there is no global attractor in the deformed dark energy cosmology [109]. We will make finite analysis of the phase space. The finite fixed points are found by setting the derivatives of the invariant submanifolds of the auxiliary variables. We can also write these autonomous equations in $q \to 1$ limit in terms of the standard auxiliary variables, such as

$$x_s' = -3x_s + s_s x_s + \sqrt{6}\xi s_s u_s - 2\sqrt{6}\xi u_s + \frac{\sqrt{6}}{2}\lambda y_s^2 - \frac{\sqrt{6}}{2}\beta\Omega_m,$$
$$y_s' = s_s y_s - \frac{\sqrt{6}}{2}\lambda y_s x_s, \tag{46}$$
$$u_s' = \sqrt{6}x_s.$$

Here we need to get the finite fixed points (critical points) of the autonomous system in (41)–(45), in order to perform the phase-space analysis of the model. We will obtain these points by equating the left-hand sides of the equations (42), (44), and (45) to zero, by using $\Omega_{\text{tot}} = 1$ in (34) and also by assuming $\omega_{\text{tot}} = -1$ and $q_d = -1$ in (37) and (40), for each critical point. After some calculations, four sets of solutions are found as the critical points which are listed in Table 1 with the existence conditions. The same critical points are also valid for x_s, y_s, and u_s instead of $x + z$, y, and u, in the $q \to 1$ standard dark energy model limit.

Now we should find δs from (39), which will exist in the perturbations $\delta x' + \delta z'$, $\delta y'$, and $\delta u'$, such that

$$\delta s = \left[2\,(1-4\xi)\,(x+z) + \frac{2\sqrt{6}}{3}\xi u\right]\frac{1}{P}\,(\delta x + \delta z) + \left[-2y - 4\xi\lambda yu\right]\frac{1}{P}\delta y + \left[\left(8\xi^2 - \xi\right)2u\right.$$

$$+\frac{2\sqrt{6}}{3}\xi(x+z)+2\xi\beta\Omega_m-2\xi\lambda y^2+\left(\frac{4}{3}\xi+8\xi^2\right)su\Bigg]\frac{1}{P}\delta u, \tag{47}$$

where $P = 2/3 - (2/3)\xi u^2 - 4\xi^2 u^2$. Then the perturbations $\delta x' + \delta z'$, $\delta y'$ and $\delta u'$ for each phase-space coordinate in our model can be found by using the variations of (42), (44), and (45), such that

$$\begin{aligned}
\delta x' + \delta z' = {} & \Bigg[2(1-4\xi)(x+z)^2+(-s+3)P+4\xi^2u^2 \\
& +\left(\frac{8}{3}\xi-8\xi^2\right)\sqrt{6}(x+z)u\Bigg]\frac{1}{P}(\delta x+\delta z) \\
& +\left[\left(-2(x+z)+\sqrt{6}\lambda P\right)y-4\xi\lambda(x+z)yu\right. \\
& \left.-2\sqrt{6}\xi yu-4\sqrt{6}\xi^2\lambda yu^2\right]\frac{1}{P}\delta y \\
& +\Bigg[\left(10\xi^2-\xi\right)2(x+z)u+\frac{2\sqrt{6}}{3}\xi(x+z)^2 \\
& +2\xi\beta(x+z)\Omega_m-2\xi\lambda(x+z)y^2 \\
& +\left(\frac{4}{3}\xi+8\xi^2\right)(x+z)su+\left(8\xi^2-\xi\right)2\sqrt{6}\xi u^2 \\
& +2\sqrt{6}\xi^2\beta u\Omega_m-2\sqrt{6}\xi^2\lambda y^2u \\
& +\left(\frac{4}{3}\xi+8\xi^2\right)\sqrt{6}\xi su^2+\sqrt{6}\xi(s-2)P\Bigg]\frac{1}{P}\delta u, \\
\delta y' = {} & \left[2(1-4\xi)(x+z)y+\frac{2\sqrt{6}}{3}\xi uy-\frac{\sqrt{6}}{2}\lambda yP\right] \\
& \cdot\frac{1}{P}(\delta x+\delta z)+\Bigg[-2y^2-4\xi\lambda y^2u+sP \\
& -\frac{\sqrt{6}}{2}\lambda(x+z)P\Bigg]\frac{1}{P}\delta y+\Bigg[\left(8\xi^2-\xi\right)uy \\
& +\frac{2\sqrt{6}}{3}\xi(x+z)y+2\xi\beta y\Omega_m-2\xi\lambda y^3 \\
& +\left(\frac{4}{3}\xi+8\xi^2\right)syu\Bigg]\frac{1}{P}\delta u, \\
\delta u' = {} & \sqrt{6}(\delta x+\delta z).
\end{aligned} \tag{48}$$

From (48), we find the 3×3 perturbation matrix M whose elements are given as

$$\begin{aligned}
M_{11} = {} & \Bigg[2(1-4\xi)(x+z)^2+(-s+3)P+4\xi^2u^2 \\
& +\left(\frac{8}{3}\xi-8\xi^2\right)\sqrt{6}(x+z)u\Bigg]\frac{1}{P}, \\
M_{12} = {} & \left[\left(-2(x+z)+\sqrt{6}\lambda P\right)y-4\xi\lambda(x+z)yu\right. \\
& \left.-2\sqrt{6}\xi yu-4\sqrt{6}\xi^2\lambda yu^2\right]\frac{1}{P}, \\
M_{13} = {} & \Bigg[\left(10\xi^2-\xi\right)2(x+z)u+\frac{2\sqrt{6}}{3}\xi(x+z)^2 \\
& +2\xi\beta(x+z)\Omega_m-2\xi\lambda(x+z)y^2 \\
& +\left(\frac{4}{3}\xi+8\xi^2\right)(x+z)su+\left(8\xi^2-\xi\right)2\sqrt{6}\xi u^2 \\
& +2\sqrt{6}\xi^2\beta u\Omega_m-2\sqrt{6}\xi^2\lambda y^2u \\
& +\left(\frac{4}{3}\xi+8\xi^2\right)\sqrt{6}\xi su^2+\sqrt{6}\xi(s-2)P\Bigg]\frac{1}{P}, \\
M_{21} = {} & \left[2(1-4\xi)(x+z)y+\frac{2\sqrt{6}}{3}\xi uy-\frac{\sqrt{6}}{2}\lambda yP\right] \\
& \cdot\frac{1}{P}, \\
M_{22} = {} & \left[-2y^2-4\xi\lambda y^2u-+sP-\frac{\sqrt{6}}{2}\lambda(x+z)P\right]\frac{1}{P}, \\
M_{23} = {} & \Bigg[\left(8\xi^2-\xi\right)uy+\frac{2\sqrt{6}}{3}\xi(x+z)y+2\xi\beta y\Omega_m \\
& -2\xi\lambda y^3+\left(\frac{4}{3}\xi+8\xi^2\right)syu\Bigg]\frac{1}{P}, \\
M_{31} = {} & \sqrt{6}, \\
M_{32} = {} & M_{33} = 0.
\end{aligned} \tag{49}$$

We insert the linear perturbations $(x + z) \to (x_c + z_c) + (\delta x + \delta z)$, $y \to y_c + \delta y$, and $u \to u_c + \delta u$ about the critical points in the autonomous system (42), (44), and (45), in order to calculate the eigenvalues of perturbation matrix M for four critical points given in Table 1, with the corresponding existing conditions. Therefore, we first give the four perturbation matrices for the critical points A, B, C, and D with the corresponding existing conditions, such that

$$M_A = M_B = \begin{pmatrix} -3 & 0 & -2\sqrt{6}\xi \\ 0 & -3 & 0 \\ \sqrt{6} & 0 & 0 \end{pmatrix}, \tag{50}$$

$$M_C = \begin{pmatrix} \frac{4\xi^2 u_C^2}{P} - 3 & -\frac{4\sqrt{6}\lambda u_C^2 \xi^2}{P} - \frac{2\sqrt{6}\xi y_C u_C}{P} + \sqrt{6} y_C \lambda & -\frac{\sqrt{6}\left(2\xi^2 - 16\xi^3\right) u_C^2}{P} - \frac{2\sqrt{6}\xi^2 \lambda y_C^2 u_C}{P} - 2\sqrt{6}\xi \\ \frac{2\sqrt{6}\xi y_C u_C}{3P} - \frac{\sqrt{6}\lambda y_C}{2} & -\frac{2y_C^2}{P} - \frac{4\xi\lambda y_C^2 u_C}{P} & -\frac{2\xi\lambda y_C^3}{P} - \frac{\left(2\xi - 16\xi^2\right) u_C y_C}{P} \\ \sqrt{6} & 0 & 0 \end{pmatrix}, \quad (51)$$

where $y_C = \sqrt{4\xi/\lambda(-2/\lambda + \sqrt{4/\lambda^2 + 1/\xi})}$ and $u_C = -2/\lambda + \sqrt{4/\lambda^2 + 1/\xi}$,

$$M_D = \begin{pmatrix} \frac{4\xi^2 u_D^2}{P} - 3 & \frac{4\sqrt{6}\lambda u_D^2 \xi^2}{P} + \frac{2\sqrt{6}\xi y_D u_D}{P} - \sqrt{6} y_D \lambda & -\frac{\sqrt{6}\left(2\xi^2 - 16\xi^3\right) u_D^2}{P} - \frac{2\sqrt{6}\xi^2 \lambda y_D^2 u_D}{P} - 2\sqrt{6}\xi \\ \frac{\sqrt{6}\lambda y_D}{2} - \frac{2\sqrt{6}\xi y_D u_D}{3P} & -\frac{2y_D^2}{P} - \frac{4\xi\lambda y_D^2 u_D}{P} & -\frac{2\xi\lambda y_D^3}{P} - \frac{\left(2\xi - 16\xi^2\right) u_D y_D}{P} \\ \sqrt{6} & 0 & 0 \end{pmatrix}, \quad (52)$$

where $y_D = -\sqrt{4\xi/\lambda(-2/\lambda + \sqrt{4/\lambda^2 + 1/\xi})}$ and $u_D = -2/\lambda + \sqrt{4/\lambda^2 + 1/\xi}$. Also by using x_s, y_s, and u_s instead of $x + z$, y, and u in the perturbation matrix elements above, we obtain the standard perturbation matrix elements in $q \to 1$ limit. Then substituting the standard critical points we again obtain the same matrices M_A, M_B, M_C, and M_D. Therefore the stability of the standard model agrees with the stability of the deformed model.

We need to obtain the four sets of eigenvalues and investigate the sign of the real parts of eigenvalues, so that we can determine the type and stability of critical points. If all the real parts of the eigenvalues are negative, the critical point is said to be stable. The physical meaning of the stable critical point is a stable attractor; namely, the Universe keeps its state forever in this state and thus it can attract the universe at a late time. Here an accelerated expansion phase occurs because $\omega_{\text{tot}} = -1 < -1/3$. However, if the suitable conditions are satisfied, there can even exist an accelerated contraction for $\omega_{\text{tot}} = -1 < -1/3$ value. Eigenvalues of the four M matrices and the stability conditions are represented in Table 2, for each critical point A, B, C, and D. From Table 2, the first two critical points A and B have the same eigenvalues, as C and D have the same eigenvalues, too. Here the eigenvalues and the stability conditions of the perturbation matrices for critical points C and D have been obtained by the numerical methods, due to the complexity of the matrices (51) and (52). The stability conditions of each critical point are listed in Table 2, according to the sign of the real part of the eigenvalues.

Now we will study the cosmological behavior of each critical point by considering the attractor solutions in scalar field cosmology [110]. We know that the energy density of a scalar field has a role in the determination of the evolution of Universe. Cosmological attractors provide the understanding of evolution and the factors affecting on this evolution, such that, from the dynamical conditions, the evolution of scalar field approaches a particular type of behavior without using the initial fine tuning conditions [111–121]. We know that the attractor solutions imply a behavior in which a collection of phase-space points evolve into a particular region and never leave from there. In order to solve the differential equation system (42), (44), and (45) we use adaptive Runge-Kutta method of 4th and 5th order, in MATLAB programming. We use the present day values for the dark matter density parameter $\Omega_m = 0.3$, interaction parameter $\beta = 14.5$, and $0 < \gamma < 2$ values in solving the differential equation system [94, 122]. Then the solutions with the stability conditions of critical points are plotted for each pair of the solution set being the auxiliary variables $x + z$, y, and u.

Critical Point A. This point exists for $\lambda = 0$ which means that the potential V is constant. Acceleration occurs at this point because of $\omega_{\text{tot}} = -1 < -1/3$, and it is an expansion phase since y is positive, so H is positive, too. Point A is stable meaning that Universe keeps its further evolution, for $0 < \xi \leq 3/16$ with $\lambda, \beta \in \mathfrak{R}$, but it is a saddle point meaning the universe evolves between different states for $\xi < 0$. In Figure 1, we illustrate the 2-dimensional projections of 4-dimensional phase-space trajectories for the stability condition $\xi = 0.15$ and for the present day values $\beta = 14.5$, $\gamma = 1.5$, and $\Omega_m = 0.3$ and three auxiliary λ values. This state corresponds to a stable attractor starting from the critical point $A = (0, 1, 0)$, as seen from the plots in Figure 1.

Critical Point B. Point B also exists for $\lambda = 0$ meaning that the potential V is constant. Acceleration phase is again valid here

Table 2: Eigenvalues and stability of critical points.

Critical points	Eigenvalues			ξ	λ	Stability
A and B	−3.0000	$-(1/2)\sqrt{9-48\xi}-3/2$	$(1/2)\sqrt{9-48\xi}-3/2$			Stable point for $0<\xi\leq 3/16$ with $\lambda,\beta\in\mathfrak{R}$ Saddle point for $\xi<0$ with $\lambda,\beta\in\mathfrak{R}$
C and D	−1.0642	−1.5576	−5.5000	0.1000	1.0000	Stable point for $0<\xi$, $\lambda=1$ and $\beta\in\mathfrak{R}$ Saddle point, if $\xi<0$ and $\lambda\neq 1$
	−1.0193	−1.0193	−7.2507	1.0000	1.0000	
	−0.8407	−0.8407	−7.7519	2.0000	1.0000	
	−0.7080	−0.7080	−8.0701	3.0000	1.0000	
	−0.6014	−0.6014	−8.3107	4.0000	1.0000	
	−0.5121	−0.5121	−8.5060	5.0000	1.0000	
	−0.4353	−0.4353	−8.6709	6.0000	1.0000	
	−0.3680	−0.3680	−8.8136	7.0000	1.0000	
	−0.3082	−0.3082	−8.9395	8.0000	1.0000	
	−0.2544	−0.2544	−9.0520	9.0000	1.0000	
	−0.2055	−0.2055	−9.1535	10.0000	1.0000	

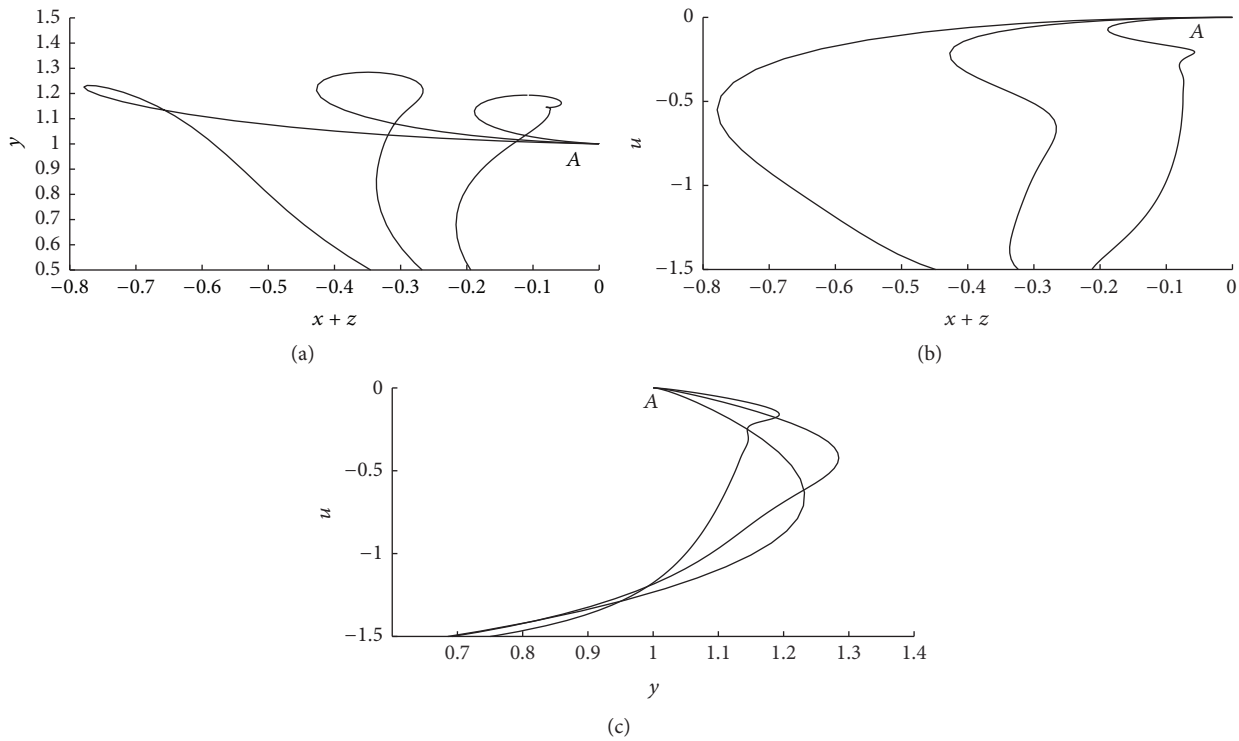

Figure 1: Two-dimensional projections of the phase-space trajectories for stability condition $\xi = 0.15$ and for present day values $\beta = 14.5$, $\gamma = 1.5$, and $\Omega_m = 0.3$. All plots begin from the critical point A being a stable attractor.

since $\omega_{\text{tot}} = -1 < -1/3$, but this point refers to contraction phase because y is negative here. For the stability of the point B, it is again stable for $0 < \xi \leq 3/16$ with $\lambda, \beta \in \mathfrak{R}$, but it is a saddle point for $\xi < 0$. Therefore the stable attractor behavior is represented for contraction starting from the critical point $B = (0, -1, 0)$, as seen from the graphs in Figure 2. We plot phase-space trajectories for the stability condition $\xi = 0.15$ and for the present day values $\beta = 14.5$, $\gamma = 1.5$, and $\Omega_m = 0.3$ and three auxiliary λ values.

Critical Point C. Critical point C occurs for $\lambda \neq 0$ meaning a field dependent potential V. The cosmological behavior is again an acceleration phase since $\omega_{\text{tot}} < -1/3$ and an expansion phase since y is positive. Point C is stable for $0 < \xi$, $\lambda = 1$,

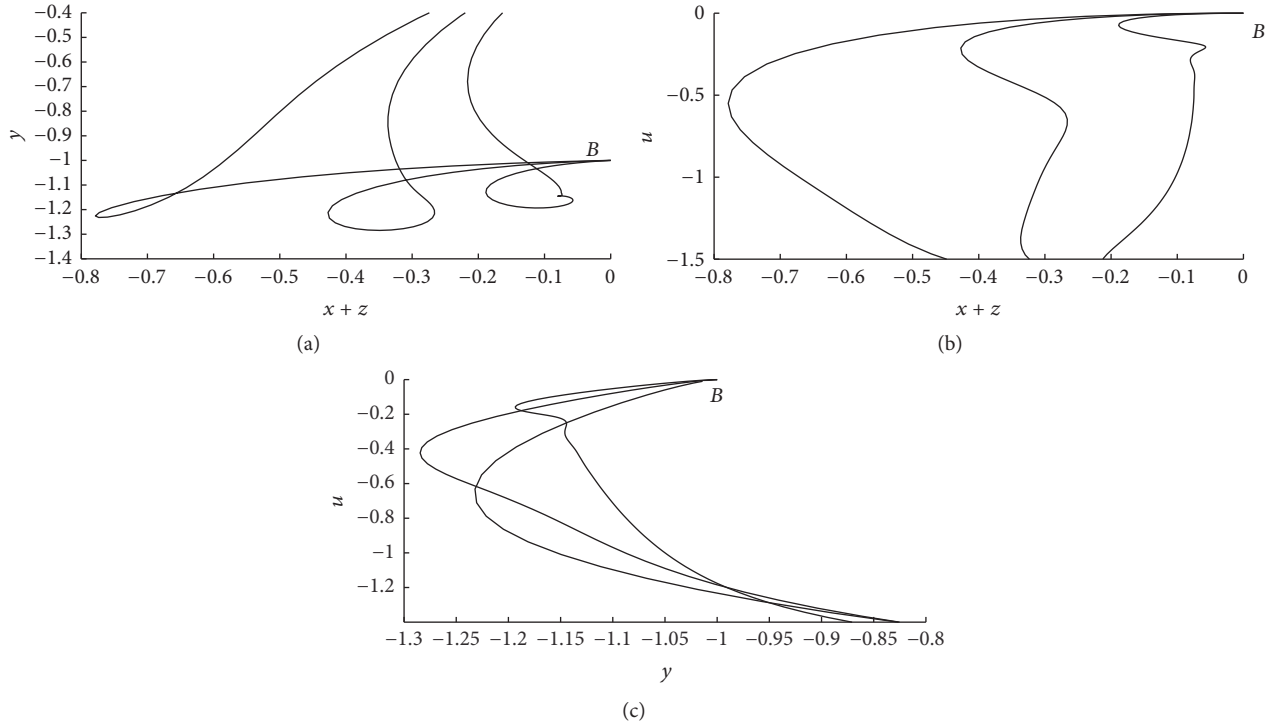

FIGURE 2: Two-dimensional projections of the phase-space trajectories for stability condition $\xi = 0.15$ and for present day values $\beta = 14.5$, $\gamma = 1.5$, and $\Omega_m = 0.3$. All plots begin from the critical point B being a stable attractor.

and $\beta \in \mathfrak{R}$ and saddle point if $\xi < 0$ and $\lambda \neq 1$. 2-dimensional projections of phase-space are represented in Figure 3, for the stability conditions $\xi = 2, \lambda = 1$ and for the present day values $\beta = 14.5, \Omega_m = 0.3$, and three auxiliary γ values in the present day value range. The stable attractor starting from the critical point C can be inferred from the plots in Figure 3.

Critical Point D. This point exists for $\lambda \neq 0$ meaning a field dependent potential V. Acceleration phase is again valid due to $\omega_{\text{tot}} < -1/3$, but this point refers to a contraction phase because y is negative. Point D is also stable for $0 < \xi, \lambda = 1$, and $\beta \in \mathfrak{R}$. However, it is a saddle point, while $\xi < 0$ and $\lambda \neq 1$. 2-dimensional plots of phase-space trajectories are shown in Figure 4, for the stability conditions $\xi = 2, \lambda = 1$ and for the present day values $\beta = 14.5, \Omega_m = 0.3$ and three auxiliary γ values in the present day value range. This state again corresponds to a stable attractor starting from the point D, as seen from the plots in Figure 4.

All the plots in Figures 1–4 have the structure of stable attractor, since each of them evolves to a single point which is in fact one of the critical points in Table 1. The three-dimensional plots of the evolution of phase-space trajectories for the stable attractors are given in Figure 5. These evolutions to the critical points are the attractor solutions of our cosmological model: interacting dark matter and q-deformed dark energy nonminimally coupled to gravity, which imply an expanding universe. On the other hand, the construction of the model in the $q \to 1$ limit reproduces the results of the phase-space analysis for the nondeformed standard dark energy case. The critical points and perturbation matrices are the same for the deformed and standard dark energy models with the equivalence of the auxiliary variables as $x + z = x_s$, $y = y_s$, and $u = u_s$. Therefore, it is confirmed that the dark energy in our model can be defined in terms of the q-deformed scalar fields obeying the q-deformed boson algebra in (2). According to the stable attractor behaviors, it makes sense to consider the dark energy as a scalar field defined by the q-deformed scalar field, with a negative pressure.

We know that the deformed dark energy model is a confirmed model since it reproduces the same stability behaviors, critical points, and perturbation matrices with the standard dark energy model, but the auxiliary variables of deformed and standard models are not the same. The relation between deformed and standard dark energy can be represented regarding auxiliary variable equations in (31):

$$x = \sqrt{\frac{1 - q^{2N}}{(1 - q^2) N}}\, x_s,$$

$$y = \sqrt{\exp\left(-c\left(\sqrt{\frac{1 - q^{2N}}{(1 - q^2) N}} - 1\right)\right)}\, y_s, \tag{53}$$

$$u = \sqrt{\frac{1 - q^{2N}}{(1 - q^2) N}}\, u_s,$$

where c is a constant. From the equations (53) we now illustrate the behavior of the deformed and standard dark energy auxiliary variables with respect to the deformation parameter q in Figure 6. We infer from the figure that the value of the

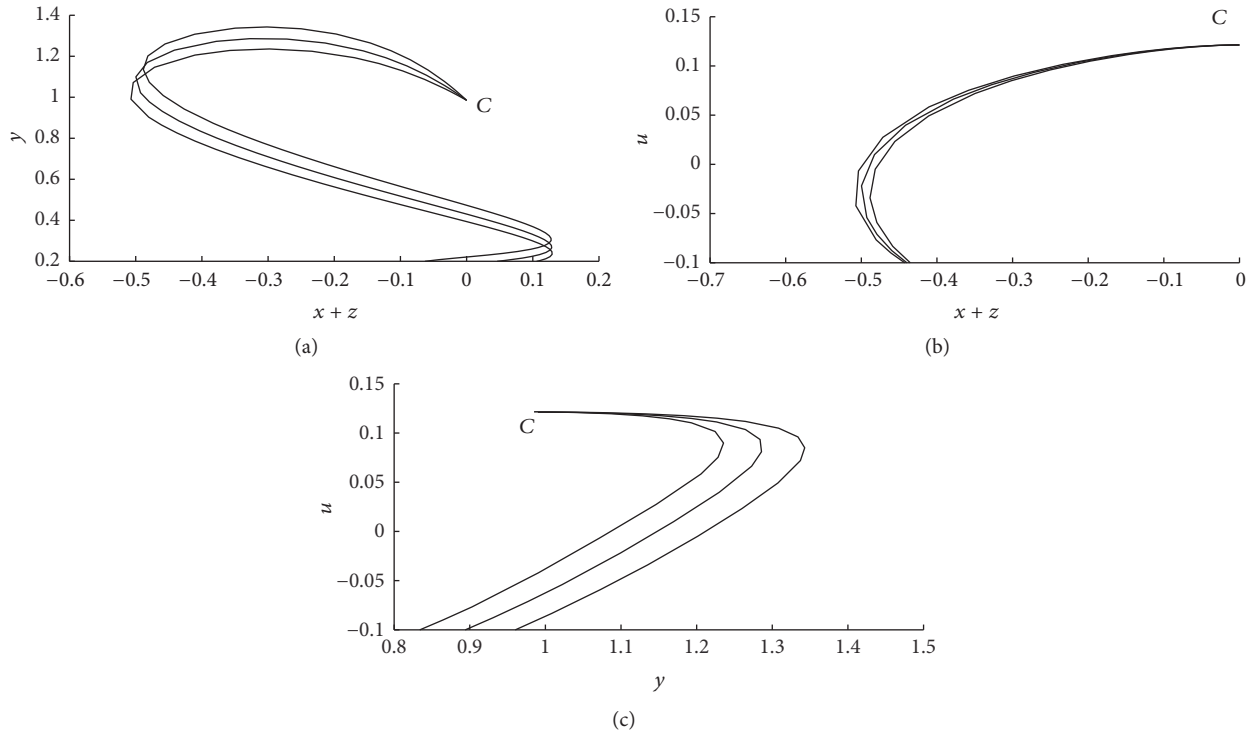

FIGURE 3: Two-dimensional projections of the phase-space trajectories for stability conditions $\xi = 2, \lambda = 1$ and for present day values $\beta = 14.5$, $\Omega_m = 0.3$. All plots begin from the critical point C being a stable attractor.

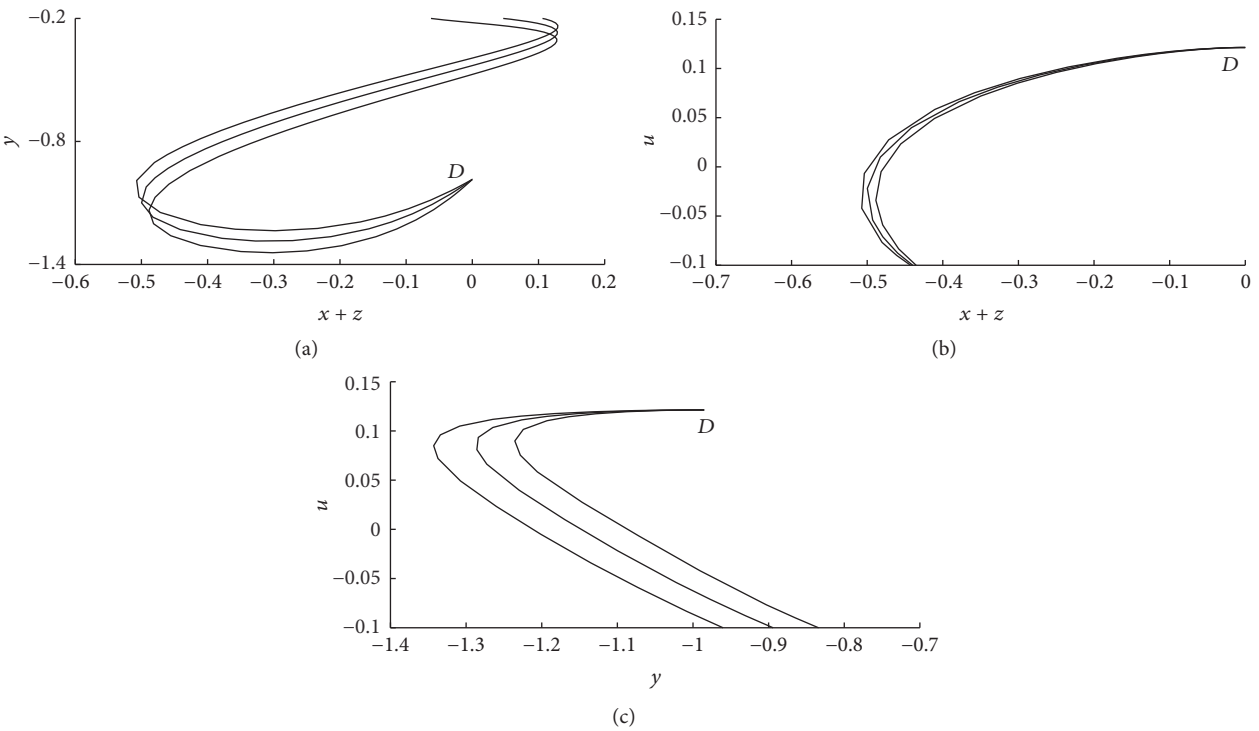

FIGURE 4: Two-dimensional projections of the phase-space trajectories for stability conditions $\xi = 2, \lambda = 1$ and for present day values $\beta = 14.5$, $\Omega_m = 0.3$. All plots begin from the critical point D being a stable attractor.

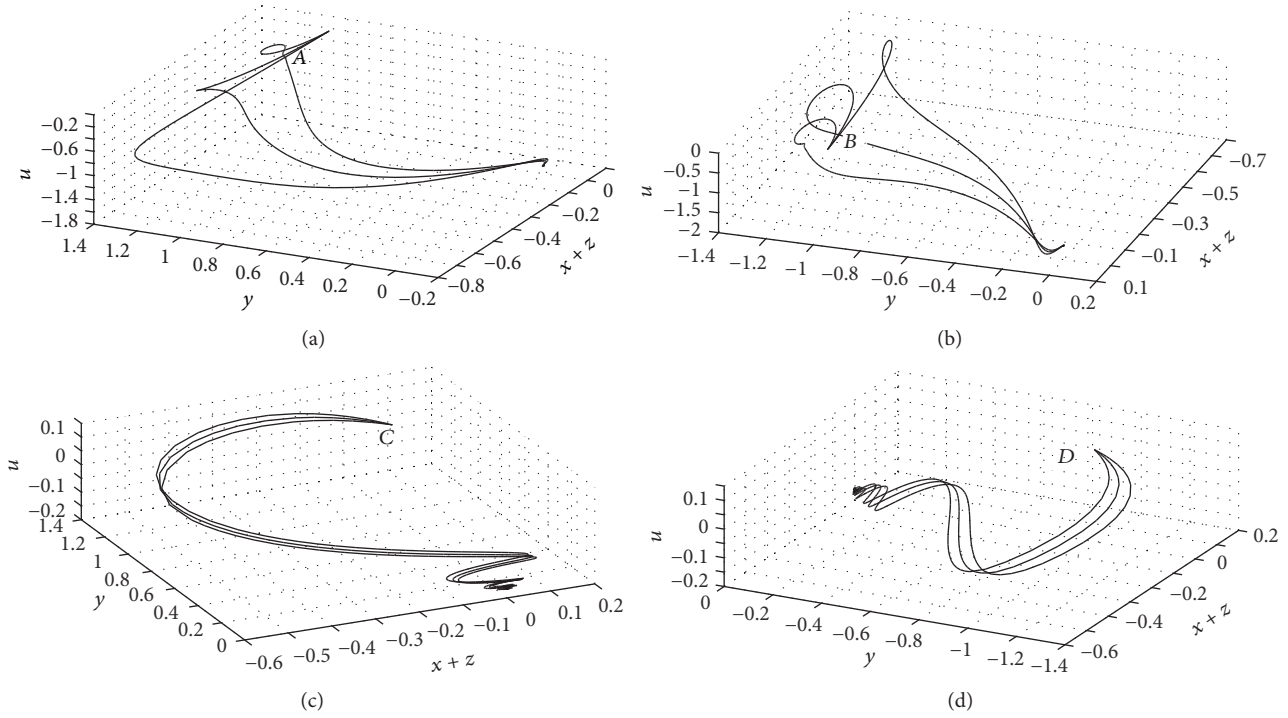

Figure 5: Three-dimensional plots of the phase-space trajectories for the critical points A, B, C, and D being the stable attractors.

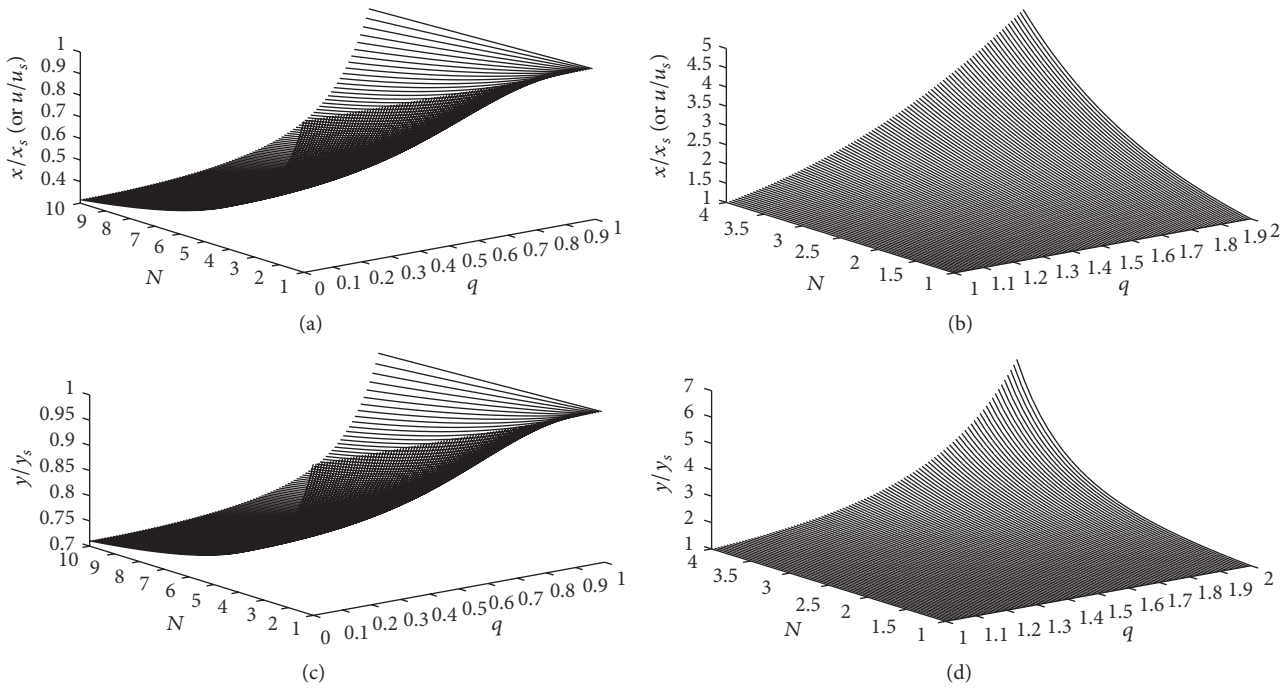

Figure 6: Behavior of the auxiliary variables x, y, and u with respect to the deformation parameter q and the particle number N.

deformed x, y, and u decreases with decreasing q for the $q < 1$ interval for large particle number, and the decrease in the variables x, y, and u refers to the decrease in deformed energy density. Also, we conclude that the value of the auxiliary variables x, y, and u increases with increasing q for the $q > 1$ interval for large particle number. In $q \to 1$ limit deformed variables goes to standard ones.

4. Conclusion

In this study, we propose that the dark energy is formed of the negative-pressure q-deformed scalar field whose field equation is defined by the q-deformed annihilation and creation operators satisfying the deformed boson algebra in (2), since it is known that the dark energy has a negative pressure—like the deformed bosons—acting as a gravitational repulsion to drive the accelerated expansion of universe. We consider an interacting dark matter and q-deformed dark energy nonminimally coupled to the gravity in the framework of Einsteinian gravity in order to confirm our proposal. Then we investigate the dynamics of the model and phase-space analysis whether it will give stable attractor solutions meaning indirectly an accelerating expansion phase of universe. Therefore, we construct the action integral of the interacting dark matter and q-deformed dark energy nonminimally coupled to gravity model in order to study its dynamics. With this the Hubble parameter and Friedmann equations of the model are obtained in the spatially flat FRW geometry. Later on, we find the energy density and pressure with the evolution equations for the q-deformed dark energy and dark matter from the variation of the action and the Lagrangian of the model. After that we translate these dynamical equations into the autonomous form by introducing the suitable auxiliary variables, in order to perform the phase-space analysis of the model. Then the critical points of autonomous system are obtained by setting each autonomous equation to zero and four perturbation matrices are obtained for each critical point by constructing the perturbation equations. We then determine the eigenvalues of four perturbation matrices to examine the stability of the critical points. We also calculate some important cosmological parameters, such as the total equation of state parameter and the deceleration parameter to check whether the critical points satisfy an accelerating universe. We obtain four stable attractors for the model depending on the coupling parameter ξ, interaction parameter β, and the potential constant λ. An accelerating universe exists for all stable solutions due to $\omega_{\text{tot}} < -1/3$. The critical points A and B are late-time stable attractors for $0 < \xi \leq 3/16$ and $\lambda, \beta \in \Re$, with the point A referring to an expansion with a stable acceleration, while the point B refers to a contraction. However, the critical points C and D are late-time stable attractors for $0 < \xi$, $\lambda = 1$, and $\beta \in \Re$, with the point C referring to an expansion with a stable acceleration, while the point D refers to a contraction. The stable attractor behavior of the model at each critical point is demonstrated in Figures 1–4. In order to solve the differential equation system (42), (44), and (45) with the critical points and plot the graphs in Figures 1–4, we use adaptive Runge-Kutta method of 4th and 5th order, in MATLAB programming. Then the solutions with the stability conditions of critical points are plotted for each pair of the solution set being the auxiliary variables in $x + z$, y, and u.

These figures show that, by using the convenient parameters of the model according to the existence and stability conditions and the present day values, we can obtain the stable attractors as A, B, C, and D.

The q-deformed dark energy is a generalization of the standard scalar field dark energy. As seen from (9) in the $q \to 1$ limit, the behavior of the deformed energy density, pressure, and scalar field functions with respect to the standard functions all approach the standard corresponding function values. Consequently, q-deformation of the scalar field dark energy gives a self-consistent model due to the existence of standard case parameters of the dark energy in the $q \to 1$ limit and the existence of the stable attractor behavior of the accelerated expansion phase of universe for the considered interacting and nonminimally coupled dark energy and dark matter model. Although the deformed dark energy model is confirmed through reproducing the same stability behaviors, critical points, and perturbation matrices with the standard dark energy model, the auxiliary variables of deformed and standard models are of course different. By using the auxiliary variable equations in (31), we find the relation between deformed and standard dark energy variables. From these equations, we represent the behavior of the deformed and standard dark energy auxiliary variables with respect to the deformation parameter for $q < 1$ and $q > 1$ intervals in Figure 6. Then, the value of the deformed x, y, and u or equivalently deformed energy density decreases with decreasing q for the $q < 1$ interval for large particle number. Also the value of the auxiliary variables x, y, and u increases with increasing q for the $q > 1$ interval for large particle number. In $q \to 1$ limit all the deformed variables transform to nondeformed variables.

The consistency of the proposed q-deformed scalar field dark energy model is confirmed by the results, since it gives the expected behavior of the universe. The idea of considering the dark energy as a q-deformed scalar field is a very recent approach. There are more deformed particle algebras in the literature which can be considered as other and maybe more suitable candidates for the dark energy. As a further study for the confirmation of whether the dark energy can be considered as a general deformed scalar field, the other interactions and couplings between deformed dark energy models, dark matter, and gravity can be investigated in the general relativity framework or in the framework of other modified gravity theories, such as teleparallelism.

Competing Interests

The author declares that there is no conflict of interests regarding the publication of this paper.

References

[1] S. Perlmutter, G. Aldering, G. Goldhaber et al., "Measurements of Ω and λ from 42 high-redshift supernovae," *The Astrophysical Journal*, vol. 517, no. 2, pp. 565–586, 1999.

[2] A. G. Riess, A. V. Filippenko, P. Challis et al., "Observational evidence from supernovae for an accelerating universe and a cosmological constant," *Astronomical Journal*, vol. 116, no. 3, pp. 1009–1038, 1998.

[3] U. Seljak, A. Makarov, P. McDonald et al., "Cosmological parameter analysis including SDSS Lyα forest and galaxy bias: constraints on the primordial spectrum of fluctuations, neutrino mass, and dark energy," *Physical Review D*, vol. 71, no. 10, Article ID 103515, 2005.

[4] M. Tegmark, M. A. Strauss, M. R. Blanton et al., "Cosmological parameters from SDSS andWMAP," *Physical Review D*, vol. 69, no. 10, Article ID 103501, 2004.

[5] D. J. Eisenstein, I. Zehavi, D. W. Hogg et al., "Detection of the baryon acoustic peak in the large-scale correlation function of SDSS luminous red galaxies," *Astrophysical Journal Letters*, vol. 633, no. 2, pp. 560–574, 2005.

[6] D. N. Spergel, L. Verde, H. V. Peiris et al., "First-year wilkinson microwave anisotropy probe (WMAP)* observations: determination of cosmological parameters," *Astrophysical Journal, Supplement Series*, vol. 148, no. 1, pp. 175–194, 2003.

[7] E. Komatsu, K. M. Smith, J. Dunkley et al., "Seven-year wilkinson microwave anisotropy probe (WMAP*) observations: cosmological interpretation," *The Astrophysical Journal, Supplement Series*, vol. 192, no. 2, 2011.

[8] G. Hinshaw, D. Larson, E. Komatsu et al., "Nine-year wilkinson microwave anisotropy probe (WMAP) observations: cosmological parameter results," *Astrophysical Journal, Supplement Series*, vol. 208, no. 2, article 19, 2013.

[9] P. A. R. Ade, N. Aghanim, C. Armitage-Caplan et al., "Planck 2013 results. XVI. Cosmological parameters," *Astronomy & Astrophysics*, vol. 571, article A16, 66 pages, 2013.

[10] P. A. R. Ade, N. Aghanim, M. Arnaud et al., "Planck 2015 results. XIII. Cosmological parameters," *Astronomy & Astrophysics*, vol. 594, article A13, 2015.

[11] F. Zwicky, "On the masses of nebulae and of clusters of nebulae," *The Astrophysical Journal*, vol. 86, pp. 217–246, 1937.

[12] H. W. Babcock, "The rotation of the Andromeda nebula," *Lick Observatory Bulletin*, vol. 498, pp. 41–51, 1939.

[13] C. Wetterich, "Cosmology and the fate of dilatation symmetry," *Nuclear Physics, Section B*, vol. 302, no. 4, pp. 668–696, 1988.

[14] B. Ratra and P. J. E. Peebles, "Cosmological consequences of a rolling homogeneous scalar field," *Physical Review D*, vol. 37, no. 12, p. 3406, 1988.

[15] E. J. Copeland, M. Sami, and S. Tsujikawa, "Dynamics of dark energy," *International Journal of Modern Physics. D. Gravitation, Astrophysics, Cosmology*, vol. 15, no. 11, pp. 1753–1935, 2006.

[16] M. Li, X.-D. Li, S. Wang, and Y. Wang, "Dark energy," *Communications in Theoretical Physics*, vol. 56, no. 3, pp. 525–604, 2011.

[17] C. Wetterich, "The cosmon model for an asymptotically vanishing time dependent cosmological 'constant'," *Astronomy & Astrophysics*, vol. 301, pp. 321–328, 1995.

[18] L. Amendola, "Coupled quintessence," *Physical Review D*, vol. 62, no. 4, Article ID 043511, 2000.

[19] N. Dalal, K. Abazajian, E. Jenkins, and A. V. Manohar, "Testing the cosmic coincidence problem and the nature of dark energy," *Physical Review Letters*, vol. 87, no. 14, Article ID 141302, 2001.

[20] W. Zimdahl, D. Pavón, and L. P. Chimento, "Interacting quintessence," *Physics Letters, Section B: Nuclear, Elementary Particle and High-Energy Physics*, vol. 521, no. 3-4, pp. 133–138, 2001.

[21] B. Gumjudpai, T. Naskar, M. Sami, and S. Tsujikawa, "Coupled dark energy: towards a general description of the dynamics," *Journal of Cosmology and Astroparticle Physics*, vol. 506, article 7, 2005.

[22] A. P. Billyard and A. A. Coley, "Interactions in scalar field cosmology," *Physical Review D*, vol. 61, no. 8, Article ID 083503, 2000.

[23] J.-Q. Xia, Y.-F. Cai, T.-T. Qiu, G.-B. Zhao, and X. Zhang, "Constraints on the sound speed of dynamical dark energy," *International Journal of Modern Physics D*, vol. 17, no. 8, pp. 1229–1243, 2008.

[24] A. Vikman, "Can dark energy evolve to the phantom?" *Physical Review D*, vol. 71, no. 2, Article ID 023515, 2005.

[25] W. Hu, "Crossing the phantom divide: dark energy internal degrees of freedom," *Physical Review D—Particles, Fields, Gravitation and Cosmology*, vol. 71, no. 4, Article ID 047301, 2005.

[26] R. R. Caldwell and M. Doran, "Dark-energy evolution across the cosmological-constant boundary," *Physical Review D—Particles, Fields, Gravitation and Cosmology*, vol. 72, no. 4, Article ID 043527, pp. 1–6, 2005.

[27] G.-B. Zhao, J.-Q. Xia, M. Li, B. Feng, and X. Zhang, "Perturbations of the quintom models of dark energy and the effects on observations," *Physical Review D*, vol. 72, no. 12, Article ID 123515, 2005.

[28] M. Kunz and D. Sapone, "Crossing the phantom divide," *Physical Review D*, vol. 74, no. 12, Article ID 123503, 2006.

[29] B. L. Spokoiny, "Inflation and generation of perturbations in broken-symmetric theory of gravity," *Physics Letters B*, vol. 147, no. 1-3, pp. 39–43, 1984.

[30] F. Perrotta, C. Baccigalupi, and S. Matarrese, "Extended quintessence," *Physical Review D*, vol. 61, no. 2, Article ID 023507, 2000.

[31] E. Elizalde, S. Nojiri, and S. D. Odintsov, "Late-time cosmology in a (phantom) scalar-tensor theory: dark energy and the cosmic speed-up," *Physical Review D*, vol. 70, no. 4, Article ID 043539, 2004.

[32] K. Bamba, S. Capozziello, S. Nojiri, and S. D. Odintsov, "Dark energy cosmology: the equivalent description via different theoretical models and cosmography tests," *Astrophysics and Space Science*, vol. 342, no. 1, pp. 155–228, 2012.

[33] O. Hrycyna and M. Szydowski, "Non-minimally coupled scalar field cosmology on the phase plane," *Journal of Cosmology and Astroparticle Physics*, vol. 2009, no. 4, article no. 26, 2009.

[34] O. Hrycyna and M. Szydłowski, "Extended quintessence with nonminimally coupled phantom scalar field," *Physical Review D*, vol. 76, no. 12, Article ID 123510, 2007.

[35] R. C. de Souza and G. M. Kremer, "Constraining non-minimally coupled tachyon fields by the Noether symmetry," *Classical and Quantum Gravity*, vol. 26, no. 13, Article ID 135008, 2009.

[36] A. A. Sen and N. C. Devi, "Cosmology with non-minimally coupled k-field," *General Relativity and Gravitation*, vol. 42, no. 4, pp. 821–838, 2010.

[37] E. Dil and E. Kolay, "Dynamics of mixed dark energy domination in teleparallel gravity and phase-space analysis," *Advances in High Energy Physics*, vol. 2015, Article ID 608252, 20 pages, 2015.

[38] S. Weinberg, "The cosmological constant problem," *Reviews of Modern Physics*, vol. 61, no. 1, pp. 1–23, 1989.

[39] S. M. Carroll, W. H. Press, and E. L. Turner, "The cosmological constant," *Annual Review of Astronomy and Astrophysics*, vol. 30, no. 1, pp. 499–542, 1992.

[40] L. M. Krauss and M. S. Turner, "The cosmological constant is back," *General Relativity and Gravitation*, vol. 27, no. 11, pp. 1137–1144, 1995.

[41] G. Huey, L. Wang, R. Dave, R. R. Caldwell, and P. J. Steinhardt, "Resolving the cosmological missing energy problem," *Physical Review D - Particles, Fields, Gravitation and Cosmology*, vol. 59, no. 6, pp. 1–6, 1999.

[42] P. Kulish and N. Reshetiknin, "Quantum linear problem for the Sine-Gordon equation and higher representations," *Journal of Soviet Mathematics*, vol. 23, no. 4, pp. 2435–2441, 1981.

[43] E. Sklyanin, L. Takhatajan, and L. Faddeev, "Quantum inverse problem method. I," *Theoretical and Mathematical Physics*, vol. 40, no. 2, pp. 688–706, 1979.

[44] L. C. Biedenharn and M. A. Lohe, *Quantum Group Symmetry and Q-Tensor Algebras* , World Scientific Publishing, River Edge, NJ, USA, 1995.

[45] M. Arik and D. D. Coon, "Hilbert spaces of analytic functions and generalized coherent states," *Journal of Mathematical Physics*, vol. 17, no. 4, pp. 524–527, 1976.

[46] A. J. Macfarlane, "On q-analogues of the quantum harmonic oscillator and the quantum group SUq(2)," *Journal of Physics A*, vol. 22, no. 21, pp. 4581–4588, 1989.

[47] L. C. Biedenharn, "The quantum group $SU_q(2)$ and a q-analogue of the boson operators," *Journal of Physics. A: Mathematical and General*, vol. 22, no. 18, pp. L873–L878, 1989.

[48] L. Tripodi and C. L. Lima, "On a q-covariant form of the BCS approximation," *Physics Letters. B*, vol. 412, no. 1-2, pp. 7–13, 1997.

[49] V. S. Timóteo and C. L. Lima, "Effect of q-deformation in the NJL gap equation," *Physics Letters B*, vol. 448, no. 1-2, pp. 1–5, 1999.

[50] C. R. Lee and J. P. Yu, "On q-analogues of the statistical distribution," *Physics Letters. A*, vol. 150, no. 2, pp. 63–66, 1990.

[51] J. A. Tuszynski, J. L. Rubin, J. Meyer, and M. Kibler, "Statistical mechanics of a q-deformed boson gas," *Physics Letters A*, vol. 175, no. 3-4, pp. 173–177, 1993.

[52] P. N. Swamy, "Interpolating statistics and q-deformed oscillator algebras," *International Journal of Modern Physics B*, vol. 20, no. 6, pp. 697–713, 2006.

[53] M. R. Ubriaco, "Thermodynamics of a free $SU_q(2)$ fermionic system," *Physics Letters. A*, vol. 219, no. 3-4, pp. 205–211, 1996.

[54] M. R. Ubriaco, "High and low temperature behavior of a quantum group fermion gas," *Modern Physics Letters A*, vol. 11, no. 29, pp. 2325–2333, 1996.

[55] M. R. Ubriaco, "Anyonic behavior of quantum group gases," *Physical Review E. Statistical, Nonlinear, and Soft Matter Physics*, vol. 55, no. 1, part A, pp. 291–296, 1997.

[56] A. Lavagno and P. N. Swamy, "Thermostatistics of a q-deformed boson gas," *Physical Review E*, vol. 61, no. 2, pp. 1218–1226, 2000.

[57] A. Lavagno and P. N. Swamy, "Generalized thermodynamics of q-deformed bosons and fermions," *Physical Review E—Statistical, Nonlinear, and Soft Matter Physics*, vol. 65, no. 3, Article ID 036101, 2002.

[58] A. Algin and M. Baser, "Thermostatistical properties of a two-parameter generalised quantum group fermion gas," *Physica A: Statistical Mechanics and Its Applications*, vol. 387, no. 5-6, pp. 1088–1098, 2008.

[59] A. Algin, M. Arik, and A. S. Arikan, "High temperature behavior of a two-parameter deformed quantum group fermion gas," *Physical Review E*, vol. 65, no. 2, Article ID 026140, p. 026140/5, 2002.

[60] A. Algin, A. S. Arikan, and E. Dil, "High temperature thermostatistics of fermionic Fibonacci oscillators with intermediate statistics," *Physica A: Statistical Mechanics and its Applications*, vol. 416, pp. 499–517, 2014.

[61] O. W. Greenberg, "Particles with small violations of Fermi or Bose statistics," *Physical Review D*, vol. 43, no. 12, pp. 4111–4120, 1991.

[62] A. M. Gavrilik, I. I. Kachurik, and Y. A. Mishchenko, "Quasi-bosons composed of two q-fermions: realization by deformed oscillators," *Journal of Physics A: Mathematical and Theoretical*, vol. 44, no. 47, Article ID 475303, 2011.

[63] P. Pouliot, "Finite number of states, de Sitter space and quantum groups at roots of unity," *Classical and Quantum Gravity*, vol. 21, no. 1, pp. 145–162, 2004.

[64] A. Strominger, "Black hole statistics," *Physical Review Letters*, vol. 71, no. 21, pp. 3397–3400, 1993.

[65] E. Dil, "Q-deformed einstein equations," *Canadian Journal of Physics*, vol. 93, no. 11, pp. 1274–1278, 2015.

[66] E. Dil and E. Kolay, "Solution of deformed Einstein equations and quantum black holes," *Advances in High Energy Physics*, vol. 2016, Article ID 3973706, 7 pages, 2016.

[67] D. Bonatsos, E. N. Argyres, and P. P. Raychev, "$SU_q(1,1)$ description of vibrational molecular spectra," *Journal of Physics A: Mathematical and General*, vol. 24, no. 8, pp. L403–L408, 1991.

[68] D. Bonatsos, P. P. Raychev, and A. Faessler, "Quantum algebraic description of vibrational molecular spectra," *Chemical Physics Letters*, vol. 178, no. 2-3, pp. 221–226, 1991.

[69] D. Bonatsos and C. Daskaloyannis, "Generalized deformed oscillators for vibrational spectra of diatomic molecules," *Physical Review A*, vol. 46, no. 1, pp. 75–80, 1992.

[70] P. P. Raychev, R. P. Roussev, and Y. F. Smirnov, "The quantum algebra $SU_q(2)$ and rotational spectra of deformed nuclei," *Journal of Physics G: Nuclear and Particle Physics*, vol. 16, no. 8, pp. L137–L141, 1990.

[71] A. I. Georgieva, K. D. Sviratcheva, M. I. Ivanov, and J. P. Draayer, "q-Deformation of symplectic dynamical symmetries in algebraic models of nuclear structure," *Physics of Atomic Nuclei*, vol. 74, no. 6, pp. 884–892, 2011.

[72] M. R-Monteiro, L. M. C. S. Rodrigues, and S. Wulck, "Quantum algebraic nature of the phonon spectrum in4He," *Physical Review Letters*, vol. 76, no. 7, 1996.

[73] A. E. Shalyt-Margolin, "Deformed quantum field theory, thermodynamics at low and high energies, and gravity. II. Deformation parameter," *International Journal of Theoretical and Mathematical Physics*, vol. 2, no. 3, pp. 41–50, 2012.

[74] A. E. Shalyt-Margolin and V. I. Strazhev, "Dark energy and deformed quantum theory in physics of the early universe. In non-eucleden geometry in modern physics," in *Proceedings of the 5th Intentional Conference of Bolyai-Gauss-Lobachevsky (BGL-5 '07)*, Y. Kurochkin and V. Red'kov, Eds., pp. 173–178, Minsk, Belarus, 2007.

[75] Y. J. Ng, "Holographic foam, dark energy and infinite statistics," *Physics Letters, Section B: Nuclear, Elementary Particle and High-Energy Physics*, vol. 657, no. 1–3, pp. 10–14, 2007.

[76] Y. J. Ng, "Spacetime foam," *International Journal of Modern Physics D*, vol. 11, no. 10, pp. 1585–1590, 2002.

[77] M. Chaichian, R. G. Felipe, and C. Montonen, "Statistics of q-oscillators, quons and relations to fractional statistics," *Journal of Physics A: Mathematical and General*, vol. 26, no. 16, pp. 4017–4034, 1993.

[78] J. Wess and B. Zumino, "Covariant differential calculus on the quantum hyperplane," *Nuclear Physics B—Proceedings Supplements*, vol. 18, no. 2, pp. 302–312, 1991.

[79] G. Vinod, *Studies in quantum oscillators and q-deformed quantum mechanics [Ph.D. thesis]*, Cochin University of Science and Technology, Department of Physics, Kochi, India, 1997.

[80] B. K. Berger, "Scalar particle creation in an anisotropic universe," *Physical Review D*, vol. 12, no. 2, pp. 368–375, 1975.

[81] S. W. Hawking, "Breakdown of predictability in gravitational collapse," *Physical Review D*, vol. 14, no. 10, pp. 2460–2473, 1976.

[82] B. K. Berger, "Classical analog of cosmological particle creation," *Physical Review D*, vol. 18, no. 12, pp. 4367–4372, 1978.

[83] L. Parker, "Quantized fields and particle creation in expanding universes. I," *Physical Review*, vol. 183, no. 5, article 1057, 1969.

[84] J. W. Goodison and D. J. Toms, "No generalized statistics from dynamics in curved spacetime," *Physical Review Letters*, vol. 71, no. 20, 1993.

[85] D. Bonatsos and C. Daskaloyannis, "Quantum groups and their applications in nuclear physics," *Progress in Particle and Nuclear Physics*, vol. 43, no. 1, pp. 537–618, 1999.

[86] R. G. Leigh, "Dirac-born-infeld action from dirichlet σ-model," *Modern Physics Letters A*, vol. 04, no. 28, pp. 2767–2772, 1989.

[87] N. A. Chernikov and E. A. Tagirov, "Quantum theory of scalar field in de Sitter space-time," *Annales de l'I.H.P. Physique Théorique*, vol. 9, pp. 109–141, 1968.

[88] C. G. Callan Jr., S. Coleman, and R. Jackiw, "A new improved energy-momentum tensor," *Annals of Physics*, vol. 59, pp. 42–73, 1970.

[89] V. Faraoni, "Inflation and quintessence with nonminimal coupling," *Physical Review D*, vol. 62, no. 2, Article ID 023504, 2000.

[90] S. C. Park and S. Yamaguchi, "Inflation by non-minimal coupling," *Journal of Cosmology and Astroparticle Physics*, vol. 2008, no. 8, p. 9, 2008.

[91] A. de Felice and S. Tsujikawa, "f(R) theories," *Living Reviews in Relativity*, vol. 13, article no. 3, 2010.

[92] S. Nojiri and S. D. Odintsov, "Unified cosmic history in modified gravity: from F(R) theory to Lorentz non-invariant models," *Physics Reports*, vol. 505, no. 2–4, pp. 59–144, 2011.

[93] S. Nojiri and S. D. Odintsov, "Introduction to modified gravity and gravitational alternative for dark energy," *International Journal of Geometric Methods in Modern Physics*, vol. 4, no. 1, pp. 115–146, 2007.

[94] A. Banijamali, "Dynamics of interacting tachyonic teleparallel dark energy," *Advances in High Energy Physics*, vol. 2014, Article ID 631630, 14 pages, 2014.

[95] B. Fazlpour and A. Banijamali, "Tachyonic teleparallel dark energy in phase space," *Advances in High Energy Physics*, vol. 2013, Article ID 279768, 9 pages, 2013.

[96] P. G. Ferreira and M. Joyce, "Structure formation with a self-tuning scalar field," *Physical Review Letters*, vol. 79, no. 24, pp. 4740–4743, 1997.

[97] E. J. Copeland, A. R. Liddle, and D. Wands, "Exponential potentials and cosmological scaling solutions," *Physical Review D*, vol. 57, no. 8, pp. 4686–4690, 1998.

[98] X.-M. Chen, Y. Gong, and E. N. Saridakis, "Phase-space analysis of interacting phantom cosmology," *Journal of Cosmology and Astroparticle Physics*, vol. 2009, no. 4, article no. 001, 2009.

[99] Z.-K. Guo, Y.-S. Piao, X. Zhang, and Y.-Z. Zhang, "Cosmological evolution of a quintom model of dark energy," *Physics Letters, Section B: Nuclear, Elementary Particle and High-Energy Physics*, vol. 608, no. 3-4, pp. 177–182, 2005.

[100] R. Lazkoz and G. León, "Quintom cosmologies admitting either tracking or phantom attractors," *Physics Letters B*, vol. 638, no. 4, pp. 303–309, 2006.

[101] Z.-K. Guo, Y.-S. Piao, X. Zhang, and Y.-Z. Zhang, "Two-field quintom models in the $w - w^{'}$ plane," *Physical Review D*, vol. 74, no. 12, Article ID 127304, 4 pages, 2006.

[102] R. Lazkoz, G. León, and I. Quiros, "Quintom cosmologies with arbitrary potentials," *Physics Letters B*, vol. 649, no. 2-3, pp. 103–110, 2007.

[103] M. Alimohammadi, "Asymptotic behavior of ω in general quintommodel," *General Relativity and Gravitation*, vol. 40, no. 1, pp. 107–115, 2008.

[104] M. R. Setare and E. N. Saridakis, "Coupled oscillators as models of quintom dark energy," *Physics Letters, Section B*, vol. 668, no. 3, pp. 177–181, 2008.

[105] M. R. Setare and E. N. Saridakis, "Quintom cosmology with general potentials," *International Journal of Modern Physics. D. Gravitation, Astrophysics, Cosmology*, vol. 18, no. 4, pp. 549–557, 2009.

[106] M. R. Setare and E. N. Saridakis, "The quintom model with O(N) symmetry," *Journal of Cosmology and Astroparticle Physics*, vol. 2008, no. 9, article no. 026, 2008.

[107] M. R. Setare and E. N. Saridakis, "Quintom dark energy models with nearly flat potentials," *Physical Review D*, vol. 79, no. 4, Article ID 043005, 2009.

[108] G. Leon, R. Cardenas, and J. L. Morales, "Equilibrium sets in quintom cosmologies: the past asymptotic dynamics," https://arxiv.org/abs/0812.0830.

[109] S. Carloni, E. Elizalde, and P. J. Silva, "An analysis of the phase space of Hořava–Lifshitz cosmologies," *Classical and Quantum Gravity*, vol. 27, no. 4, Article ID 045004, 2010.

[110] Z.-K. Guo, Y.-S. Piao, R.-G. Cai, and Y.-Z. Zhang, "Inflationary attractor from tachyonic matter," *Physical Review D*, vol. 68, no. 4, Article ID 043508, 2003.

[111] L. A. Ureña-López and M. J. Reyes-Ibarra, "On the dynamics of a quadratic scalar field potential," *International Journal of Modern Physics D*, vol. 18, no. 4, pp. 621–634, 2009.

[112] V. A. Belinsky, L. P. Grishchuk, I. M. Khalatnikov, and Y. B. Zeldovich, "Inflationary stages in cosmological models with a scalar field," *Physics Letters B*, vol. 155, no. 4, pp. 232–236, 1985.

[113] T. Piran and R. M. Williams, "Inflation in universes with a massive scalar field," *Physics Letters B*, vol. 163, no. 5-6, pp. 331–335, 1985.

[114] A. R. Liddle and D. H. Lyth, *Cosmological inflation and large-scale structure*, Cambridge University Press, Cambridge, England, 2000.

[115] V. V. Kiselev and S. A. Timofeev, "Quasiattractor dynamics of $\lambda\phi$4-inflation," https://arxiv.org/abs/0801.2453.

[116] S. Downes, B. Dutta, and K. Sinha, "Attractors, universality, and inflation," *Physical Review D*, vol. 86, no. 10, Article ID 103509, 2012.

[117] J. Khoury and P. J. Steinhardt, "Generating scale-invariant perturbations from rapidly-evolving equation of state," *Physical Review D—Particles, Fields, Gravitation and Cosmology*, vol. 83, no. 12, Article ID 123502, 2011.

[118] S. Clesse, C. Ringeval, and J. Rocher, "Fractal initial conditions and natural parameter values in hybrid inflation," *Physical Review D*, vol. 80, no. 12, Article ID 123534, 2009.

[119] V. V. Kiselev and S. A. Timofeev, "Quasiattractor in models of new and chaotic inflation," *General Relativity and Gravitation*, vol. 42, no. 1, pp. 183–197, 2010.

[120] G. F. R. Ellis, R. Maartens, and M. A. H. MacCallum, *Relativistic cosmology*, Cambridge University Press, Cambridge, UK, 2012.

[121] Y. Wang, J. M. Kratochvil, A. Linde, and M. Shmakova, "Current observational constraints on cosmic doomsday," *Journal of Cosmology and Astroparticle Physics*, vol. 412, article 6, 2004.

[122] L. Amendola and D. Tocchini-Valentini, "Stationary dark energy: the present universe as a global attractor," *Physical Review D*, vol. 64, no. 4, Article ID 043509, 2001.

Hindawi Publishing Corporation
Advances in High Energy Physics
Volume 2016, Article ID 3740957, 10 pages
http://dx.doi.org/10.1155/2016/3740957

Research Article

Spinor Quintom Cosmology with Intrinsic Spin

Emre Dil

Department of Physics, Sinop University, Korucuk, 57000 Sinop, Turkey

Correspondence should be addressed to Emre Dil; emredil@sakarya.edu.tr

Received 5 October 2016; Revised 5 November 2016; Accepted 7 November 2016

Academic Editor: Dandala R. K. Reddy

We consider a spinor quintom dark energy model with intrinsic spin, in the framework of Einstein-Cartan-Sciama-Kibble theory. After constructing the mathematical formalism of the model, we obtain the spin contributed total energy-momentum tensor giving the energy density and the pressure of the quintom model, and then we find the equation of state parameter, Hubble parameter, deceleration parameter, state finder parameter, and some distance parameter in terms of the spinor potential. Choosing suitable potentials leads to the quintom scenario crossing between quintessence and phantom epochs, or vice versa. Analyzing three quintom scenarios provides stable expansion phases avoiding Big Rip singularities and yielding matter dominated era through the stabilization of the spinor pressure via spin contribution. The stabilization in spinor pressure leads to neglecting it as compared to the increasing energy density and constituting a matter dominated stable expansion epoch.

1. Introduction

The astrophysical observations show that the universe is experiencing an accelerating expansion due to an unknown component of energy, named as the dark energy (DE) which is distributed all over the universe and having a negative pressure in order to drive the acceleration of the universe [1–9]. Various DE scenarios have been proposed: cosmological constant Λ is the oldest DE model which has a constant energy density filling the space homogeneously [10–13]. Equation of state (EoS) parameter of a cosmological fluid is $\omega = p/\rho$, where p and ρ are the pressure and energy density and the DE scenario formed by the cosmological constant refers to a perfect fluid with EoS $\omega_\Lambda = -1$.

Other DE scenarios can be constructed from the dynamical components, such as the quintessence, phantom, K-essence, or quintom [14–16]. Quintessence is considered as a DE scenario with EoS $\omega > -1$. Such a model can be described by using a canonical scalar field. Recent observational data presents the idea that the EoS of DE can be in a region where $\omega < -1$. The most common scenario generalizing this regime is to use a scalar field with a negative kinetic term. This DE model is known as the phantom scenario which is also named as a ghost [17]. This model experiences the shortcoming, such that its energy state is unbounded from below and this leads to the quantum instability problem [18]. If the potential value is not bounded from above, this scenario is even instable at the classical regime known as the Big Rip singularity [19]. Another DE scenario, K-essence, is constructed by using kinetic term in the domain of a general function in the field Lagrangian. This model can realize both $\omega > -1$ and $\omega < -1$ due to the existence of a positive energy density but cannot allow a consistent crossing of the cosmological constant boundary -1 [20].

The time variation of the EoS of DE has been restricted by the data obtained by Supernovae Ia (SNIa). According to the SNIa data, some attempts have come out to estimate the band power and density of the DE EoS as a function of the redshift [21]. There occur two main models for the variation of EoS with respect to time; Model A and Model B. While Model A is valid in low redshift, Model B suffers in low redshift; therefore, it works in high redshift values. These models imply that the evolution of the DE EoS begins from $\omega > -1$ in the past to $\omega < -1$ in the present time, namely, the observational and theoretical results allow the EoS ω of DE crossing the cosmological constant boundary or phantom divide during the evolution of the universe [22–25].

Crossing of the DE EoS the cosmological constant boundary is named as the quintom scenario and this can be constructed in some special DE models. For instance, if we consider a single perfect fluid or single scalar field DE constituent, this model does not allow the DE EoS to cross the $\omega = -1$ boundary according to the no-go theorem [26–31]. To overcome no-go theorem and to realize crossing phantom divide line, some modifications can be made to the single scalar field DE models. One can construct a quintom scenario by considering two scalar fields, such as quintessence and quintom [22]. The components cannot cross the −1 boundary alone but can cross it combined together. Another quintom scenario is achieved by constructing a scalar field model with nonlinear or higher order derivative kinetic term [27, 32] or a phantom model coupled to dark matter [33]. Also the scalar field DE models nonminimally coupled to gravity satisfy the crossing cosmological constant boundary [34, 35].

The aforementioned quintom models are constructed from the scalar fields providing various phantom behaviors, but the ghost field may cause some instable solutions. By considering the linearized perturbations in the effective quantum field equation at two-loop order one can obtain an acceleration phase [36–40]. On the other hand, there is another quintom model satisfying the acceleration of the universe, which is constructed from the classical homogeneous spinor field ψ [41–44]. In recent years, many studies for spinor fields in cosmology can be found [20], such as those for inflation and cyclic universe driven by spinor fields, for spinor matter in Bianchi Type I spacetime, and for a DE model with spinor matter [45–50].

The consistent quintom cosmology has been proposed by using spinor matter in Friedmann-Robertson-Walker (FRW) geometry, in Einstein's general relativity framework [51]. The spinor quintom scenario allows EoS crossing −1 boundary without using a ghost field. When the derivative of the potential term with respect to the scalar bilinear $\overline{\psi}\psi$ becomes negative, the spinor field shows a phantom-like behavior. But the spinor quintom exhibits a quintessence-like behavior for the positive definite potential derivative [20]. In this quintom model, there exist three categories of scenario depending on the choice of the type of potentials; one scenario is that the universe evolves from a quintessence-like phase $\omega > -1$ to a phantom-like phase $\omega < -1$, another scenario is for the universe evolving from a phantom-like phase $\omega < -1$ to a quintessence-like phase $\omega > -1$, and the third scenario is that the EoS of spinor quintom DE crosses the −1 boundary more than one time.

In this study, we consider the spinor quintom DE, in the framework of Einstein-Cartan-Sciama-Kibble (ECSK) theory which is a generalization of the metric-affine formulation of Einstein's general relativity with intrinsic spin [52–61]. Since the ECSK theory is the simplest theory including the intrinsic spin and avoiding the big-bang singularity [62], it is worth considering the spinor quintom in ECSK theory for investigating the acceleration phase of the universe with the phantom behavior. Therefore, we analyze the spinor quintom model with intrinsic spin in ECSK theory whether it provides the crossing cosmological constant boundary. Then if the model provides the crossing −1 boundary, we will find the suitable conditions on the potential for the crossing −1 boundary.

2. Algebra of Spinor Quintom with Intrinsic Spin

The most complicated example of the quantum field theories lying in curved spacetime is the theory of Dirac spinors. There occurs a conceptual problem related to obtaining the energy-momentum tensor of the spinor matter field from the variation of the matter field Lagrangian. For the scalar or tensor fields, energy-momentum tensor is the quantity describing the reaction of the matter field Lagrangian to the variations of the metric, while the matter field is held constant during the change of the metric. But for the spinor fields, the above procedure does not hold for obtaining the energy-momentum tensor from the variation with respect to metric only, because the spinor fields are the sections of a spinor bundle obtained as an associated vector bundle from the bundle of spin frames. The bundle of spin frames is double covering of the bundle of oriented and time-oriented orthonormal frames. For spinor fields, when one varies the metric, the components of the spinor fields cannot be held fixed with respect to some fixed holonomic frame induced by a coordinate system, as in the tensor field case [63]. Therefore, the intrinsic spin of matter field in curved spacetime requires ECSK theory which is the simplest generalization of the metric-affine formulation of general relativity.

According to the metric-affine formulation of the gravity, the dynamical variables are the tetrad (vierbein or frame) field e^i_a and the spin connection $\omega^a_{bk} = e^a_j e^j_{b;k} = e^a_j(e^j_{b,k} + \Gamma^j_{ik}e^i_b)$. Here comma denotes the partial derivative with respect to the x^k coordinate, while the semicolon refers to the covariant derivative with respect to the affine connection Γ^i_{jk}. The antisymmetric lower indices of the affine connection give the torsion tensor $S^i_{jk} = \Gamma^i_{[jk]}$. The tetrad gives the relation between spacetime coordinates denoted by the indices $i, j, k, \ldots$ and local Lorentz coordinates denoted by the indices $a, b, c, \ldots$, such that $V^a = V^i e^a_i$, where V^a is a Lorentz vector and V^i is a usual vector. Covariant derivative of a Lorentz vector is defined with respect to the spin connection and denoted by a bar: $V^a_{|i} = V^a_{,i} + \omega^a_{bi}V^b$ and $V_{a|i} = V_{a,i} - \omega^b_{ai}V_b$. Also the covariant derivative of a vector is defined in terms of the affine connection: $V^k_{;i} = V^k_{,i} + \Gamma^k_{li}V^l$ and $V_{k;i} = V_{k,i} - \Gamma^l_{ki}V_l$. Local Lorentz coordinates are lowered or raised by the Minkowski metric η_{ab} of the flat spacetime, while the spacetime coordinates are lowered or raised by the metric tensor g_{ik}. Metric compatibility condition $g_{ij;k} = 0$ leads to the definition of affine connection $\Gamma^k_{ij} = \left\{ {k \atop ij} \right\} + C^k_{ij}$ in terms of the Christoffel symbols $\left\{ {k \atop ij} \right\} = (1/2)g^{km}(g_{mi,j} + g_{mj,i} - g_{ij,m})$ and the contortion tensor $C^i_{jk} = S^i_{jk} + 2S^i_{(jk)}$. Throughout the paper, the $A_{(jk)} = (1/2)(A_{jk} + A_{kj})$ notation is used for symmetrization and $A_{[jk]} = A_{jk} - A_{kj}$ is used for the antisymmetrization. With the definitions $g_{ik} = \eta_{ab}e^a_i e^b_k$ and $S^j_{ik} =$

$\omega^{j}_{[ik]} + e^{a}_{[i,k]}e^{j}_{a}$, the metric tensor and the torsion tensor can be considered as the dynamical variable instead of the tetrad and spin connection.

A tensor density $\mathrm{A}^{ij\cdots}_{kl\cdots}$ is given in terms of the corresponding tensor $A^{ij\cdots}_{kl\cdots}$ as $\mathrm{A}^{ij\cdots}_{kl\cdots} = eA^{ij\cdots}_{kl\cdots}$, where $e = \det e^{a}_{i} = \sqrt{-\det g_{ik}}$. Therefore, we represent the spin density and the energy-momentum density, such as $\sigma_{ijk} = es_{ijk}$ and $\mathrm{T}_{ik} = eT_{ik}$. Here we call these tensors metric spin tensor and metric energy-momentum tensor, since the spacetime coordinate indices label these tensors and are obtained from the variation of the Lagrangian with respect to the torsion (or contortion) tensor C^{ij}_{k} and the metric tensor g^{ij}, respectively. The metric spin tensor is written as $s^{k}_{ij} = (2/e)(\delta\ell_m/\delta C^{ij}_{k}) = (2/e)(\partial\ell_m/\partial C^{ij}_{k})$, while the metric energy-momentum tensor is given by $T_{ij} = (2/e)(\delta\ell_m/\delta g^{ij}) = (2/e)[\partial\ell_m/\partial g^{ij} - \partial_k(\partial\ell_m/\partial(g^{ij}_{,k}))]$. Here, the Lagrangian density of the source matter field is $\ell_m = eL_m$. When the local Lorentz coordinates are also used in these tensors as $\sigma^{i}_{ab} = es^{i}_{ab}$ and $\mathrm{T}^{a}_{i} = eT^{a}_{i}$, we call s^{i}_{ab} and T^{a}_{i} dynamical spin tensor and dynamical energy-momentum tensor, respectively, and they are obtained from the variation of the Lagrangian with respect to the tetrad e^{i}_{a} and the spin connection ω^{ab}_{i}. The dynamical spin tensor is $s^{i}_{ab} = (2/e)(\delta\ell_m/\delta\omega^{ab}_{i}) = (2/e)(\partial\ell_m/\partial\omega^{ab}_{i})$, and energy-momentum tensor is $T^{a}_{i} = (1/e)(\delta\ell_m/\delta e^{i}_{a}) = (1/e)[\partial\ell_m/\partial e^{i}_{a} - \partial_j(\partial\ell_m/\partial(e^{i}_{a,j}))]$.

Total action of the gravitational field and the source matter in metric-affine ECSK theory is given in the same form with the classical Einstein-Hilbert action, such as $S = \kappa\int(\ell_g + \ell_m)d^4x$, where $\kappa = 8\pi G$ and $\ell_g = -(1/2\kappa)eR$ is the gravitational Lagrangian density. Here Ricci scalar is constructed from the spin connection containing curvature tensor, such that $R = R^{b}_{j}e^{j}_{b}$, where $R^{b}_{j} = R^{bc}_{jk}e^{k}_{c}$ is the Ricci tensor obtained from the curvature tensor R^{bc}_{jk} and finally this curvature tensor is expressed in terms of the spin connection, such that $R^{a}_{bij} = \omega^{a}_{bj,i} - \omega^{a}_{bi,j} + \omega^{a}_{ci}\omega^{c}_{bj} - \omega^{a}_{cj}\omega^{c}_{bi}$. Variation of the total action with respect to the contortion tensor gives Cartan equations $S^{j}_{ik} - S_i\delta^{j}_{k} + S_k\delta^{j}_{i} = -(\kappa/2e)\sigma^{j}_{ik}$ and with respect to the metric tensor gives Einstein equations in the form of $G_{ik} = \kappa(T_{ik} + U_{ik})$, where $G_{ik} = P^{j}_{ijk} - (1/2)P^{lm}_{lm}g_{ik}$ is the Einstein tensor and P^{j}_{ijk} is the Riemann curvature tensor satisfying $R^{i}_{klm} = P^{i}_{klm} + C^{i}_{km:l} - C^{i}_{kl:m} + C^{j}_{km}C^{i}_{jl} - C^{j}_{kl}C^{i}_{jm}$, where colon denotes the Riemannian covariant derivative with respect to the Levi-Civita connection, such as $V^{k}_{:i} = V^{k}_{,i} + \left\{ {k \atop li} \right\}V^{l}$ and $V_{k:i} = V_{k,i} - \left\{ {l \atop ki} \right\}V_l$. Also for torsion-free general relativity theory, curvature tensor turns out to be the Riemann tensor. Right hand side of Einstein equations contains an extra term U_{ik} which is the contribution to the energy-momentum tensor from the torsion and it is quadratic in the spin tensor, such as $U_{ik} = \kappa(-s^{ij}_{[l}s^{kl}_{j]} - (1/2)s^{ijl}s^{k}_{jl} + (1/4)s^{jli}s^{k}_{jl} + (1/8)g^{ik}(-4s^{l}_{j[m}s^{jm}_{l]} + s^{jlm}s_{jlm}))$. Therefore, the total energy-momentum tensor is $\Theta_{ik} = T_{ik} + U_{ik}$.

In metric-affine ECSK formulation of gravity, a spinor quintom field with intrinsic spin has a Lagrangian density of the form $\ell_m = e(i/2)(\overline{\psi}\gamma^{k}\psi_{;k} - \overline{\psi}_{;k}\gamma^{k}\psi) - eV$, where V is the potential of the spinor field ψ and the adjoint spinor $\overline{\psi} = \psi^{+}\gamma^{0}$. The covariant derivative of the spinor field is given as $\psi_{;k} = \psi_{,k} - \Gamma_k\psi$ and $\overline{\psi}_{;k} = \overline{\psi}_{,k} - \Gamma_k\overline{\psi}$, where $\Gamma_k = -(1/4)\omega_{abk}\gamma^{a}\gamma^{b}$ is the Fock-Ivanenko spin connection, and then γ^{k} and γ^{a} are the metric and dynamical Dirac gamma matrices satisfying $\gamma^{k} = e^{k}_{a}\gamma^{a}$, $\gamma^{(k}\gamma^{m)} = g^{km}I$, and $\gamma^{(a}\gamma^{b)} = \eta^{ab}I$. The covariant derivative of the spinor can be decomposed into the Riemannian covariant derivative plus a contortion tensor C_{ijk} containing term, such as $\psi_{;k} = \psi_{:k} + (1/4)C_{ijk}\gamma^{[i}\gamma^{j]}\psi$ and $\overline{\psi}_{;k} = \overline{\psi}_{:k} - (1/4)C_{ijk}\overline{\psi}\gamma^{[i}\gamma^{j]}$. The Riemannian covariant derivative of the spinor and adjoint spinor fields for quintom DE are given: $\psi_{:k} = \psi_{,k} + (1/4)g_{ik}\left\{ {i \atop jm} \right\}\gamma^{j}\gamma^{m}\psi$ and $\overline{\psi}_{:k} = \overline{\psi}_{,k} - (1/4)g_{ik}\left\{ {i \atop jm} \right\}\gamma^{j}\gamma^{m}\overline{\psi}$. These covariant derivatives including the contortion tensor C_{ijk} are embedded in the spinor quintom Lagrange density. However, the explicit form of the contortion tensor which can be obtained from the Cartan equations is needed. Since the right hand side of Cartan equations contains the spin tensor density, we obtain the spin tensor from the variation of the spinor Lagrangian with respect to the contortion tensor, such that $s^{ijk} = (1/e)\sigma^{ijk} = -(1/e)\varepsilon^{ijkl}s_l$, where ε^{ijkl} is the Levi-Civita symbol, $s^{i} = (1/2)\,\overline{\psi}\gamma^{i}\gamma^{5}\psi$ is the spin pseudovector, and $\gamma^{5} = i\gamma^{0}\gamma^{1}\gamma^{2}\gamma^{3}$. Inserting the spin tensor for spinor quintom field in the Cartan equations gives the torsion tensor $S_{ijk} = C_{ijk} = (1/2)\kappa\varepsilon_{ijkl}s^{l}$ which will take place in the spinor quintom Lagrange density [52–62].

The variation of the spinor quintom matter Lagrangian density with respect to the adjoint spinor gives the ECSK Dirac equation, such as

$$i\gamma^{k}\psi_{:k} - \frac{\partial V}{\partial\overline{\psi}} + \frac{3}{8}\kappa\left(\overline{\psi}\gamma^{k}\gamma^{5}\psi\right)\gamma_k\gamma^{5}\psi = 0, \tag{1}$$

and the variation with respect to the spinor itself gives adjoint Dirac equation as

$$i\overline{\psi}_{:k}\gamma^{k} + \frac{\partial V}{\partial\psi} - \frac{3}{8}\kappa\left(\overline{\psi}\gamma^{k}\gamma^{5}\psi\right)\overline{\psi}\gamma_k\gamma^{5} = 0. \tag{2}$$

Then the total energy-momentum tensor of the spinor quintom field is obtained from $\Theta_{ik} = T_{ik} + U_{ik}$. Here the metric energy-momentum tensor is obtained by the variation of spinor quintom Lagrange density with respect to the metric tensor, such as

$$\begin{aligned} T_{ik} &= \frac{2}{e}\left[\frac{\partial\ell_m/\partial g^{ik}}{-\partial_j\left(\partial\ell_m/\partial\left(g^{ik}_{,j}\right)\right)}\right] \\ &= \frac{i}{2}\left(\overline{\psi}\delta^{j}_{(i}\gamma_{k)}\psi_{;j} - \overline{\psi}_{;j}\delta^{j}_{(i}\gamma_{k)}\psi\right) \\ &\quad - \frac{i}{2}\left(\overline{\psi}\gamma^{j}\psi_{;j} - \overline{\psi}_{;j}\gamma^{j}\psi\right)g_{ik} + Vg_{ik}, \end{aligned} \tag{3}$$

and the spin contributing metric energy-momentum tensor is obtained by substituting the spin tensor for spinor quintom

field in U_{ik}. Then the total metric energy-momentum tensor is found to be

$$\Theta_{ik} = \frac{i}{2}\left(\overline{\psi}\delta^{j}_{(i}\gamma_{k)}\psi_{:j} - \overline{\psi}_{:j}\delta^{j}_{(i}\gamma_{k)}\psi\right) + \frac{3}{4}\kappa s^{l}s_{l}g_{ik}. \quad (4)$$

Here, the semicolon covariant derivatives of the spinor field in (3) are decoupled into colon covariant derivatives in (4) and the contortion tensor containing parts of the decoupled covariant derivatives are suppressed in the spin pseudovector s^{l} by the contribution of U_{ik}. In order to rewrite (4) in a more convenient form for our further calculations, we multiply (1) by adjoint spinor $\overline{\psi}$ from the left and multiply (2) by spinor ψ from right, such that

$$i\overline{\psi}\gamma^{k}\psi_{:k} - V'\overline{\psi}\psi + \frac{3}{8}\kappa\left(\overline{\psi}\gamma^{k}\gamma^{5}\psi\right)\left(\overline{\psi}\gamma_{k}\gamma^{5}\psi\right) = 0, \quad (5)$$

$$i\overline{\psi}_{:k}\gamma^{k}\psi + V'\overline{\psi}\psi - \frac{3}{8}\kappa\left(\overline{\psi}\gamma^{k}\gamma^{5}\psi\right)\left(\overline{\psi}\gamma_{k}\gamma^{5}\psi\right) = 0, \quad (6)$$

where $V' = \partial V/\partial(\overline{\psi}\psi)$ for which $\overline{\psi}(\partial V/\partial\overline{\psi}) = (\partial V/\partial\psi)\psi = V'\overline{\psi}\psi$. By using (5) and writing the symmetrizations explicitly in (4), we obtain the total energy-momentum tensor Θ_{ik} of the spinor field dark energy in the form of

$$\begin{aligned}\Theta_{ik} = {} & \frac{i}{4}\left(\overline{\psi}\gamma_{i}\psi_{:k} + \overline{\psi}\gamma_{k}\psi_{:i} - \overline{\psi}_{:i}\gamma_{k}\psi - \overline{\psi}_{:k}\gamma_{i}\psi\right) \\ & + \frac{1}{2}\left(V'\overline{\psi}\psi - i\overline{\psi}\gamma^{l}\psi_{:l}\right)g_{ik}.\end{aligned} \quad (7)$$

We consider the spinor quintom DE model in FRW spacetime whose metric is given as

$$ds^{2} = dt^{2} - a^{2}(t)\left[dx^{2} + dy^{2} + dz^{2}\right], \quad (8)$$

and the corresponding tetrad components read

$$\begin{aligned} e^{i}_{0} &= \delta^{i}_{0}, \\ e^{i}_{a} &= \frac{1}{a(t)}\delta^{i}_{a}. \end{aligned} \quad (9)$$

Therefore, by performing the Riemannian covariant derivatives explicitly in (7), the time-like components Θ^{ψ}_{00} and the space-like components Θ^{ψ}_{u} of the space independent spinor field dark energy energy-momentum tensor can be obtained, such as

$$\Theta_{00} = -\frac{i}{2}\dot{\overline{\psi}}\gamma_{0}\psi + \frac{1}{2}V'\overline{\psi}\psi - \frac{3i}{8}H\overline{\psi}\gamma_{0}\psi, \quad (10)$$

$$\Theta_{u} = -\frac{i}{2}\overline{\psi}\gamma_{0}\dot{\psi}g_{u} + \frac{1}{2}V'\overline{\psi}\psi g_{u} - \frac{3i}{8}H\overline{\psi}\gamma_{0}\psi g_{u}. \quad (11)$$

Here $H = \dot{a}(t)/a(t)$ is the Hubble parameter and it comes from the Levi-Civita connections in the Riemannian covariant derivatives. We now write ECSK Dirac equations (4) and (5) for a space independent spinor field as

$$\begin{aligned} & i\overline{\psi}\gamma^{0}\dot{\psi} + \frac{3i}{4}H\overline{\psi}\gamma^{0}\psi - V'\overline{\psi}\psi \\ & \quad + \frac{3}{8}\kappa\left(\overline{\psi}\gamma^{0}\gamma^{5}\psi\right)\left(\overline{\psi}\gamma_{0}\gamma^{5}\psi\right) = 0, \end{aligned} \quad (12)$$

$$\begin{aligned} & i\dot{\overline{\psi}}\gamma^{0}\psi + \frac{3i}{4}H\overline{\psi}\gamma^{0}\psi + V'\overline{\psi}\psi \\ & \quad - \frac{3}{8}\kappa\left(\overline{\psi}\gamma^{0}\gamma^{5}\psi\right)\left(\overline{\psi}\gamma_{0}\gamma^{5}\psi\right) = 0. \end{aligned} \quad (13)$$

The solution of (12) and (13) by adding them leads to

$$\overline{\psi}\dot{\psi} + \dot{\overline{\psi}}\psi + \frac{3}{2}H\overline{\psi}\psi = 0, \quad (14)$$

$$\overline{\psi}\psi = \frac{N}{a^{3/2}}. \quad (15)$$

Here N is the integration constant, and then, by using the scale factor $a \propto e^{\beta t}$ for a cosmological fluid [64], we can also obtain $\overline{\psi}\psi = Ne^{-3\beta t/2}$. Using (13) in (10) leads to the energy density

$$\rho = \Theta^{0}_{0} = V'\overline{\psi}\psi - \frac{3}{16}\kappa\left(\overline{\psi}\gamma^{0}\gamma^{5}\psi\right)\left(\overline{\psi}\gamma_{0}\gamma^{5}\psi\right), \quad (16)$$

and similarly using (12) in (11) leads to the pressure of the spinor field dark energy

$$p = -\Theta^{t}_{t} = -\frac{3}{16}\kappa\left(\overline{\psi}\gamma^{0}\gamma^{5}\psi\right)\left(\overline{\psi}\gamma_{0}\gamma^{5}\psi\right), \quad (17)$$

respectively. Then the EoS of the spinor field is given as

$$\omega = \frac{p}{\rho} = \frac{(3/16)\kappa\left(\overline{\psi}\gamma^{0}\gamma^{5}\psi\right)^{2}}{(3/16)\kappa\left(\overline{\psi}\gamma^{0}\gamma^{5}\psi\right)^{2} - V'\overline{\psi}\psi}, \quad (18)$$

where $\gamma^{0} = \gamma_{0}$ for a FRW metric. We rewrite the EoS in the form of

$$\omega = -1 + \alpha, \quad (19)$$

where

$$\alpha = \frac{6\kappa\left(\overline{\psi}\gamma^{0}\gamma^{5}\psi\right)^{2} - 16V'\overline{\psi}\psi}{3\kappa\left(\overline{\psi}\gamma^{0}\gamma^{5}\psi\right)^{2} - 16V'\overline{\psi}\psi}. \quad (20)$$

It is known that for $\alpha = 4/3$ the EoS of the spinor field is $\omega = 1/3$ and it behaves like radiation, but for $\alpha = 1$, $\omega = 0$, and it is normal matter. On the other hand, if $\alpha < 2/3$, the EoS $\omega < -1/3$ meaning that the spinor field behaves like a DE leading to the acceleration of universe. The $\alpha < 2/3$ region allows us to investigate the dynamical evolution of the spinor quintom DE described in ECSK formalism with intrinsic spin.

3. Dynamical Evolution of Spinor Quintom

From (20) we deduce that the spinor field can have an EoS of $-1 < \omega < -1/3$ for $0 < \alpha < 2/3$ and shows a quintessence-like behavior, but it has $\omega = -1$ cosmological constant value if $\alpha = 0$, and then it behaves like a phantom for $\omega < -1$ if $\alpha < 0$. Therefore, the spinor field exhibits a quintom picture by crossing the cosmological constant boundary $\omega = -1$ from above or below this boundary depending on the sign of α in (20).

There exist three categories of spinor quintom evolution depending on the behavior of the potential V. The quintom scenario may exhibit an evolution starting from $-1 < \omega$ quintessence phase to $\omega < -1$ phantom phase, called Quintom-A. Another scenario may evolve from $\omega < -1$ to $-1 < \omega$, Quintom-B scenario. The last quintom scenario contains the evolution for crossing $\omega = -1$ more than one time, and it is called Quintom-C model.

Considering the quintom scenario in which the spinor field comes from $-1 < \omega$ quintessence phase to $\omega < -1$ phantom phase, we first need to find the condition $0 < \alpha$. Since the energy density (16) must be positive definite, V' is positive. Therefore, the condition of occurring $-1 < \omega$ phase reads from (20) as

$$16V'\overline{\psi}\psi > 6\kappa\left(\overline{\psi}\gamma^0\gamma^5\psi\right)^2. \tag{21}$$

Similarly, $\omega = -1$ boundary occurs for

$$16V'\overline{\psi}\psi = 6\kappa\left(\overline{\psi}\gamma^0\gamma^5\psi\right)^2, \tag{22}$$

and $\omega < -1$ phantom phase occurs for

$$16V'\overline{\psi}\psi < 6\kappa\left(\overline{\psi}\gamma^0\gamma^5\psi\right)^2. \tag{23}$$

Since prime denotes the derivative with respect to $\overline{\psi}\psi$, the solution of (22) is found as $V_\Lambda = (6\kappa/16)(\overline{\psi}\gamma^0\gamma^5\psi)^2 \ln\overline{\psi}\psi$, in which the dynamical evolution of potential goes to the cosmological constant boundary.

In order to obtain Quintom-A scenario, we define the potential to be

$$V = \left(\frac{6\kappa}{16}\right)\left(\overline{\psi}\gamma^0\gamma^5\psi\right)^2 \ln\overline{\psi}\psi - \left(c - \overline{\psi}\psi\right)\overline{\psi}\psi, \tag{24}$$

for the early times of the universe. Then the potential leads the EoS from (20) as

$$\omega = -1 + \frac{16\left(2\overline{\psi}\psi - c\right)\overline{\psi}\psi}{16\left(2\overline{\psi}\psi - c\right)\overline{\psi}\psi + (3\kappa/16)\left(\overline{\psi}\gamma^0\gamma^5\psi\right)^2}, \tag{25}$$

and the term $(2\overline{\psi}\psi - c)$ in this potential satisfies $-1 < \omega$ quintessence scenario (21) with (15), since the scaling factor a is very small at the beginning of the evolution of the universe. When $\overline{\psi}\psi$ becomes equal to $c/2$, this potential leads the spinor field to approach $\omega = -1$ boundary (22). After that scaling factor evolves to a greater value, then $\overline{\psi}\psi$ reaches a value smaller than $c/2$. This gives the condition (23) phantom phase $\omega < -1$. We illustrate this behavior in Figure 1

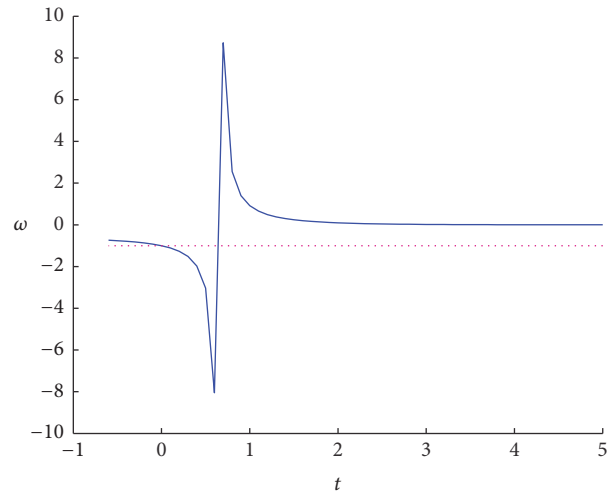

Figure 1: Evolution of ω with potential (24) as a function of time. For the numerical analysis we assume $N = 3$, $c = 6$, and $\beta = 1$. From [51].

by numerical analysis. According to the figure, ω starts its evolution from above -1 to below -1. We set the crossing cosmological constant boundary as at $t = 0$. After crossing the -1 boundary, spinor quintom picks up and is avoided from a Big Rip singularity and then enters a stable matter dominated expansion with $\omega = 0$ value.

We can also find other important cosmological quantities, such as luminosity distance, Hubble parameter, deceleration parameter, and jerk and state finder parameters. For this we use the Friedmann equations

$$\frac{\ddot{a}}{a} = -\frac{4\pi G}{3}(\rho + 3p), \tag{26}$$

$$\left(\frac{\dot{a}}{a}\right)^2 = \frac{8\pi G}{3}\rho. \tag{27}$$

By using (16) for the potential (24), we obtain spinor energy density as

$$\rho = \left(\frac{3\kappa}{16}\right)\left(\overline{\psi}\gamma^0\gamma^5\psi\right)^2 + \left(2\overline{\psi}\psi - c\right)\overline{\psi}\psi, \tag{28}$$

and substituting (15) and (28) in (27) we obtain

$$H = \frac{\dot{a}}{a} = \sqrt{\frac{8\pi G}{3}}\sqrt{\left(-\frac{3\kappa N^2}{8} + 2N^2\right)e^{-3\beta t} - cNe^{-3\beta t/2}}. \tag{29}$$

Solving the differential equation in (29) gives the scale factor as

$$a = \exp\left\{\sqrt{\frac{8\pi G}{3}}\left[C_1 + t\sqrt{2N^2 - \frac{3\kappa N^2}{8} - cN} + t^2\frac{3\beta\left(4N^2 - 3\kappa N^2/4 - cN\right)}{\sqrt{2N^2 - 3\kappa N^2/8 - cN}} + \cdots\right]\right\}, \tag{30}$$

from which we obtain the redshift

$$z = -1 + \exp\left\{-\sqrt{\frac{8\pi G}{3}}\left[C_1 + t\sqrt{2N^2 - \frac{3\kappa N^2}{8} - cN} + t^2\frac{3\beta\left(4N^2 - 3\kappa N^2/4 - cN\right)}{\sqrt{2N^2 - 3\kappa N^2/8 - cN}} + \cdots\right]\right\}. \quad (31)$$

Therefore, we can find the Luminosity distance

$$d_L = H_0^{-1}\left[z + \frac{1}{2}\left(1 - q_0\right)z^2 + \cdots\right], \quad (32)$$

in terms of the measurable quantities present time Hubble parameter H_0 and deceleration parameter q_0. Moreover, to find the deceleration parameter, we use (16) and (17) for the potential (24) and obtain the term in (26), such that

$$\rho + 3p = \left(-\frac{3\kappa}{8}\right)\left(\overline{\psi}\gamma^0\gamma^5\psi\right)^2 + \left(2\overline{\psi}\psi - c\right)\overline{\psi}\psi, \quad (33)$$

and inserting (15) and (33) in (26) we find

$$\frac{\ddot{a}}{a} = -\frac{4\pi G}{3}\left[\left(\frac{3\kappa N^2}{4} + 2N^2\right)e^{-3\beta t} - cNe^{-3\beta t/2}\right]. \quad (34)$$

Then, the deceleration parameter is obtained from (29) and (34), such as

$$q = -\frac{a\ddot{a}}{\dot{a}^2} = -H^{-2}\frac{\ddot{a}}{a} = \frac{1}{2}\frac{\left(3\kappa N^2/4 + 2N^2\right)e^{-3\beta t} - cNe^{-3\beta t/2}}{\left(-3\kappa N^2/8 + 2N^2\right)e^{-3\beta t} - cNe^{-3\beta t/2}}. \quad (35)$$

Also, we finally obtain the state finder parameters for spinor Quintom-A by taking time derivative of (34), such that

$$\left(\frac{\ddot{a}}{a}\right)^{\bullet} = 12\pi\beta G\left[\left(\frac{3\kappa N^2}{4} + 2N^2\right)e^{-3\beta t} - \frac{cN}{2}e^{-3\beta t/2}\right]. \quad (36)$$

Then the state finder parameter is

$$r = \frac{\dddot{a}}{aH^3} = \left(\frac{\ddot{a}}{a}\right)^{\bullet}H^{-3} - q = \frac{9\beta}{\sqrt{32\pi G}}\frac{\left(3\kappa N^2/4 + 2N^2\right)e^{-3\beta t} - (cN/2)e^{-3\beta t/2}}{\left(\left(-3\kappa N^2/8 + 2N^2\right)e^{-3\beta t} - cNe^{-3\beta t/2}\right)^{3/2}} - \frac{1}{2}\frac{\left(3\kappa N^2/4 + 2N^2\right)e^{-3\beta t} - cNe^{-3\beta t/2}}{\left(-3\kappa N^2/8 + 2N^2\right)e^{-3\beta t} - cNe^{-3\beta t/2}}, \quad (37)$$

and one can obtain the second state finder parameter $s = 2(r-1)/3(2q-1)$.

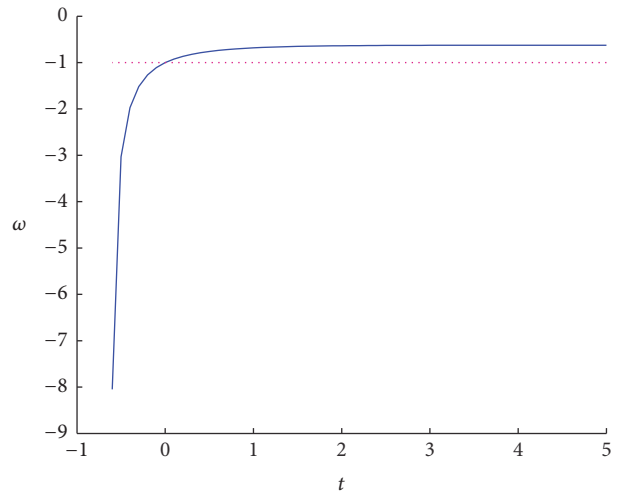

Figure 2: Evolution of ω with potential (38) as a function of time. For the numerical analysis we assume $N = 3$, $c = 3$, and $\beta = 1$. From [51].

For a Quintom-B model, the potential can be defined as

$$V = \left(\frac{6\kappa}{16}\right)\left(\overline{\psi}\gamma^0\gamma^5\psi\right)^2\ln\overline{\psi}\psi - \left(c - \overline{\psi}\psi\right)^2, \quad (38)$$

and then the EoS is obtained, such that

$$\omega = -1 + \frac{32\left(c - \overline{\psi}\psi\right)\overline{\psi}\psi}{32\left(c - \overline{\psi}\psi\right)\overline{\psi}\psi + (3\kappa/16)\left(\overline{\psi}\gamma^0\gamma^5\psi\right)^2}, \quad (39)$$

which lead to $\omega < -1$ phantom phase (23) at the beginning of the evolution of universe. With the increasing of the scale factor, $\overline{\psi}\psi$ decreases to c and the term $2(c - \overline{\psi}\psi)$ becomes zero. This gives $\omega = -1$ cosmological constant phase (22). As the evolution continues $\overline{\psi}\psi$ gets smaller than c and spinor quintom reaches a quintessence scenario $-1 < \omega$ in (21). The behavior of the spinor Quintom-B scenario is represented in Figure 2 which states that the spinor field starts the evolution from below $\omega = -1$ to above $\omega = -1$. Crossing from phantom to quintessence phase continues in this phase with an EoS value of $-1 < \omega < -1/3$ which imitates a stable de Sitter accelerated expansion for a scalar field dark energy model.

We proceed to find the other cosmological quantities; by using (16) for the potential (38), we get the quintom energy density

$$\rho = \left(\frac{3\kappa}{16}\right)\left(\overline{\psi}\gamma^0\gamma^5\psi\right)^2 + 2\left(c - \overline{\psi}\psi\right)\overline{\psi}\psi, \quad (40)$$

and inserting (15) and (40) in (27) we find

$$H = \frac{\dot{a}}{a} = \sqrt{\frac{8\pi G}{3}}\sqrt{\left(-\frac{3\kappa N^2}{8} - 2N^2\right)e^{-3\beta t} + 2cNe^{-3\beta t/2}}. \quad (41)$$

By solving the differential equation in (41), we obtain the scale factor as

$$a = \exp\left\{\sqrt{\frac{8\pi G}{3}}\left[C_2 + t\sqrt{2cN - 2N^2 - \frac{3\kappa N^2}{8}} + t^2\frac{3\beta\left(2cN - 4N^2 - 3\kappa N^2/4\right)}{\sqrt{2cN - 2N^2 - 3\kappa N^2/8}} + \cdots\right]\right\}, \tag{42}$$

which gives the redshift as

$$z = -1 + \exp\left\{-\sqrt{\frac{8\pi G}{3}}\left[C_2 + t\sqrt{2cN - 2N^2 - 3\kappa N^2/8} + t^2\frac{3\beta\left(2cN - 4N^2 - 3\kappa N^2/4\right)}{\sqrt{2cN - 2N^2 - 3\kappa N^2/8}} + \cdots\right]\right\}. \tag{43}$$

Thus we obtain the Luminosity distance $d_L = H_0^{-1}[z + (1/2)(1-q_0)z^2 + \cdots]$ in terms of the measurable quantities H_0 and q_0. Then to find the deceleration parameter, we use (16) and (17) for the potential (24) and obtain the term in (26), such that

$$\rho + 3p = \left(-\frac{3\kappa}{8}\right)\left(\overline{\psi}\gamma^0\gamma^5\psi\right)^2 + 2\left(c - \overline{\psi}\psi\right)\overline{\psi}\psi, \tag{44}$$

and inserting (15) and (44) in (26) we obtain

$$\frac{\ddot{a}}{a} = -\frac{4\pi G}{3}\left[\left(\frac{3\kappa N^2}{4} - 2N^2\right)e^{-3\beta t} + 2cNe^{-3\beta t/2}\right]. \tag{45}$$

The deceleration parameter is obtained from (41) and (45) as

$$q = -\frac{a\ddot{a}}{\dot{a}^2} = -H^{-2}\frac{\ddot{a}}{a} = \frac{1}{2}\frac{\left(3\kappa N^2/4 - 2N^2\right)e^{-3\beta t} + cNe^{-3\beta t/2}}{\left(-3\kappa N^2/8 - 2N^2\right)e^{-3\beta t} + cNe^{-3\beta t/2}}. \tag{46}$$

We can obtain the state finder parameters for spinor Quintom-B from the time derivative of (45) as

$$\left(\frac{\ddot{a}}{a}\right)^{\bullet} = 12\pi\beta G\left[\left(\frac{3\kappa N^2}{4} - 2N^2\right)e^{-3\beta t} + cNe^{-3\beta t/2}\right], \tag{47}$$

and the state finder parameter is

$$r = \frac{\dddot{a}}{aH^3} = \left(\frac{\ddot{a}}{a}\right)^{\bullet}H^{-3} - q = \frac{9\beta}{\sqrt{32\pi G}} \cdot \frac{\left(3\kappa N^2/4 - 2N^2\right)e^{-3\beta t} + cNe^{-3\beta t/2}}{\left(\left(-3\kappa N^2/8 - 2N^2\right)e^{-3\beta t} + 2cNe^{-3\beta t/2}\right)^{3/2}} - \frac{1}{2} \cdot \frac{\left(3\kappa N^2/4 - 2N^2\right)e^{-3\beta t} + cNe^{-3\beta t/2}}{\left(-3\kappa N^2/8 - 2N^2\right)e^{-3\beta t} + cNe^{-3\beta t/2}}, \tag{48}$$

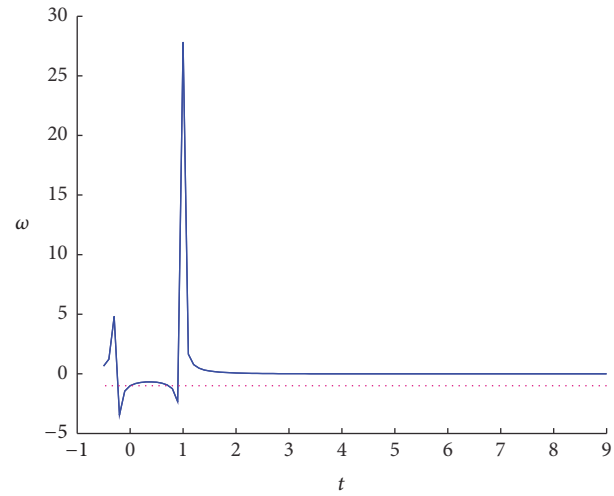

Figure 3: Evolution of ω with potential (49) as a function of time. For the numerical analysis we assume $N = 3$, $c = 3$, and $\beta = 1$. From [51].

from which we can obtain the second state finder parameter $s = 2(r-1)/3(2q-1)$.

Third case Quintom-C scenario can be obtained for the potential

$$V = \left(\frac{6\kappa}{16}\right)\left(\overline{\psi}\gamma^0\gamma^5\psi\right)^2 \ln\overline{\psi}\psi - \left(c - \overline{\psi}\psi\right)^2\overline{\psi}\psi, \tag{49}$$

which leads the EoS as

$$\omega = -1 + \frac{16\left(c - 3\overline{\psi}\psi\right)\left(\overline{\psi}\psi - c\right)\overline{\psi}\psi}{16\left(c - 3\overline{\psi}\psi\right)\left(\overline{\psi}\psi - c\right)\overline{\psi}\psi + (3\kappa/16)\left(\overline{\psi}\gamma^0\gamma^5\psi\right)^2}. \tag{50}$$

This potential provides two roots in $V'\overline{\psi}\psi$ for crossing the $\omega = -1$ boundary. The term coming from the derivative of V is $-3(\overline{\psi}\psi)^2 + 4c\overline{\psi}\psi - c^2$ which determines the sign of $16V'\overline{\psi}\psi$ in (21)–(23). During the evolution of universe with the increase in scale factor, $\overline{\psi}\psi$ decreases firstly to the value c which is the bigger root. This is a transition from phantom phase to quintessence phase by crossing -1 boundary. After continuing the evolution $\overline{\psi}\psi$ decreases to the second root $c/3$ which is recrossing the -1 boundary as a transition from quintessence phase to phantom phase again. This scenario is obviously a Quinton-C scenario and is illustrated in Figure 3. We see from the figure that the EoS of the quintom model crosses the $\omega = -1$ boundary twice, firstly from below $\omega = -1$ to above $\omega = -1$ and secondly from above to below $\omega = -1$, then it picks up and then is avoided from Big Rip singularities, and finally it asymptotically evolves to a stable matter dominated expansion epoch with a value of $\omega = 0$.

Although considering the phantom scenarios normally leads to the Big Rip singularities due to the unbound of EoS from below $\omega = -1$, our spinor quintom model with intrinsic spin in ECSK theory is avoided from the Big Rip singularities by picking up to a bound value and approaching a stable value, as seen in Figures 1 and 3. Diverging EoS of a dark fluid

from a constant bound toward a lower singularity refers to continuous increase in the pressure of the fluid. This scenario is avoided in spinor quintom with intrinsic spin, which may be interpreted as the intrinsic spin of the fluid quanta leads to a bound pressure value. The increase of the pressure with the energy density is bounded due to the effect of intrinsic spin, then singular values of EoS are avoided, and the universe enters a stable expansion in the final era.

We now obtain other cosmological quantities; by using (16) for the potential (49), we get the Quintom-C energy density as

$$\rho = \left(\frac{3\kappa}{16}\right)\left(\overline{\psi}\gamma^0\gamma^5\psi\right)^2 + \left(c - 3\overline{\psi}\psi\right)\left(\overline{\psi}\psi - c\right)\overline{\psi}\psi, \tag{51}$$

and inserting (15) and (51) in (27) we find

$$H = \frac{\dot{a}}{a} = \sqrt{\frac{8\pi G}{3}}\sqrt{\left(-\frac{3\kappa N^2}{8} + 4cN^2\right)e^{-3\beta t} - c^2 N e^{-3\beta t/2} - 3N^3 e^{-9\beta t/2}}. \tag{52}$$

We now solve the differential equation in (52) to obtain the scale factor, such that

$$a = \exp\left\{\sqrt{\frac{8\pi G}{3}}\left[C_{3+}t\sqrt{4cN^2 - c^2N - 3N^3 - 3\kappa N^2/8} + t^2\frac{3\beta\left(8cN^2 - c^2N + 9N^3 - 3\kappa N^2/4\right)}{\sqrt{4cN^2 - c^2N - 3N^3 - 3\kappa N^2/8}} + \cdots\right]\right\}, \tag{53}$$

and this gives the redshift, such as

$$z = -1 + \exp\left\{-\sqrt{\frac{8\pi G}{3}}\left[C_3 + t\sqrt{4cN^2 - c^2N - 3N^3 - 3\kappa N^2/8} + t^2\frac{3\beta\left(8cN^2 - c^2N + 9N^3 - 3\kappa N^2/4\right)}{\sqrt{4cN^2 - c^2N - 3N^3 - 3\kappa N^2/8}} + \cdots\right]\right\}. \tag{54}$$

Therefore, we can find the luminosity distance as $d_L = H_0{}^{-1}[z + (1/2)(1 - q_0)z^2 + \cdots]$ in terms of the quantities H_0 and q_0. Here the deceleration parameter is again obtained by using (16) and (17) for the potential (49) and obtaining the term in (26), such that

$$\rho + 3p = \left(-\frac{3\kappa}{8}\right)\left(\overline{\psi}\gamma^0\gamma^5\psi\right)^2 + \left(c - 3\overline{\psi}\psi\right)\left(\overline{\psi}\psi - c\right)\overline{\psi}\psi, \tag{55}$$

and by substituting (15) and (55) in (26) we obtain

$$\frac{\ddot{a}}{a} = -\frac{4\pi G}{3}\left[\left(-\frac{3\kappa N^2}{4} + 4cN^2\right)e^{-3\beta t} - c^2 N e^{-3\beta t/2} - 3N^3 e^{-9\beta t/2}\right]. \tag{56}$$

The deceleration parameter is obtained from (52) and (56) as

$$q = -\frac{a\ddot{a}}{\dot{a}^2} = -H^{-2}\frac{\ddot{a}}{a} = \frac{1}{2} \cdot \frac{\left(-3\kappa N^2/4 + 4cN^2\right)e^{-3\beta t} - c^2 N e^{-3\beta t/2} - 3N^3 e^{-9\beta t/2}}{\left(-3\kappa N^2/8 + 4cN^2\right)e^{-3\beta t} - c^2 N e^{-3\beta t/2} - 3N^3 e^{-9\beta t/2}}. \tag{57}$$

By using the time derivative of (56), we obtain the state finder parameters for Quintom-C model as

$$\left(\frac{\ddot{a}}{a}\right)^{\bullet} = 12\pi\beta G\left[\left(-\frac{3\kappa N^2}{4} + 4cN^2\right)e^{-3\beta t} - \frac{c^2 N}{2}e^{-3\beta t/2} + \frac{9N^3}{2}e^{-9\beta t/2}\right], \tag{58}$$

and the state finder parameter is

$$r = \frac{\dddot{a}}{aH^3} = \frac{9\beta}{\sqrt{32\pi G}}\frac{\left(-3\kappa N^2/4 + 4cN^2\right)e^{-3\beta t} - \left(c^2 N/2\right)e^{-3\beta t/2} + \left(9N^3/2\right)e^{-9\beta t/2}}{\left(\left(-3\kappa N^2/8 + 4cN^2\right)e^{-3\beta t} - c^2 N e^{-3\beta t/2} - 3N^3 e^{-9\beta t/2}\right)^{3/2}} - \frac{1}{2}\frac{\left(-3\kappa N^2/4 + 4cN^2\right)e^{-3\beta t} - c^2 N e^{-3\beta t/2} - 3N^3 e^{-9\beta t/2}}{\left(-3\kappa N^2/8 + 4cN^2\right)e^{-3\beta t} - c^2 N e^{-3\beta t/2} - 3N^3 e^{-9\beta t/2}}, \tag{59}$$

from which we can obtain the second state finder parameter $s = 2(r - 1)/3(2q - 1)$.

4. Conclusion

By using the spinor field dark energy in a FRW geometry, a consistent quintom model, in which EoS crosses −1 boundary without using a ghost field, has recently been obtained in the framework of general relativity [51]. Here, we consider the spinor field dark energy with intrinsic spin in the formalism of metric-affine ECSK theory. We first introduce the ECSK formalism and then define the model Lagrangian whose variations with respect to the tetrad field and torsion tensor give the total energy-momentum tensor consisting of metric

and spin contributions. Also from the variation of Lagrangian with respect to the spinor field we obtain the ECSK Dirac equation. By using the total energy-momentum tensor and ECSK Dirac equation, the energy density and the pressure values of the spinor quintom DE are obtained, from which the EoS of the model is obtained for an arbitrary potential. The dependence of the potential on the spinor field leads to the evolution of potential with the change of scale factor, since the scale factor increases by time. Constructing the ECSK spinor potential suitably the quintom scenario is reached, for three different cases as Quintom-A, Quintom-B, and Quintom-C models. We also obtained the redshift values for three quintom scenarios from the scale factors of each quintom model. Then, we find other cosmological parameters, such as the Hubble parameter, deceleration parameter, and state finder parameters for three different potential values of each quintom scenario, respectively.

The Quintom-A case exhibits the transition of EoS from quintessence phase to phantom phase, evolving to a stable matter dominated expansion with $\omega \to 0$. This scenario is avoided from the Big Rip singularities due to the balancing of energy density and pressure of spinor DE by intrinsic spin. Similarly, in the Quintom-B scenario, the EoS of the model evolves from phantom region $\omega < -1$ to quintessence region $\omega > -1$ and approaches an EoS value of $-1 < \omega < -1/3$ referring to a stable de Sitter accelerated expansion for a scalar field dark energy model. On the other hand, the Quintom-C scenario exhibits the evolution of EoS which crossed the cosmological constant boundary $\omega = -1$ more than one time. The spinor Quintom-C firstly crosses the -1 boundary from phantom epoch, and then it again enters the phantom epoch from quintessence epoch. Then it converges to $\omega = 0$ stable matter dominated expansion phase by picking up from avoiding the singularities.

The proposed ECSK spinor quintom model differs from the spinor Quintom model in the framework of general relativity with the existence of matter dominated expansion phases in cases A and C. In both Quintom-A and Quintom-C cases, after the spinor field crosses the -1 boundary from a quintessence epoch toward the phantom epoch, it suddenly picks and enters the stable matter dominated expansion with $\omega = 0$. This can be interpreted as the intrinsic spin causes to fix the pressure of the fluid to a certain value as the energy density increases. After the spinor field reaches a very large energy density value, this allows neglecting the pressure relative to energy density value, which imitates a pressure-free matter dominated era with zero EoS.

Competing Interests

The author declares that he has no competing interests.

References

[1] S. Perlmutter, G. Aldering, G. Goldhaber et al., "Measurements of Ω and Λ from 42 high-redshift supernovae," *The Astrophysical Journal*, vol. 517, no. 2, p. 565, 1999.

[2] A. G. Riess, A. V. Filippenko, P. Challis et al., "Observational evidence from supernovae for an accelerating universe and a cosmological constant," *Astronomical Journal*, vol. 116, no. 3, pp. 1009–1038, 1998.

[3] U. Seljak, A. Makarov, P. McDonald et al., "Cosmological parameter analysis including SDSS Lyα forest and galaxy bias: constraints on the primordial spectrum of fluctuations, neutrino mass, and dark energy," *Physical Review D*, vol. 71, Article ID 103515, 2005.

[4] M. Tegmark, M. Strauss, M. Blanton et al., "Cosmological parameters from SDSS and WMAP," *Physical Review D*, vol. 69, no. 10, Article ID 103501, 2004.

[5] D. J. Eisenstein, I. Zehavi, D. W. Hogg et al., "Detection of the baryon acoustic peak in the large-scale correlation function of SDSS luminous red galaxies," *The Astrophysical Journal*, vol. 633, no. 2, p. 560, 2005.

[6] D. N. Spergel, L. Verde, H. V. Peiris et al., "First-year Wilkinson Microwave Anisotropy Probe (WMAP) observations: determination of cosmological parameters," *Astrophysical Journal, Supplement Series*, vol. 148, no. 1, pp. 175–194, 2003.

[7] D. Larson, J. Dunkley, G. Hinshaw et al., "Seven-year wilkinson microwave anisotropy probe (WMAP*) observations: power spectra and WMAP-derived parameters," *The Astrophysical Journal, Supplement Series*, vol. 192, no. 2, 2011.

[8] G. Hinshaw, D. Larson, E. Komatsu et al., "Nine-year wilkinson microwave anisotropy probe (WMAP) observations: cosmological parameter results," *Astrophysical Journal, Supplement Series*, vol. 208, no. 2, 2013.

[9] K. Bamba, S. Capozziello, S. Nojiri, and S. D. Odintsov, "Dark energy cosmology: the equivalent description via different theoretical models and cosmography tests," *Astrophysics and Space Science*, vol. 342, no. 1, pp. 155–228, 2012.

[10] S. Weinberg, "The cosmological constant problem," *Reviews of Modern Physics*, vol. 61, no. 1, pp. 1–23, 1989.

[11] S. M. Carroll, W. H. Press, and E. L. Turner, "The cosmological constant," *Annual Review of Astronomy and Astrophysics*, vol. 30, no. 1, pp. 499–542, 1992.

[12] L. M. Krauss and M. S. Turner, "The cosmological constant is back," *General Relativity and Gravitation*, vol. 27, no. 11, pp. 1137–1144, 1995.

[13] G. Huey, L. M. Wang, R. Dave, R. R. Caldwell, and P. J. Steinhardt, "Resolving the cosmological missing energy problem," *Physical Review D*, vol. 59, Article ID 063005, 1999.

[14] B. Ratra and P. J. E. Peebles, "Cosmological consequences of a rolling homogeneous scalar field," *Physical Review D*, vol. 37, no. 12, pp. 3406–3427, 1988.

[15] C. Wetterich, "Cosmology and the fate of dilatation symmetry," *Nuclear Physics B*, vol. 302, no. 4, pp. 668–696, 1988.

[16] R. R. Caldwell, M. Kamionkowski, and N. N. Weinberg, "Phantom energy: dark energy with w < −1 causes a cosmic doomsday," *Physical Review Letters*, vol. 91, no. 7, Article ID 071301, 2003.

[17] R. R. Caldwell, "A phantom menace? Cosmological consequences of a dark energy component with super-negative equation of state," *Physics Letters B*, vol. 545, no. 1-2, pp. 23–29, 2002.

[18] S. M. Carroll, M. Hoffman, and M. Trodden, "Can the dark energy equation-of-state parameter w be less than –1?" *Physical Review D*, vol. 68, no. 2, Article ID 023509, 2003.

[19] R. R. Caldwell, M. Kamionkowski, and N. N. Weinberg, "Phantom energy: dark energy with $\omega < -1$ causes a cosmic doomsday," *Physical Review Letters*, vol. 91, Article ID 071301, 2003.

[20] Y.-F. Cai, E. N. Saridakis, M. R. Setare, and J.-Q. Xia, "Quintom cosmology: theoretical implications and observations," *Physics Reports*, vol. 493, no. 1, pp. 1–60, 2010.

[21] D. Huterer and A. Cooray, "Uncorrelated estimates of dark energy evolution," *Physical Review D*, vol. 71, no. 2, Article ID 023506, 2005.

[22] B. Feng, X. L. Wang, and X. M. Zhang, "Dark energy constraints from the cosmic age and supernova," *Physics Letters B*, vol. 607, no. 1-2, pp. 35–41, 2005.

[23] E. Komatsu, J. Dunkley, M. R. Nolta et al., "FIVE-*Year Wilkinson Microwave Anisotropy Probe*∗ observations: cosmological interpretation," *The Astrophysical Journal Supplement Series*, vol. 180, no. 2, pp. 330–376, 2009.

[24] E. Elizalde, S. Nojiri, and S. D. Odintsov, "Late-time cosmology in a (phantom) scalar-tensor theory: dark energy and the cosmic speed-up," *Physical Review D*, vol. 70, no. 4, Article ID 043539, 2004.

[25] H. Li, J. Liua, J. Q. Xiac, and L. Sund, "Constraining cosmological parameters with observational data including weak lensing effects," *Physics Letters B*, vol. 675, no. 2, pp. 164–169, 2009.

[26] J.-Q. Xia, Y.-F. Cai, T.-T. Qiu, G.-B. Zhao, and X. Zhang, "Constraints on the sound speed of dynamical dark energy," *International Journal of Modern Physics D*, vol. 17, no. 8, pp. 1229–1243, 2008.

[27] A. Vikman, "Can dark energy evolve to the phantom?," *Physical Review D*, vol. 71, no. 2, Article ID 023515, 2005.

[28] W. Hu, "Crossing the phantom divide: dark energy internal degrees of freedom," *Physical Review D*, vol. 71, no. 4, Article ID 047301, 2005.

[29] R. R. Caldwell and M. Doran, "Dark-energy evolution across the cosmological-constant boundary," *Physical Review D*, vol. 72, no. 4, Article ID 043527, 2005.

[30] G. B. Zhao, J. Q. Xia, M. Li, B. Feng, and X. Zhang, "Perturbations of the quintom models of dark energy and the effects on observations," *Physical Review D*, vol. 72, Article ID 123515, 2005.

[31] M. Kunz and D. Sapone, "Crossing the phantom divide," *Physical Review D*, vol. 74, no. 12, Article ID 123503, 2006.

[32] S. Nojiri, S. D. Odintsov, and M. Sami, "Dark energy cosmology from higher-order, string-inspired gravity, and its reconstruction," *Physical Review D*, vol. 74, Article ID 046004, 2006.

[33] M.-Z. Li, B. Feng, and X.-M. Zhang, "A single scalar field model of dark energy with equation of state crossing −1," *Journal of Cosmology and Astroparticle Physics*, vol. 2005, no. 12, p. 2, 2005.

[34] L. Perivolaropoulos, "Crossing the phantom divide barrier with scalar tensor theories," *Journal of Cosmology and Astroparticle Physics*, vol. 2005, no. 10, p. 1, 2005.

[35] J. Sadeghi, M. R. Setare, A. Banijamali, and F. Milani, "Crossing of the phantom divide using tachyon-Gauss-Bonnet gravity," *Physical Review D*, vol. 79, no. 12, Article ID 123003, 2009.

[36] V. K. Onemli and R. P. Woodard, "Super-acceleration from massless, minimally coupled $\emptyset^4$," *Classical and Quantum Gravity*, vol. 19, no. 17, pp. 4607–4626, 2002.

[37] V. K. Onemli and R. P. Woodard, "Quantum effects can render $w < -1$ on cosmological scales," *Physical Review D*, vol. 70, no. 10, Article ID 107301, 2004.

[38] T. Brunier, V. K. Onemli, and R. P. Woodard, "Two-loop scalar self-mass during inflation," *Classical and Quantum Gravity*, vol. 22, no. 1, pp. 59–84, 2005.

[39] E. O. Kahya and V. K. Onemli, "Quantum stability of a $w < -1$ phase of cosmic acceleration," *Physical Review D*, vol. 76, no. 4, Article ID 043512, 2007.

[40] E. O. Kahya, V. K. Onemli, and R. P. Woodard, "A Completely Regular Quantum Stress Tensor with $\omega < -1$," *Physical Review D*, vol. 81, no. 2, Article ID 023508, 2010.

[41] A. H. Taub, "Quantum equations in cosmological spaces," *Physical Review*, vol. 51, no. 6, pp. 512–525, 1937.

[42] D. R. Brill and J. A. Wheeler, "Interaction of neutrinos and gravitational fields," *Reviews of Modern Physics*, vol. 29, pp. 465–479, 1957.

[43] L. Parker, "Quantized fields and particle creation in expanding universes. II," *Physical Review D*, vol. 3, no. 2, p. 346, 1971.

[44] L. Parker, "Quantized fields and particle creation in expanding universes. II," *Physical Review D*, vol. 3, no. 10, p. 2546, 1971.

[45] Y. N. Obukhov, "Spin-driven inflation," *Physics Letters A*, vol. 182, no. 2-3, pp. 214–216, 1993.

[46] C. Armendáriz-Picón and P. B. Greene, "Spinors, inflation, and non-singular cyclic cosmologies," *General Relativity and Gravitation*, vol. 35, no. 9, pp. 1637–1658, 2003.

[47] S. Kasuya, "Difficulty of a spinning complex scalar field to be dark energy," *Physics Letters B*, vol. 515, no. 1-2, pp. 121–124, 2001.

[48] B. Saha, "Dirac spinor in Bianchi-I universe with time-dependent gravitational and cosmological constants," *Modern Physics Letters A*, vol. 16, no. 20, pp. 1287–1296, 2001.

[49] M. O. Ribas, F. P. Devecchi, and G. M. Kremer, "Fermions as sources of accelerated regimes in cosmology," *Physical Review D*, vol. 72, no. 12, Article ID 123502, 2005.

[50] L. P. Chimento, F. P. Devecchi, M. Forte, and G. M. Kremer, "Phantom cosmologies and fermions," *Classical and Quantum Gravity*, vol. 25, no. 8, Article ID 085007, 2008.

[51] Y.-F. Cai and J. Wang, "Dark energy model with spinor matter and its quintom scenario," *Classical and Quantum Gravity*, vol. 25, no. 16, Article ID 165014, 12 pages, 2008.

[52] E. A. Lord, *Tensors, Relativity and Cosmology*, McGraw-Hill, 1976.

[53] T. W. B. Kibble, "Lorentz invariance and the gravitational field," *Journal of Mathematical Physics*, vol. 2, pp. 212–221, 1961.

[54] D. W. Sciama, *Recent Developments in General Relativity*, Pergamon, 1962.

[55] V. de Sabbata and C. Sivaram, *Spin and Torsion in Gravitation*, World Scientific, 1994.

[56] R. Utiyama, "Invariant theoretical interpretation of interaction," *APS Journals Archive*, vol. 101, no. 5, p. 1597, 1956.

[57] T. P. Sotiriou and V. Faraoni, "$f(R)$ theories of gravity," *Reviews of Modern Physics*, vol. 82, no. 1, pp. 451–497, 2010.

[58] S. Capozziello and M. De Laurentis, "Extended theories of gravity," *Physics Reports*, vol. 509, no. 4-5, pp. 167–321, 2011.

[59] N. J. Popławski, "Nonsingular dirac particles in spacetime with torsion," *Physics Letters. B*, vol. 690, no. 1, pp. 73–77, 2010.

[60] I. L. Shapiro, "Physical aspects of the space–time torsion," *Physics Reports. A Review Section of Physics Letters*, vol. 357, no. 2, pp. 113–213, 2002.

[61] F. W. Hehl and B. K. Datta, "Nonlinear spinor equation and asymmetric connection in general relativity," *Journal of Mathematical Physics*, vol. 12, pp. 1334–1339, 1971.

[62] N. Poplawski, "Intrinsic spin requires gravity with torsion and curvature," (https://arxiv.org/abs/1304.0047).

[63] M. Forger and H. Römer, "Currents and the energy-momentum tensor in classical field theory: a fresh look at an old problem," *Annals of Physics*, vol. 309, no. 2, pp. 306–389, 2004.

[64] S. Carroll, *Spacetime and geometry: an introduction to general relativity*, Addison Wesley, San Francisco, California, USA, 2004.

Hindawi Publishing Corporation
Advances in High Energy Physics
Volume 2016, Article ID 9753208, 20 pages
http://dx.doi.org/10.1155/2016/9753208

Research Article

Coupling q-Deformed Dark Energy to Dark Matter

Emre Dil

Department of Physics, Sinop University, 57000 Korucuk, Sinop, Turkey

Correspondence should be addressed to Emre Dil; emredil@sakarya.edu.tr

Received 10 June 2016; Revised 6 September 2016; Accepted 3 October 2016

Academic Editor: Tiberiu Harko

We propose a novel coupled dark energy model which is assumed to occur as a q-deformed scalar field and investigate whether it will provide an expanding universe phase. We consider the q-deformed dark energy as coupled to dark matter inhomogeneities. We perform the phase-space analysis of the model by numerical methods and find the late-time accelerated attractor solutions. The attractor solutions imply that the coupled q-deformed dark energy model is consistent with the conventional dark energy models satisfying an acceleration phase of universe. At the end, we compare the cosmological parameters of deformed and standard dark energy models and interpret the implications.

1. Introduction

The standard model of cosmology states that approximately 5% of the energy content of the universe belongs to ordinary baryonic matter of standard model of particle physics. The other 95% of the energy content of the universe is made of the dark sector. Particularly, 25% of the content is an unknown form of matter having a mass but in nonbaryonic form that is called dark matter. The remaining 70% of the content consists of an unknown form of energy named dark energy. On the other hand, it is known that the universe is experiencing accelerating expansion by astrophysical observations, Supernova Ia, large-scale structure, baryon acoustic oscillations, and cosmic microwave background radiation. The dark energy is assumed to be responsible for the late-time accelerated expansion of the universe. The dark energy component of the universe is not clustered but spreads all over the universe and it generates gravitational repulsion due to its negative pressure for driving the acceleration of the expansion of the universe [1–10].

In order to explain the viable mechanism for the accelerated expansion of the universe, cosmologists have proposed various dynamical models for dark energy and dark matter, which include possible interactions between dark energy, dark matter, and other fields, such as gravitation. Particularly, the coupling between dark energy and dark matter is proposed since the energy densities of two dark components are of the same order of magnitude today [11–18].

Since there are a great number of candidates for the constitution of the dark energy, such as cosmological constant, quintessence, phantom, and tachyon fields, different interactions have been proposed between these constituents, dark matter, and gravitational field in the framework of general relativity [19–29]. However, the corresponding dynamical analyses of the interactions between different dark energy models and the dark matter and the gravity have been studied in the framework of teleparallel gravity which uses the torsion tensor instead of the curvature tensor of general relativity [30–39].

The main motivation of this study comes from the recent studies in the literature [40–45] which involves the deformation of the standard scalar field equations representing the dark energy. In this study, we propose a novel dark energy model as a q-deformed scalar field interacting with the dark matter. Since the dark energy is a negative-pressure scalar field, this scalar field can be considered as a q-deformed scalar field. The q-deformed scalar field is in fact a q-deformed boson model, and the statistical mechanical studies of q-deformed boson models have shown that the pressure of the deformed bosons is generally negative. Not only do the

different deformed boson models have a negative pressure, but also the different deformed fermion models can take negative pressure values [46–50]. Here, we consider the q-deformed bosons and propose that the scalar field which is produced by these deformed bosons constitutes the dark energy in the universe. We also investigate the dynamics of the coupling q-deformed dark energy and dark matter inhomogeneities in the Friedmann-Robertson-Walker (FRW) space-time. In order to confirm our proposal, we perform the phase-space analysis of the model whether the late-time stable attractor solutions exist or not, since the stable attractor solutions imply the accelerating expansion of the universe. We finally compare the cosmological parameters of the q-deformed and standard dark energy model and interpret the implications of the comparison.

2. Dynamics of the Model: Coupling q-Deformed Dark Energy to Dark Matter

In our model, the dark energy consists of the scalar field whose field equations are defined by the q-deformed boson fields. Since the idea of q-deformation to the single particle quantum mechanics is a previous establishment in the literature [51–53], it has been natural to construct a q-deformed quantum field theory [54–56]. While the bosonic counterpart of the deformed particle fields corresponds to the deformed scalar field, the fermionic one corresponds to the deformed vector field. Here, we take into account the q-deformed boson field as the q-deformed scalar field which constitutes the dark energy under consideration. The q-deformed dark energy couples to dark matter inhomogeneities in our model. Now, we begin with defining the q-deformed dark energy in the FRW geometry.

Quantum field theory in curved space-time is important in the understanding of the scenario in the Early Universe. Quantum mechanically, constructing the coherent states for any mode of the scalar field translates the behavior of the classical scalar field around the initial singularity into quantum field regime. At the present universe, the quantum mechanical state of the scalar field around the initial singularity cannot be determined by an observer. Therefore, Hawking states that this indeterministic nature can be described by taking the random superposition of all possible states in that space-time. Berger has realized this by taking the superposition of coherent states randomly. Parker has studied the particle creation in the expanding universe with a nonquantized gravitational metric. When the evolution of the scalar field is considered in an expanding universe, Goodison and Toms stated that if the field quanta obey the Bose or Fermi statistics, then the particle creation does not occur in the vacuum state. Therefore, the scalar field dark energy must be described in terms of the deformed bosons or fermions in the coherent states or squeezed state [56–62]. Also, the q-deformed dark energy is a generalization of the standard scalar field dark energy. The free parameter q makes it possible to obtain a desired dark energy model with a preferred interaction or coupling by setting up the deformation parameter to the suitable value.

This motivates us to describe the dark energy as a q-deformed scalar field interacting with the dark matter. We can give the Dirac-Born-Infeld type action of the model as $S = \kappa^2 \int (\ell_g + \ell_{\phi_q} + \ell_m + \ell_r) d^4x$, where $\kappa^2 = 8\pi G$, $\ell_g = -(1/2\kappa) gR$, and ℓ_m and ℓ_r are the gravitational, dark matter, and radiation Lagrangian densities. Then, the deformed dark energy Lagrangian density is given for $(+,-,-,-)$ metric signature as [63]

$$\ell_{\phi_q} = g \frac{1}{2} \left[g^{\mu\nu} \left(\nabla_\mu \phi_q \right) \left(\nabla_\nu \phi_q \right) - m^2 {\phi_q}^2 \right], \tag{1}$$

where $g = \sqrt{-\det g_{\mu\nu}}$ and ϕ_q is the q-deformed scalar field operator for the dark energy and ∇_μ is the covariant derivative which is in fact the ordinary partial derivative ∂_μ for the scalar field. From the variation of the q-deformed scalar field Lagrangian density with respect to the deformed field, we obtain the deformed Klein-Gordon equation:

$$\begin{aligned} \frac{\partial \ell_{\phi_q}}{\partial \phi_q} - \partial_\mu \left(\frac{\partial \ell_{\phi_q}}{\partial \left(\partial_\mu \phi_q \right)} \right) = 0, \\ \left(\partial_\mu \partial^\mu \right) \phi_q + m^2 \phi_q = 0. \end{aligned} \tag{2}$$

Also, we get the energy-momentum tensor of the scalar field dark energy from the variation of Lagrangian ℓ_{ϕ_q} with respect to the metric tensor, such that

$$\begin{aligned} T^{\phi_q}_{\mu\nu} &= \frac{2}{g} \left(\frac{\partial \ell_{\phi_q}}{\partial g^{\mu\nu}} - g_{\mu\nu} \ell_{\phi_q} \right) \\ &= \partial_\mu \phi_q \partial_\nu \phi_q - \frac{1}{2} g_{\mu\nu} \left(g^{\alpha\beta} \partial_\alpha \phi_q \partial_\beta \phi_q - m^2 {\phi_q}^2 \right), \end{aligned} \tag{3}$$

from which the timelike and spacelike parts of $T^{\phi_q}_{\mu\nu}$ read as follows:

$$\begin{aligned} T^{\phi_q}_{00} &= \frac{1}{2} {\dot{\phi}_q}^2 - \frac{1}{2} g^{ii} \left(\partial_i \phi_q \right)^2 + \frac{1}{2} m^2 {\phi_q}^2, \\ T^{\phi_q}_{ii} &= -\frac{1}{2} g_{ii} {\dot{\phi}_q}^2 + \frac{1}{2} \left(\partial_i \phi_q \right)^2 - \frac{1}{2} g_{ii} g^{jj} \left(\partial_j \phi_q \right)^2 \\ &\quad + \frac{1}{2} g_{ii} m^2 {\phi_q}^2, \end{aligned} \tag{4}$$

where $i, j = 1, 2, 3$ represent the spacelike components.

In order to calculate the deformed energy density and the pressure functions of the q-deformed energy from the energy-momentum components (4), we need to consider the quantum field theoretical description of the deformed scalar field in a FRW background with the metric

$$ds^2 = dt^2 - a^2(t) \left[dx^2 + dy^2 + dz^2 \right]. \tag{5}$$

Then, the canonically quantized q-deformed scalar field ϕ_q is introduced in terms of the Fourier expansion [57]

$$\phi_q = \int d^3k \left[a_q(k) f_k + a_q^+(k) f_k^* \right], \tag{6}$$

where $a_q(k)$ and $a_q^+(k)$ are the q-deformed boson annihilation and creation operators for the quanta of the q-deformed scalar field dark energy in the kth mode. k denotes the spatial wave vector and obeys the relativistic energy conservation law $\omega^2 = -g^{ii}k^2 + m^2$. Here, f_k is a set of orthonormal mode solutions of the deformed Klein-Gordon equation, such that

$$f_k(x^\mu) = \frac{\exp\left(ik_\mu x^\mu\right)}{\sqrt{(2\pi)^3\, 2\omega}}, \tag{7}$$

where $k_\mu = (\omega, -k)$ is the four-momentum vector and satisfies the relations

$$\begin{aligned}
\int d^3x f_k f_{k'}^* &= \frac{\delta^3\left(-k+k'\right)}{2\omega},\\
\int d^3x f_k f_{k'} &= \frac{e^{2i\omega t}\delta^3\left(-k-k'\right)}{2\omega},\\
\int d^3x f_k^* f_{k'} &= \frac{\delta^3\left(k-k'\right)}{2\omega},\\
\int d^3x f_k^* f_{k'}^* &= \frac{e^{-2i\omega t}\delta^3\left(k+k'\right)}{2\omega}.
\end{aligned} \tag{8}$$

We can give the spatial average of the q-deformed scalar field energy-momentum tensor $T_{\mu\nu}^{\phi_q}$ as [59]

$$\overline{T}_{\mu\nu}^{\phi_q} = \int d^3x T_{\mu\nu}^{\phi_q}. \tag{9}$$

By using (9), the spatial average of the timelike energy-momentum tensor component is obtained as

$$\overline{T}_{00}^{\phi_q} = \int d^3x \left[\frac{1}{2}\dot{\phi}_q^{\,2} - \frac{1}{2}g^{ii}\left(\partial_i\phi_q\right)^2 + \frac{1}{2}m^2\phi_q^{\,2}\right]. \tag{10}$$

This can be determined from (6)–(8) term by term, as follows:

$$\begin{aligned}
&\frac{1}{2}m^2\int d^3x\phi_q^{\,2} = \frac{1}{2}\\
&\cdot m^2\int d^3x\iint d^3k d^3k'\left[a_q(k) f_k + a_q^+(k) f_k^*\right]\\
&\cdot\left[a_q\left(k'\right) f_{k'} + a_q^+\left(k'\right) f_{k'}^*\right] = \frac{1}{2}\int d^3k\frac{m^2}{2\omega}\left[a_q(k)\right.\\
&\cdot a_q(-k)\, e^{2i\omega t} + a_q^+(k)\, a_q(k) + a_q(k)\, a_q^+(k)\\
&\left.+ a_q^+(k)\, a_q^+(-k)\, e^{-2i\omega t}\right],
\end{aligned} \tag{11}$$

$$\begin{aligned}
&\frac{1}{2}\int d^3x\dot{\phi}_q^{\,2} = \frac{1}{2}\int d^3k\frac{\omega}{2}\left[-a_q(k)\, a_q(-k)\, e^{2i\omega t} + a_q^+(k)\right.\\
&\left.\cdot a_q(k) + a_q(k)\, a_q^+(k) - a_q^+(k)\, a_q^+(-k)\, e^{-2i\omega t}\right],
\end{aligned} \tag{12}$$

$$\begin{aligned}
&\frac{1}{2}g^{ii}\int d^3x\left(\partial_i\phi_q\right)^2 = \frac{1}{2}\int d^3k\frac{g^{ii}k^2}{2\omega}\left[a_q(k)\, a_q(-k)\, e^{2i\omega t}\right.\\
&+ a_q^+(k)\, a_q(k) + a_q(k)\, a_q^+(k) + a_q^+(k)\, a_q^+(-k)\\
&\left.\cdot e^{-2i\omega t}\right].
\end{aligned} \tag{13}$$

Combining (11), (12), and (13) gives

$$\overline{T}_{00}^{\phi_q} = \frac{1}{2}\int d^3k\omega\left[a_q(k)\, a_q^+(k) + a_q^+(k)\, a_q(k)\right], \tag{14}$$

where $\omega^2 = m^2 - k^2/a^2(t)$ for the FRW space-time. Correspondingly, the average of the spacelike energy-momentum tensor component can be determined, such that

$$\begin{aligned}
\overline{T}_{ii}^{\phi_q} &= \int d^3x\left[-\frac{1}{2}g_{ii}\dot{\phi}_q^{\,2} + \frac{1}{2}\left(\partial_i\phi_q\right)^2 - \frac{1}{2}g_{ii}g^{jj}\left(\partial_j\phi_q\right)^2\right.\\
&\left.+ \frac{1}{2}g_{ii}m^2\phi_q^{\,2}\right] = -\frac{1}{2}\int d^3k\frac{g_{ii}\omega}{2}\\
&\cdot\left[-a_q(k)\, a_q(-k)\, e^{2i\omega t} + a_q^+(k)\, a_q(k)\right.\\
&\left.+ a_q(k)\, a_q^+(k) - a_q^+(k)\, a_q^+(-k)\, e^{-2i\omega t}\right] + \int d^3k\frac{k_i^2}{2\omega}\\
&\cdot\left[a_q(k)\, a_q(-k)\, e^{2i\omega t} + a_q^+(k)\, a_q(k) + a_q(k)\, a_q^+(k)\right.\\
&\left.+ a_q^+(k)\, a_q^+(-k)\, e^{-2i\omega t}\right] + \frac{1}{2}\int d^3k\frac{g_{ii}g^{jj}k^2}{2\omega}\\
&\cdot\left[a_q(k)\, a_q(-k)\, e^{2i\omega t} + a_q^+(k)\, a_q(k) + a_q(k)\, a_q^+(k)\right.\\
&\left.+ a_q^+(k)\, a_q^+(-k)\, e^{-2i\omega t}\right] + \frac{1}{2}\int d^3k\frac{g_{ii}m^2}{2\omega}\\
&\cdot\left[a_q(k)\, a_q(-k)\, e^{2i\omega t} + a_q^+(k)\, a_q(k) + a_q(k)\, a_q^+(k)\right.\\
&\left.+ a_q^+(k)\, a_q^+(-k)\, e^{-2i\omega t}\right].
\end{aligned} \tag{15}$$

From the identities $a_q(-k)e^{2i\omega t} = a_q^+(k)$ and $a_q^+(-k)e^{-2i\omega t} = a_q(k)$, (15) turns out to be

$$\begin{aligned}
\overline{T}_{ii}^{\phi_q} &= \frac{1}{2}\int d^3k\frac{1}{\omega}\left[2k_i^2 - a^2(t)\,\omega^2\right]\\
&\cdot\left[a_q(k)\, a_q^+(k) + a_q^+(k)\, a_q(k)\right],
\end{aligned} \tag{16}$$

for the FRW geometry, and k_i is the ith spatial component of the wave vector.

The q-deformation of a quantum field theory is constructed from the standard algebra satisfied by the annihilation and creation operators introduced in the canonical quantization of the field. The deformation of a standard boson algebra satisfied by the annihilation and creation operators of a bosonic quantum field theory was firstly realized by Arik-Coon [51], and then Macfarlane and Biedenharn [52, 53] independently realized the deformation of boson algebra different from Arik-Coon. Hence, the q-deformed bosonic quantum field theory of the scalar field dark energy is constructed by the q-deformed algebra of the operators $a_q(k)$ and $a_q^+(k)$ in (6), such that

$$a_q(k)\, a_q^+\left(k'\right) - q^2 a_q^+\left(k'\right) a_q(k) = \delta^3\left(k-k'\right), \tag{17}$$

$$a_q(k)\, a_q\left(k'\right) - q^2 a_q\left(k'\right) a_q(k) = 0, \tag{18}$$

$$\left[N_k\right] = a_q^+(k)\, a_q(k). \tag{19}$$

Here, q is a real deformation parameter, and $[N_k]$ is the deformed number operator whose eigenvalue spectrum is given as [51]

$$[n_k] = \frac{1 - q^{2n_k}}{1 - q^2}, \tag{20}$$

where n_k is the eigenvalue of the standard number operator N_k.

The corresponding vector spaces of the annihilation and creation operators for the q-deformed scalar field dark energy are the q-deformed Fock space state vectors, which give information about the number of particles in the corresponding state. The q-deformed bosonic annihilation and creation operators $a_q(k)$ and $a_q^+(k)$ act on the Fock states $|n_k\rangle$ as follows:

$$\begin{aligned} a_q(k)|n_k\rangle &= \sqrt{[n_k]}\,|n_k - 1\rangle, \\ a_q^+(k)|n_k\rangle &= \sqrt{[n_k + 1]}\,|n_k + 1\rangle, \\ [N_k]|n_k\rangle &= a_q^+(k)\,a_q(k)|n_k\rangle = [n_k]|n_k\rangle. \end{aligned} \tag{21}$$

By taking the quantum expectation values of the spatial averages of energy-momentum tensor with respect to the Fock basis $|n_k\rangle$, we obtain the energy density and the pressure of the q-deformed dark energy. Using $\rho_{\phi_q} = T_0^0$ and $p_{\phi_q} = -T_i^i$ for the energy density and pressure of the q-deformed scalar field dark energy, we obtain

$$\begin{aligned} \int \rho_{\phi_q} d^3x &= \langle n_k|\,\overline{T}_0^{0\phi_q}\,|n_k\rangle \\ &= \int d^3k \frac{\omega}{2} \langle n_k| \left[a_q(k)\,a_q^+(k) + a_q^+(k)\,a_q(k)\right]|n_k\rangle \\ &= \left(\left(1 + q^2\right)[n_k] + 1\right) \int d^3k_\phi \frac{\omega_\phi}{2}, \end{aligned} \tag{22}$$

where q-deformed boson algebra in (17) is used in the second line. Because the q-deformed boson algebra in (17)–(19) transforms to be the standard boson algebra and $[n_k] = n_k$ in the $q \to 1$ limit, the energy density ρ_{ϕ_q} of the q-deformed dark energy transforms into the energy density ρ_ϕ of the standard dark energy as

$$\int \rho_\phi d^3x = (2n_k + 1) \int d^3k_\phi \frac{\omega_\phi}{2}. \tag{23}$$

Hence, the energy density ρ_{ϕ_q} of the q-deformed dark energy can be written in terms of the energy density ρ_ϕ of the standard dark energy by

$$\rho_{\phi_q} = \frac{\left(1 + q^2\right)[n_k] + 1}{2n_k + 1} \rho_\phi = \Delta_q(n_k)\,\rho_\phi. \tag{24}$$

Accordingly, the pressure of the q-deformed scalar field dark energy can be written from (6) as

$$\begin{aligned} \int p_{\phi_q} d^3x &= \langle n_k| - \overline{T}_i^{i\phi_q}\,|n_k\rangle = \int d^3k \\ &\cdot \frac{1}{2\omega}\left[\frac{2k^2}{a^2(t)} - \omega^2\right]\langle n_k| \\ &\cdot \left[a_q(k)\,a_q^+(k) + a_q^+(k)\,a_q(k)\right]|n_k\rangle = \left(\left(1 + q^2\right) \right. \\ &\left. \cdot [n_k] + 1\right) \int d^3k \frac{1}{2\omega}\left[\frac{2k^2}{a^2(t)} - \omega^2\right], \end{aligned} \tag{25}$$

where $g^{ii}k_i^2 = (1/a^2(t))(k_1^2 + k_2^2 + k_3^2) = k^2/a^2(t)$ is used. In the $q \to 1$ limit, the q-deformed pressure p_{ϕ_q} of dark energy transforms to the standard pressure p_ϕ of the dark energy, such that

$$\int p_\phi d^3x = (2n_k + 1) \int d^3k \frac{1}{2\omega}\left[\frac{2k^2}{a^2(t)} - \omega^2\right]. \tag{26}$$

Consequently, the q-deformed pressure p_{ϕ_q} of dark energy can be obtained in terms of the standard pressure p_ϕ of the dark energy; thus,

$$p_{\phi_q} = \frac{\left(1 + q^2\right)[n_k] + 1}{2n_k + 1} p_\phi = \Delta_q(n_k)\,p_\phi. \tag{27}$$

Also, the commutation relations and plane-wave expansion of the q-deformed scalar field $\phi_q(x)$ are given by using (17)–(19) in (6), as follows:

$$\phi_q(x)\,\phi_q^+\left(x'\right) - q^2\phi_q^+\left(x'\right)\phi_q(x) = i\Delta\left(x - x'\right), \tag{28}$$

where

$$\Delta\left(x - x'\right) = \frac{-1}{(2\pi)^3} \int \frac{d^3k}{w_k} \sin w_k\left(x - x_0\right). \tag{29}$$

On the other hand, the deformed and standard annihilation operators, a_q and a_s, are written as [62]

$$a_q = a_s \sqrt{\frac{[N_k]}{N_k}}. \tag{30}$$

From this, we can express the deformed bosonic scalar fields in terms of the standard one by using (20) in (30) and (6):

$$\phi_q = \sqrt{\frac{1 - q^{2n_k}}{\left(1 - q^2\right)n_k}}\,\phi = \Delta(q)\,\phi, \tag{31}$$

where we use the Hermiticity of the number operator N.

Now, we will derive the Friedmann equations for our coupling q-deformed dark energy to dark matter model with a radiation field in FRW space-time by using the scale factor $a(t)$ in Einstein's equations. We can achieve this by relating the scale factor with the energy-momentum tensor of the objects in the considered universe model. It is a common

fact to consider energy and matter as a perfect fluid, which will naturally be generalized to dark energy and matter. An isotropic fluid in one coordinate frame gives an isotropic metric in another frame which coincides with the first frame. This means that the fluid is at rest in commoving coordinates. Then, the four-velocity vector is given as [63]

$$U^{\mu} = (1, 0, 0, 0), \tag{32}$$

while the energy-momentum tensor reads

$$T_{\mu\nu} = (\rho + p) U_{\mu} U_{\nu} + p g_{\mu\nu} = \begin{pmatrix} \rho & 0 & 0 & 0 \\ 0 & & & \\ 0 & & g_{ij} p & \\ 0 & & & \end{pmatrix}. \tag{33}$$

Raising one index gives a more suitable form

$$T^{\mu}_{\nu} = \mathrm{diag}(-\rho, p, p, p). \tag{34}$$

For a model of universe described by Dirac-Born-Infeld type action and consisting of more than one form of energy momentum, we have totally three types of energy density and pressure, such that

$$\rho_{\mathrm{tot}} = \rho_{\phi_q} + \rho_m + \rho_r, \tag{35}$$

$$p_{\mathrm{tot}} = p_{\phi_q} + p_r, \tag{36}$$

where the pressure of the dark matter p_m is explicitly zero in the total pressure p_{tot} (36). From the conservation of equation for the zero component $\nabla_{\mu} T^{\mu}_{0} = 0$, one obtains $\rho \propto a^{-3(1+w)}$. Here, w is the parameter of the equation of state $p = w\rho$ which relates the pressure and the energy density of the cosmological fluid component under consideration. Therefore, pressure is zero for the matter component and $w_m = 0$, but for the radiation component $w_r = 1/3$ due to the vanishing trace of the energy-momentum tensor of the electromagnetic field. We then express the total equation of state parameter as

$$w_{\mathrm{tot}} = \frac{p_{\mathrm{tot}}}{\rho_{\mathrm{tot}}} = w_{\phi_q} \Omega_{\phi_q} + w_r \Omega_r. \tag{37}$$

While the equations of state parameters are given as $w_{\phi_q} = p_{\phi_q}/\rho_{\phi_q}$ and $w_r = p_r/\rho_r = 1/3$, the density parameters are defined by $\Omega_{\phi_q} = \rho_{\phi_q}/\rho_{\mathrm{tot}}$, $\Omega_r = \rho_r/\rho_{\mathrm{tot}}$ for the q-deformed dark energy and the radiation fields, respectively. Since the pressure of the dark matter is $p_m = 0$, then the equation of state parameter is $w_m = p_m/\rho_m = 0$ and the density parameter is $\Omega_m = \rho_m/\rho_{\mathrm{tot}}$ for the dark matter field having no contribution to w_{tot} (37), but contributing to the total density parameter, such that

$$\Omega_{\mathrm{tot}} = \Omega_{\phi_q} + \Omega_m + \Omega_r = \frac{\kappa^2 \rho_{\mathrm{tot}}}{3H^2} = 1. \tag{38}$$

We now turn to Einstein's equations of the form $R_{\mu\nu} = \kappa^2 (T_{\mu\nu} - (1/2) g_{\mu\nu} T)$. Then, by using the components of the Ricci tensor for FRW space-time (5) and the energy-momentum tensor in (34), we rewrite Einstein's equations, for $\mu\nu = 00$ and $\mu\nu = ij$:

$$-3\frac{\ddot{a}}{a} = \frac{\kappa^2}{2}(\rho + 3p), \tag{39}$$

$$\frac{\ddot{a}}{a} + 2\left(\frac{\dot{a}}{a}\right)^2 = \frac{\kappa^2}{2}(\rho - p), \tag{40}$$

respectively. Here, the dot also represents the derivative with respect to cosmic time t. Using (39) and (40) gives the Friedmann equations for FRW metric as

$$\begin{aligned} H^2 &= \frac{\kappa^2}{3}\left(\rho_{\phi_q} + \rho_m + \rho_r\right), \\ \dot{H} &= -\frac{\kappa^2}{2}\left(\rho_{\phi_q} + p_{\phi_q} + \rho_m + \rho_r + p_r\right), \end{aligned} \tag{41}$$

where $H = \dot{a}/a$ is the Hubble parameter and $\rho_r = 3p_r$. From the conservation of energy, we can obtain the continuity equations for q-deformed dark energy, dark matter, and the radiation constituents in the form of evolution equations, such as

$$\dot{\rho}_{\phi_q} + 3H\left(\rho_{\phi_q} + p_{\phi_q}\right) = -Q', \tag{42}$$

$$\dot{\rho}_m + 3H\rho_m = Q, \tag{43}$$

$$\dot{\rho}_r + 3H(\rho_r + p_r) = Q' - Q, \tag{44}$$

where Q is an interaction current between the q-deformed dark energy and the dark matter which transfers the energy and momentum from the dark matter to dark energy and vice versa. Q and Q' vanish for the models having no coupling between the dark energy and the dark matter. For the models including only the interactions between dark energy and dark matter, the interaction terms become equal $Q' = Q$. The case $Q < 0$ corresponds to energy transfer from dark matter to the other two constituents, the case $Q' > 0$ corresponds to energy transfer from dark energy to the other constituents, and the case $Q' < 0$ corresponds to an energy loss from radiation. Here, we consider that the model only has interaction between dark energy and dark matter and $Q' = Q$ [64].

The energy density ρ and pressure p of this dark energy are rewritten explicitly from the energy-momentum tensor components (4) obtained by the Dirac-Born-Infeld type action of coupling q-deformed dark energy and dark matter, such that [65–68]

$$\begin{aligned} \rho_{\phi_q} &= T_0^{0\phi_q} = \frac{1}{2}\dot{\phi}_q^{\,2} + \frac{1}{2}m^2\phi_q^{\,2}, \\ p_{\phi_q} &= -T_i^{i\phi_q} = \frac{1}{2}\dot{\phi}_q^{\,2} - \frac{1}{2}m^2\phi_q^{\,2}, \end{aligned} \tag{45}$$

where the dark energy is space-independent due to the isotropy and homogeneity. Now, the equation of motion for

the q-deformed dark energy can be obtained by inserting (45) into the evolution equation, such that

$$\ddot{\phi}_q + 3H\dot{\phi}_q + m^2\phi_q = -\frac{Q}{\dot{\phi}_q}. \tag{46}$$

In order to obtain the energy density and pressure and equation of motion in terms of the deformation parameter q, (31) and its time derivative will be used. Because the number of particles in each mode of the q-deformed scalar field varies in time by the particle creation and annihilation, the time derivative of $\Delta(q)$ is given as

$$\dot{\Delta}(q) = \frac{-q^{2n_k}\dot{n}_k \ln q}{\sqrt{(1-q^2)(1-q^{2n_k})\,n_k}} - \frac{\dot{n}_k\sqrt{1-q^{2n_k}}}{2\sqrt{(1-q^2)\,n_k^3}}. \tag{47}$$

Substituting (31) and (47) in (45) and (46), we obtain

$$\begin{aligned}\rho_{\phi_q} &= \frac{1}{2}\Delta^2(q)\,\dot{\phi}^2 + \frac{1}{2}\Delta^2(q)\,m^2\phi^2 + \frac{1}{2}\dot{\Delta}^2(q)\,\phi^2 \\ &\quad + \Delta(q)\,\dot{\Delta}(q)\,\phi\dot{\phi},\end{aligned} \tag{48}$$

$$\begin{aligned}p_{\phi_q} &= \frac{1}{2}\Delta^2(q)\,\dot{\phi}^2 - \frac{1}{2}\Delta^2(q)\,m^2\phi^2 + \frac{1}{2}\Delta^2(q)\,\phi^2 \\ &\quad + \Delta(q)\,\dot{\Delta}(q)\,\phi\dot{\phi},\end{aligned} \tag{49}$$

$$\begin{aligned}&\Delta(q)\,\ddot{\phi} + 3\Delta(q)\,H\dot{\phi} - \Delta(q)\,m^2\phi + 2\dot{\Delta}(q)\,\dot{\phi} \\ &\quad + \ddot{\Delta}(q)\,\phi + 3H\dot{\Delta}(q)\,\phi = -\beta\kappa\rho_m.\end{aligned} \tag{50}$$

Here, we consider the commonly used interaction current as $Q = \beta\kappa\rho_m\dot{\phi}_q$ in the literature [15], in order to obtain stationary and stable cosmological solutions in our dark model. The deformed energy density and pressure equations (24) and (27) are the same as (48) and (49), respectively. While (24) and (48) are the expression of the deformed energy density, accordingly (27) and (49) are the deformed pressure of the dark energy in terms of the deformation parameter q. The functions of the deformation parameter in (24) and (48) are

$$\begin{aligned}&\Delta_q(n_k) \approx \Delta(q), \\ &\frac{\left(1+q^2\right)[n_k]+1}{2n_k+1} \approx \sqrt{\frac{1-q^{2n_k}}{(1-q^2)\,n_k}},\end{aligned} \tag{51}$$

since n_k values are very large, and n_k is given as a function of time:

$$n_k \approx \frac{t}{3} + \frac{\sqrt{16t^2+16t-14}}{12} + \frac{1}{6}. \tag{52}$$

We now perform the phase-space analysis of our coupling q-deformed dark energy to dark matter model if the late-time solutions of the universe can be obtained, in order to confirm our proposal.

3. Phase-Space Analysis

We investigate the cosmological properties of the proposed q-deformed dark energy model by performing the phase-space analysis. We need to transform the equations of the dynamical system into their autonomous form [26–28, 36, 37, 69–71]. The auxiliary variables are defined to be

$$\begin{aligned}x_{\phi_q} &= \frac{\kappa\left(\Delta\dot{\phi} + \dot{\Delta}\phi\right)}{\sqrt{6}H}, \\ y_{\phi_q} &= \frac{\kappa\sqrt{e^{-\kappa\lambda\Delta\phi}}}{\sqrt{3}H}.\end{aligned} \tag{53}$$

We consider an exponential potential as $V = V_0 e^{-\kappa\lambda\phi_q}$ instead of the potential $V = (1/2)m^2{\phi_q}^2$ in Lagrangian (1), as the usual assumption in the literature, because the power-law potential does not provide a stable attractor solution [16, 18, 72–76].

We also express the density parameters for the q-deformed scalar field dark energy, dark matter, and the radiation in the autonomous system by using (35), (36), and (48) with (53):

$$\Omega_{\phi_q} = \frac{\kappa^2\rho_{\phi_q}}{3H^2} = x_{\phi_q}^2 + y_{\phi_q}^2, \tag{54}$$

$$\Omega_m = \frac{\kappa^2\rho_m}{3H^2}, \tag{55}$$

$$\Omega_r = \frac{\kappa^2\rho_r}{3H^2}, \tag{56}$$

and then the total density parameter is given by

$$\Omega_{\text{tot}} = \frac{\kappa^2\rho_{\text{tot}}}{3H^2} = x_{\phi_q}^2 + y_{\phi_q}^2 + \Omega_m + \Omega_r = 1. \tag{57}$$

Also, the equation of state parameter for the dark energy is written in the autonomous form by using (35) and (36) with (53):

$$w_{\phi_q} = \frac{p_{\phi_q}}{\rho_{\phi_q}} = \frac{x_{\phi_q}^2 - y_{\phi_q}^2}{x_{\phi_q}^2 + y_{\phi_q}^2}. \tag{58}$$

Then, the total equation of state parameter in the autonomous system from (37) and (54)–(56) and (58) is obtained as

$$w_{\text{tot}} = x_{\phi_q}^2 - y_{\phi_q}^2 + \frac{\Omega_r}{3}. \tag{59}$$

We also define $s = -\dot{H}/H^2$ in the autonomous system by using (41) and (59), such that

$$s = -\frac{\dot{H}}{H^2} = \frac{3}{2}\left(1 + w_{\text{tot}}\right) = \frac{3}{2}\left(1 + x_{\phi_q}^2 - y_{\phi_q}^2 + \frac{\Omega_r}{3}\right). \tag{60}$$

s is here only a jerk parameter which is used in other equations of cosmological parameters. However, the deceleration

Table 1: Critical points and existence conditions.

Label	x_{ϕ_q}	y_{ϕ_q}	Ω_m	Ω_r	Ω_{ϕ_q}	ω_{ϕ_q}	ω_{tot}
A	$\frac{3}{\sqrt{6}(\lambda+\beta)}$	$\frac{\sqrt{2\beta(\lambda+\beta)+3}}{\sqrt{2}(\lambda+\beta)}$	$\frac{\lambda(\lambda+\beta)-3}{(\lambda+\beta)^2}$	0	$\frac{\beta(\lambda+\beta)+3}{(\lambda+\beta)^2}$	$\frac{-\beta(\lambda+\beta)}{\beta(\lambda+\beta)+3}$	$\frac{-\beta}{(\lambda+\beta)}$
B	$\frac{3}{\sqrt{6}(\lambda+\beta)}$	$\frac{-\sqrt{2\beta(\lambda+\beta)+3}}{\sqrt{2}(\lambda+\beta)}$	$\frac{\lambda(\lambda+\beta)-3}{(\lambda+\beta)^2}$	0	$\frac{\beta(\lambda+\beta)+3}{(\lambda+\beta)^2}$	$\frac{-\beta(\lambda+\beta)}{\beta(\lambda+\beta)+3}$	$\frac{-\beta}{(\lambda+\beta)}$
C	$\frac{\sqrt{6}\lambda}{6}$	$\sqrt{1-\frac{\lambda^2}{6}}$	0	0	1	$\frac{\lambda^2}{3}-1$	$\frac{\lambda^2}{3}-1$
D	$\frac{4}{\sqrt{6}\lambda}$	$\frac{2}{\sqrt{3}\lambda}$	0	$1-\frac{4}{\lambda^2}$	$\frac{4}{\lambda^2}$	$\frac{1}{3}$	$\frac{1}{3}$
E	$\frac{-1}{\sqrt{6}\beta}$	0	$\frac{1}{3\beta^2}$	$1-\frac{1}{2\beta^2}$	$\frac{1}{6\beta^2}$	1	$\frac{1}{3}$

parameter q_d which is not used in the equations but is not also a jerk parameter is defined as

$$q_d = -1 - \frac{\dot{H}}{H^2}. \tag{61}$$

Now, we convert the Friedmann equation (41), the continuity equations (43) and (44), and the equation of motion (50) into the autonomous system by using the auxiliary variables in (53)–(56) and their derivatives with respect to $N = \ln a$, for which the time derivative of any quantity F is $\dot{F} = H(dF/dN)$. Thus, we will obtain $X' = f(X)$, where X is the column vector including the auxiliary variables and $f(X)$ is the column vector of the autonomous equations. We then find the critical points X_c of X, by setting $X' = 0$. We then expand $X' = f(X)$ around $X = X_c + U$, where U is the column vector of perturbations of the auxiliary variables, such as δx_{ϕ_q}, δy_{ϕ_q}, $\delta\Omega_m$, and $\delta\Omega_r$ for each constituent in our model. Thus, we expand the perturbation equations up to the first order for each critical point as $U' = MU$, where M is the matrix of perturbation equations. The eigenvalues of perturbation matrix M determine the type and stability of the critical points for each critical point [77–79].

With the definitions for the interaction current and the potential, the autonomous form of the cosmological system reads [80–89]

$$\begin{aligned}
x'_{\phi_q} &= -3x_{\phi_q} + sx_{\phi_q} + \frac{\sqrt{6}}{2}\lambda y^2_{\phi_q} - \frac{\sqrt{6}}{2}\beta\Omega_m,\\
y'_{\phi_q} &= sy_{\phi_q} - \frac{\sqrt{6}}{2}\lambda y_{\phi_q} x_{\phi_q},\\
\Omega'_m &= \Omega_m\left[-3 + \sqrt{6}\beta x_{\phi_q} + 2s\right],\\
\Omega'_r &= \Omega_r\left[-4 + 2s\right].
\end{aligned} \tag{62}$$

In order to perform the phase-space analysis of the model, we obtain the critical points of the autonomous system in (62). We will obtain these points by equating the left hand sides of (62) to zero for stationary solutions, by using the condition $\Omega_{\text{tot}} = 1$. After some calculations, five critical points are found as listed in Table 1 with the existence conditions.

Now, we will get the perturbations $\delta x'_{\phi_q}$, $\delta y'_{\phi_q}$, $\delta\Omega'_m$, and $\delta\Omega'_r$ for each constituent in our model by using the variations of (62), such as

$$\begin{aligned}
\delta x'_{\phi_q} &= \left[-\frac{3}{2} + \frac{9}{2}x^2_{\phi_q} - \frac{3}{2}y^2_{\phi_q} + \frac{\Omega_r}{2}\right]\delta x_{\phi_q}\\
&\quad + \left[\sqrt{6}\lambda - 3x_{\phi_q}y_{\phi_q}\right]\delta y_{\phi_q} + \frac{\sqrt{6}}{2}\beta\delta\Omega_m\\
&\quad + \frac{x_{\phi_q}}{2}\delta\Omega_r,
\end{aligned} \tag{63}$$

$$\begin{aligned}
\delta y'_{\phi_q} &= \left[3x_{\phi_q}y_{\phi_q} - \frac{\sqrt{6}}{2}\lambda y_{\phi_q}\right]\delta x_{\phi_q}\\
&\quad + \left[\frac{3}{2} + \frac{\sqrt{6}}{2}\lambda x_{\phi_q} + \frac{3}{2}x^2_{\phi_q} - \frac{9}{2}y^2_{\phi_q} + \frac{\Omega_r}{2}\right]\delta y_{\phi_q}\\
&\quad + \frac{y_{\phi_q}}{2}\delta\Omega_r,
\end{aligned} \tag{64}$$

$$\begin{aligned}
\delta\Omega'_m &= \left[6x_{\phi_q}\Omega_m + \sqrt{6}\beta\Omega_m\right]\delta x_{\phi_q} - 6y_{\phi_q}\Omega_m\delta y_{\phi_q}\\
&\quad + \left[\sqrt{6}\beta x_{\phi_q} + 3x^2_{\phi_q} - 3y^2_{\phi_q} + \Omega_r\right]\delta\Omega_m\\
&\quad + \Omega_m\delta\Omega_r,
\end{aligned} \tag{65}$$

$$\begin{aligned}
\delta\Omega'_r &= 6x_{\phi_q}\Omega_r\delta x_{\phi_q} - 6y_{\phi_q}\Omega_r\delta y_{\phi_q}\\
&\quad + \left[-1 + 3x^2_{\phi_q} - 3y^2_{\phi_q} + 2\Omega_r\right]\delta\Omega_r.
\end{aligned} \tag{66}$$

Thus, we obtain a 4×4 perturbation matrix M whose nonzero elements are given as

$$
\begin{aligned}
M_{11} &= -\frac{3}{2} + \frac{9}{2}x_{\phi_q}^2 - \frac{3}{2}y_{\phi_q}^2 + \frac{\Omega_r}{2},\\
M_{12} &= \sqrt{6}\lambda y_{\phi_q} - 3x_{\phi_q}y_{\phi_q},\\
M_{13} &= \frac{\sqrt{6}}{2}\beta,\\
M_{14} &= \frac{x_{\phi_q}}{2},\\
M_{21} &= 3x_{\phi_q}y_{\phi_q} - \frac{\sqrt{6}}{2}\lambda y_{\phi_q},\\
M_{22} &= \frac{3}{2} + \frac{\sqrt{6}}{2}\lambda x_{\phi_q} + \frac{3}{2}x_{\phi_q}^2 - \frac{9}{2}y_{\phi_q}^2 + \frac{\Omega_r}{2},\\
M_{24} &= \frac{y_{\phi_q}}{2},\\
M_{31} &= 6x_{\phi_q}\Omega_m + \sqrt{6}\beta\Omega_m,\\
M_{32} &= -6y_{\phi_q}\Omega_m,\\
M_{33} &= \sqrt{6}\beta x_{\phi_q} + 3x_{\phi_q}^2 - 3y_{\phi_q}^2 + \Omega_r,\\
M_{34} &= \Omega_m,\\
M_{41} &= 6x_{\phi_q}\Omega_r,\\
M_{42} &= -6y_{\phi_q}\Omega_r,\\
M_{44} &= -1 + 3x_{\phi_q}^2 - 3y_{\phi_q}^2 + 2\Omega_r.
\end{aligned}
\tag{67}
$$

Then, we insert linear perturbations $x_{\phi_q} \to x_{\phi_q,c} + \delta x_{\phi_q}$, $y_{\phi_q} \to y_{\phi_q,c} + \delta y_{\phi_q}$, $\Omega_m \to \Omega_{m,c} + \delta\Omega_m$, and $\Omega_r \to \Omega_{r,c} + \delta\Omega_r$ about the critical points for three constituents in the autonomous system (62). So, we can calculate the eigenvalues of perturbation matrix M for five critical points given in Table 1, with the corresponding existing conditions.

In what follows, we find and represent five perturbation matrices for each of the five critical points. We obtain five sets of eigenvalues. In order to determine the type and stability of critical points, we investigate the sign of the real parts of eigenvalues. A critical point is stable if all the real part of eigenvalues is negative. The physical meaning of the negative eigenvalue is always stable attractor; namely, if the universe is in this state, it keeps its state forever and thus it can attract the universe at a late time. There can occur accelerated expansion only for $w_{\text{tot}} < -1/3$.

A:

$$
M = \begin{pmatrix}
\dfrac{9}{2(\lambda+\beta)^2} + \dfrac{3\lambda}{2(\lambda+\beta)} - 3 & \left[\dfrac{-9}{6(\lambda+\beta)} + \sqrt{6}\lambda\right]\dfrac{\sqrt{2\beta(\lambda+\beta)+3}}{\sqrt{2}(\lambda+\beta)} & \dfrac{-\sqrt{6}\beta}{2} & \dfrac{\sqrt{6}}{4(\lambda+\beta)} \\
\left[\dfrac{9}{6(\lambda+\beta)} - \dfrac{\sqrt{6}\lambda}{2}\right]\dfrac{\sqrt{2\beta(\lambda+\beta)+3}}{\sqrt{2}(\lambda+\beta)} & \dfrac{-3(2\beta(\lambda+\beta)+3)}{2(\lambda+\beta)^2} & 0 & \dfrac{\sqrt{2\beta(\lambda+\beta)+3}}{2\sqrt{2}(\lambda+\beta)} \\
\left[\dfrac{18}{\sqrt{6}(\lambda+\beta)} + \sqrt{6}\beta\right]\dfrac{\lambda(\lambda+\beta)-3}{(\lambda+\beta)^2} & \dfrac{-6(\lambda(\lambda+\beta)-3)\sqrt{2\beta(\lambda+\beta)+3}}{\sqrt{2}(\lambda+\beta)^3} & 0 & \dfrac{\lambda(\lambda+\beta)-3}{(\lambda+\beta)^2} \\
0 & 0 & 0 & -4 + \dfrac{3\lambda}{\lambda+\beta}
\end{pmatrix}
\tag{68}
$$

B:

$$
M = \begin{pmatrix}
\dfrac{9}{2(\lambda+\beta)^2} + \dfrac{3\lambda}{2(\lambda+\beta)} - 3 & \left[\dfrac{9}{6(\lambda+\beta)} - \sqrt{6}\lambda\right]\dfrac{\sqrt{2\beta(\lambda+\beta)+3}}{\sqrt{2}(\lambda+\beta)} & \dfrac{-\sqrt{6}\beta}{2} & \dfrac{\sqrt{6}}{4(\lambda+\beta)} \\
\left[\dfrac{-9}{6(\lambda+\beta)} + \dfrac{\sqrt{6}\lambda}{2}\right]\dfrac{\sqrt{2\beta(\lambda+\beta)+3}}{\sqrt{2}(\lambda+\beta)} & \dfrac{-3(2\beta(\lambda+\beta)+3)}{2(\lambda+\beta)^2} & 0 & \dfrac{-\sqrt{2\beta(\lambda+\beta)+3}}{2\sqrt{2}(\lambda+\beta)} \\
\left[\dfrac{18}{\sqrt{6}(\lambda+\beta)} + \sqrt{6}\beta\right]\dfrac{\lambda(\lambda+\beta)-3}{(\lambda+\beta)^2} & \dfrac{6(\lambda(\lambda+\beta)-3)\sqrt{2\beta(\lambda+\beta)+3}}{\sqrt{2}(\lambda+\beta)^3} & 0 & \dfrac{\lambda(\lambda+\beta)-3}{(\lambda+\beta)^2} \\
0 & 0 & 0 & -4 + \dfrac{3\lambda}{\lambda+\beta}
\end{pmatrix}
\tag{69}
$$

C:

$$M = \begin{pmatrix} \lambda^2 - 3 & \frac{\sqrt{6}\lambda}{2}\sqrt{1-\frac{\lambda^2}{6}} & \frac{-\sqrt{6}\beta}{2} & \frac{\sqrt{6}\lambda}{12} \\ 0 & \frac{\lambda^2}{2} - 3 & 0 & \frac{1}{2}\sqrt{1-\frac{\lambda^2}{6}} \\ 0 & 0 & \lambda^2 + \lambda\beta - 3 & 0 \\ 0 & 0 & 0 & \lambda^2 - 4 \end{pmatrix} \quad (70)$$

D:

$$M = \begin{pmatrix} \frac{8}{\lambda^2} - 1 & 2\sqrt{2} - \frac{4\sqrt{2}}{\lambda^2} & \frac{-\sqrt{6}\beta}{2} & \frac{2}{\sqrt{6}\lambda} \\ -\sqrt{2} + \frac{4\sqrt{2}}{\lambda^2} & \frac{4}{\lambda^2} & 0 & \frac{1}{\sqrt{3}\lambda} \\ 0 & 0 & \frac{4\beta}{\lambda} + 1 & 0 \\ \frac{24}{\sqrt{6}\lambda}\left(1 - \frac{4}{\lambda^2}\right) & \frac{-12}{\sqrt{3}\lambda}\left(1 - \frac{4}{\lambda^2}\right) & 0 & 1 - \frac{4}{\lambda^2} \end{pmatrix} \quad (71)$$

E:

$$M = \begin{pmatrix} \frac{1}{2\beta^2} - 1 & 0 & \frac{-\sqrt{6}\beta}{2} & \frac{-1}{2\sqrt{6}\beta} \\ 0 & 2 + \frac{\lambda}{\beta} & 0 & 0 \\ 0 & 0 & 0 & \frac{1}{3\beta^2} \\ \frac{\sqrt{6}}{\beta}\left(1 - \frac{1}{2\beta^2}\right) & 0 & 0 & 1 - \frac{1}{2\beta^2} \end{pmatrix} \quad (72)$$

Eigenvalues of the five M matrices with the existence conditions, stability conditions, and acceleration condition are represented in Table 2, for each of the critical points A, B, C, D, and E. As seen in Table 2, the first two critical points A and B have the same eigenvalues. Here, the eigenvalues and the stability conditions of the perturbation matrices for critical points A, B, D, and E have been obtained by the numerical methods, due to the complexity of the matrices. The stability conditions of each critical point are listed in Table 2, according to the sign of the eigenvalues.

We now analyze the cosmological behavior of each critical point by noting the attractor solutions in scalar field cosmology [90]. From the theoretical cosmology studies, we know that the energy density of a scalar field has an effect on the determination of the evolution of the universe. Cosmological attractors provide the understanding of the evolution and the affecting factors on this evolution; for example, from the dynamical conditions, the scalar field evolution approaches a certain kind of behavior without initial fine tuning conditions [91–101]. Attractor behavior is known as a situation in which a collection of phase-space points evolve into a particular region and never leave from there.

Critical Point A. This point exists for $\beta(\lambda + \beta) > -3/2$ and $\lambda(\lambda + \beta) > 3$. Because of $w_{\text{tot}} < -1/3$, acceleration occurs at this point if $\lambda < 2\beta$ and it is an expansion phase since y_{ϕ_q} is positive, so H is positive, too. Point A is stable, meaning that the universe keeps its further evolution, if λ and β take the values for the negative eigenvalues given in the second column of Table 2. In Figure 1, we also represent the 2-dimensional and 3-dimensional projections of 4-dimensional phase-space trajectories for $\beta = 2.51$, $\lambda = 3.1$, $\lambda = 3.6$, and $\lambda = 4.1$. This state corresponds to a stable attractor starting from the critical point $A = (0.21, 0.70, 0.45, 0)$, as seen from the plots in Figure 1. Also, zero value of critical point Ω_r cancels the total behavior Ω_r' in (66).

Critical Point B. Point B also exists for $\beta(\lambda + \beta) > -3/2$ and $\lambda(\lambda + \beta) > 3$. Acceleration phase is again valid here if $\lambda < 2\beta$ leading $w_{\text{tot}} < -1/3$, but this point refers to contraction phase because y_{ϕ_q} is negative here. Stability of the point B is again satisfied for λ and β values given in the second column of Table 2. Therefore, the stable attractor behavior is represented starting from the critical point $B = (0.21, -0.70, 0.45, 0)$ for $\beta = 2.51$, $\lambda = 3.1$, $\lambda = 3.6$, and $\lambda = 4.1$ values, in Figure 2. The zero value of critical point Ω_r again cancels the total behavior Ω_r' in (66).

Critical Point C. Critical point C occurs for all values of β, while $\lambda < \sqrt{6}$. The cosmological behavior is again an acceleration phase that occurs if $\lambda < \sqrt{2}$ providing $w_{\text{tot}} < -1/3$ and an expansion phase since y_{ϕ_q} is positive. Point C is stable if $\beta < (3 - \lambda^2)/\lambda$ and $\lambda < \sqrt{3}$. Two-dimensional projection of phase-space is represented in Figure 3, for $\beta = 1.5$, $\lambda = 0.001$, $\lambda = 0.5$, and $\lambda = 1.1$. The stable attractor starting from the critical point $C = (0.48, 0.87, 0, 0)$ can be inferred from Figure 3. We again find zero plots containing zero values Ω_m and Ω_r, since they cancel the total behaviors Ω_m' and Ω_r' in (65) and (66).

Critical Point D. This point exists for any values of β, while $\lambda > 2$. Acceleration phase never occurs due to $w_{\text{tot}} = 1/3$. Point D is always unstable for any values of β and λ. This state corresponds to an unstable saddle point starting from the point $D = (0.54, 0.38, 0, 0.55)$ for $\beta = 1.5$, $\lambda = 3$, $\lambda = 4$, and $\lambda = 6$, as seen from the plots in Figure 4. Zero plots containing the axis Ω_m lead to the cancellation of the total behavior Ω_m' in (65), since $\Omega_m = 0$, so they are not represented in Figure 4.

Critical Point E. This point exists for any values of λ, while $\beta > 1/\sqrt{2}$. Acceleration phase never occurs due to $w_{\text{tot}} = 1/3$. Point E is always unstable for any values of β and λ. This state corresponds to an unstable saddle point starting from the point $= (-0.24, 0, 0.11, 0.82)$ for $\lambda = 1$, $\beta = 1.7$, $\beta = 2.6$, and $\beta = 3.5$, as seen from the plots in Figure 5. Zero plots containing the axis y_{ϕ_q} lead to the cancellation of the total behavior y_{ϕ_q}' in (64), since $y_{\phi_q} = 0$, so they are not represented in Figure 5.

All the plots in Figures 1–3 have the structure of stable attractor, since each of them evolves to a single point which is in fact one of the critical points in Table 1. These evolutions

Table 2: Eigenvalues and stability of critical points.

	Eigenvalues				λ	β	
A and B	−0.7516	−0.7516	−0.0065	−1.0065	4.6000	0.0100	Existing condition is $\beta(\lambda+\beta) > -3/2$ and $\lambda(\lambda+\beta) > 3$. Stable point if λ and β are the given values for the negative eigenvalues in the second column. Acceleration phase occurs if $\lambda < 2\beta$.
	−0.7518	−0.7518	−0.0073	−1.0073	4.1000	0.0100	
	−0.7521	−0.7521	−0.0083	−1.0083	3.6000	0.0100	
	−0.7524	−0.7524	−0.0096	−1.0096	3.1000	0.0100	
	−0.8249	−0.8249	−0.2994	−1.2994	4.6000	0.5100	
	−0.8330	−0.8330	−0.3319	−1.3319	4.1000	0.5100	
	−0.8431	−0.8431	−0.3723	−1.3723	3.6000	0.5100	
	−0.8560	−0.8560	−0.4238	−1.4238	3.1000	0.5100	
	−0.8850	−0.8850	−0.5401	−1.5401	4.6000	1.0100	
	−0.8982	−0.8982	−0.5930	−1.5930	4.1000	1.0100	
	−0.9143	−0.9143	−0.6573	−1.6573	3.6000	1.0100	
	−0.9343	−0.9343	−0.7372	−1.7372	3.1000	1.0100	
	−0.9354	−0.9354	−0.7414	−1.7414	4.6000	1.5100	
	−0.9519	−0.9519	−0.8075	−1.8075	4.1000	1.5100	
	−0.9716	−0.9716	−0.8865	−1.8865	3.6000	1.5100	
	−0.9781	−0.9781	−0.9123	−1.9123	4.6000	2.0100	
	−0.9957	−0.9957	−0.9826	−1.9826	3.1000	1.5100	
	−0.9967	−0.9967	−0.9869	−1.9869	4.1000	2.0100	
	−1.0148	−1.0148	−1.0591	−2.0591	4.6000	2.5100	
	−1.0187	−1.0187	−1.0749	−2.0749	3.6000	2.0100	
	−1.0348	−1.0348	−1.1392	−2.1392	4.1000	2.5100	
	−1.0450	−1.0450	−1.1800	−2.1800	3.1000	2.0100	
	−1.0581	−1.0581	−1.2324	−2.2324	3.6000	2.5100	
	−1.0856	−1.0856	−1.3422	−2.3422	3.1000	2.5100	
	Eigenvalues						
C	$\lambda^2 + \lambda\beta - 3$, $\lambda^2 - 3$, $\lambda^2 - 4$, $\frac{\lambda^2}{2} - 3$,						Existing condition is $\lambda < \sqrt{6}$. Stable point if $\beta < (3-\lambda^2)/\lambda$ and $\lambda < \sqrt{3}$. Acceleration phase occurs if $\lambda < \sqrt{2}$.

Table 2: Continued.

	Eigenvalues				λ	β	
	−0.5000	−0.5000	1.0000	0.2000	2.5000	−0.5000	
	−0.5000	−0.5000	1.0000	0.3333	3.0000	−0.5000	
	−0.5000	−0.5000	1.0000	0.4286	3.5000	−0.5000	
	−0.5000	−0.5000	1.0000	0.5000	4.0000	−0.5000	
	1.0000	−1.0000	0	0	2.0000	−0.5000	
	1.0000	−1.0000	2.0000	0	2.0000	0.5000	
	1.0000	−1.0000	4.0000	0	2.0000	1.5000	
	1.0000	−1.0000	−2.0000	0	2.0000	−1.5000	
	−0.5000	−0.5000	1.0000	0	4.0000	−1.0000	
	−0.5000	−0.5000	1.0000	1.0000	2.5000	0	
	−0.5000	−0.5000	1.0000	1.0000	3.5000	0	
	−0.5000	−0.5000	1.0000	1.0000	4.0000	0	
	−0.5000	−0.5000	1.0000	1.5000	4.0000	0.5000	
	−0.5000	−0.5000	1.0000	1.5714	3.5000	0.5000	
	−0.5000	−0.5000	1.0000	1.6667	3.0000	0.5000	
	−0.5000	−0.5000	1.0000	1.8000	2.5000	0.5000	
	−0.5000	−0.5000	1.0000	2.0000	4.0000	1.0000	
	−0.5000	−0.5000	1.0000	2.1429	3.5000	1.0000	Existing condition is $\lambda > 2$ and $\forall\beta$.
	−0.5000	−0.5000	1.0000	2.3333	3.0000	1.0000	Unstable point.
D	−0.5000	−0.5000	1.0000	2.5000	4.0000	1.5000	Acceleration phase never occurs.
	−0.5000	−0.5000	1.0000	2.6000	2.5000	1.0000	
	−0.5000	−0.5000	1.0000	2.7143	3.5000	1.5000	
	−0.5000	−0.5000	1.0000	3.0000	3.0000	1.5000	
	−0.5000	−0.5000	1.0000	3.0000	4.0000	2.0000	
	−0.5000	−0.5000	1.0000	3.2857	3.5000	2.0000	
	−0.5000	−0.5000	1.0000	3.4000	2.5000	1.5000	
	−0.5000	−0.5000	1.0000	3.6667	3.0000	2.0000	
	−0.5000	−0.5000	1.0000	4.2000	2.5000	2.0000	
	−0.5000	−0.5000	1.0000	−0.1429	3.5000	−1.0000	
	−0.5000	−0.5000	1.0000	−0.3333	3.0000	−1.0000	
	−0.5000	−0.5000	1.0000	−0.5000	4.0000	−1.5000	
	−0.5000	−0.5000	1.0000	−0.6000	2.5000	−1.0000	
	−0.5000	−0.5000	1.0000	−0.7143	3.5000	−1.5000	
	−0.5000	−0.5000	1.0000	−1.0000	3.0000	−1.5000	
	−0.5000	−0.5000	1.0000	−1.0000	4.0000	−2.0000	
	−0.5000	−0.5000	1.0000	−1.2857	3.5000	−2.0000	
	−0.5000	−0.5000	1.0000	−1.4000	2.5000	−1.5000	
	−0.5000	−0.5000	1.0000	−1.6667	3.0000	−2.0000	
	−0.5000	−0.5000	1.0000	−2.2000	2.5000	−2.0000	

Table 2: Continued.

	Eigenvalues				λ	β	
	0.2634	−0.1317	−0.1317	2.0704	0.1000	0.7100	
	0.2634	−0.1317	−0.1317	2.4225	0.6000	0.7100	
	0.2634	−0.1317	−0.1317	2.7746	1.1000	0.7100	
	0.2634	−0.1317	−0.1317	3.1268	1.6000	0.7100	
	0.2634	−0.1317	−0.1317	3.4789	2.1000	0.7100	
	0.2634	−0.1317	−0.1317	3.8310	2.6000	0.7100	
	0.2634	−0.1317	−0.1317	4.1831	3.1000	0.7100	
	0.2634	−0.1317	−0.1317	4.5352	3.6000	0.7100	
	1.0273	−0.8883	−0.1390	2.0185	0.1000	2.7100	
	1.0273	−0.8883	−0.1390	2.1107	0.6000	2.7100	
	1.0273	−0.8883	−0.1390	2.2030	1.1000	2.7100	
	1.0273	−0.8883	−0.1390	2.2952	1.6000	2.7100	
	1.0273	−0.8883	−0.1390	2.3875	2.1000	2.7100	
	1.0273	−0.8883	−0.1390	2.4797	2.6000	2.7100	
	1.0273	−0.8883	−0.1390	2.5720	3.1000	2.7100	
	1.0273	−0.8883	−0.1390	2.6642	3.6000	2.7100	
	1.0368	−0.8208	−0.2160	2.0226	0.1000	2.2100	
	1.0368	−0.8208	−0.2160	2.1357	0.6000	2.2100	Existing condition is $\beta > 1/\sqrt{2}$ and $\forall\lambda$.
	1.0368	−0.8208	−0.2160	2.2489	1.1000	2.2100	Unstable point.
E	1.0368	−0.8208	−0.2160	2.3620	1.6000	2.2100	Acceleration phase never occurs.
	1.0368	−0.8208	−0.2160	2.4751	2.1000	2.2100	
	1.0368	−0.8208	−0.2160	2.5882	2.6000	2.2100	
	1.0368	−0.8208	−0.2160	2.7014	3.1000	2.2100	
	1.0368	−0.8208	−0.2160	2.8145	3.6000	2.2100	
	1.0437	−0.5219	−0.5219	2.0413	0.1000	1.2100	
	1.0437	−0.5219	−0.5219	2.2479	0.6000	1.2100	
	1.0437	−0.5219	−0.5219	2.4545	1.1000	1.2100	
	1.0437	−0.5219	−0.5219	2.6612	1.6000	1.2100	
	1.0437	−0.5219	−0.5219	2.8678	2.1000	1.2100	
	1.0437	−0.5219	−0.5219	3.0744	2.6000	1.2100	
	1.0437	−0.5219	−0.5219	3.2810	3.1000	1.2100	
	1.0437	−0.5219	−0.5219	3.4876	3.6000	1.2100	
	1.0485	−0.5910	−0.4575	2.0292	0.1000	1.7100	
	1.0485	−0.5910	−0.4575	2.1754	0.6000	1.7100	
	1.0485	−0.5910	−0.4575	2.3216	1.1000	1.7100	
	1.0485	−0.5910	−0.4575	2.4678	1.6000	1.7100	
	1.0485	−0.5910	−0.4575	2.6140	2.1000	1.7100	
	1.0485	−0.5910	−0.4575	2.7602	2.6000	1.7100	
	1.0485	−0.5910	−0.4575	2.9064	3.1000	1.7100	

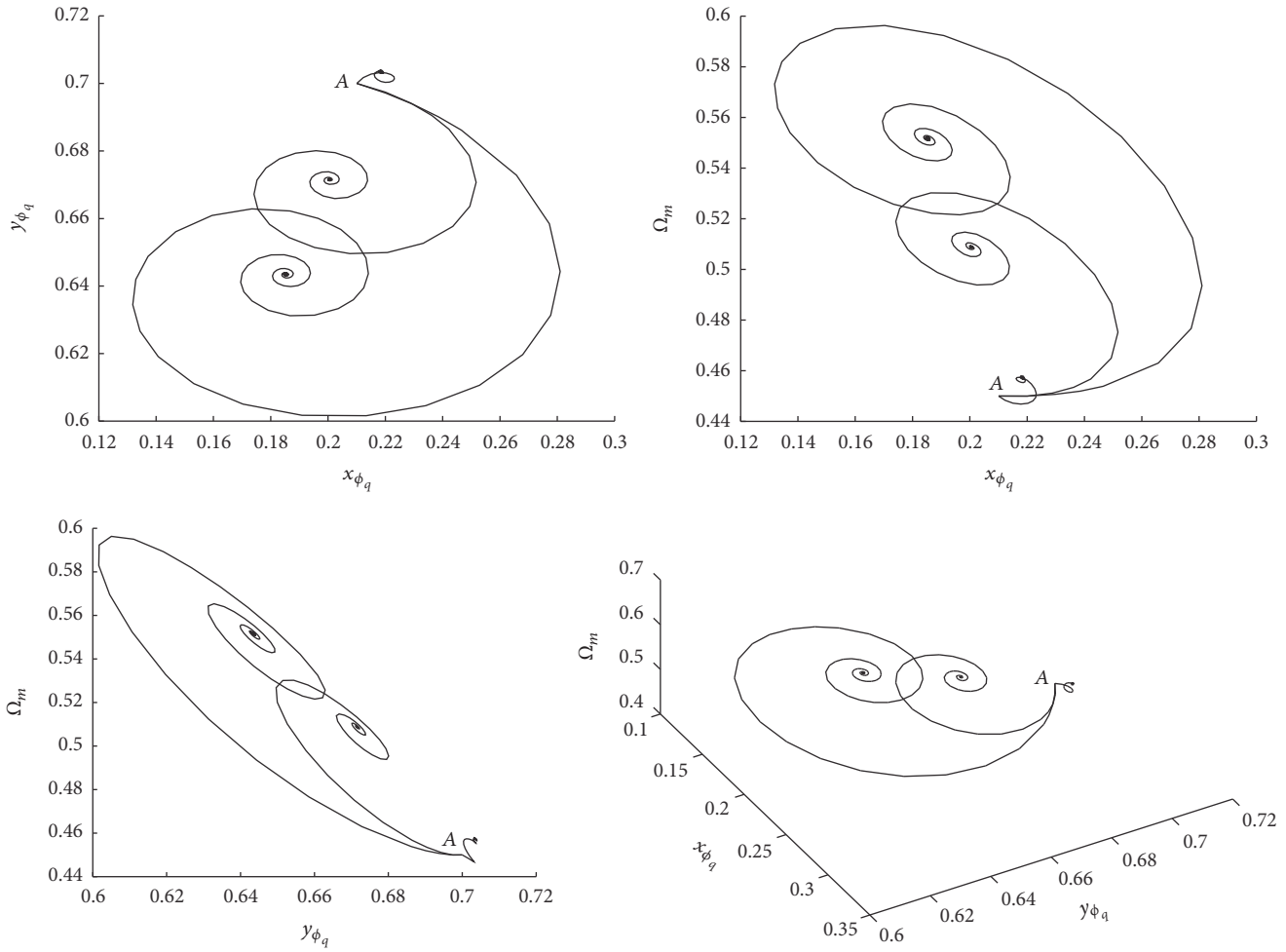

Figure 1: Two- and three-dimensional projections of the phase-space trajectories for $\beta = 2.51$, $\lambda = 3.1$, $\lambda = 3.6$, and $\lambda = 4.1$. All plots begin from the critical point $A = (0.21, 0.70, 0.45, 0)$ being a stable attractor.

to the critical points are the attractor solutions in coupling q-deformed dark energy to dark matter cosmology of our model, which imply an expanding universe. Therefore, we confirm that the dark energy in our model can be defined in terms of the q-deformed scalar fields obeying the q-deformed boson algebra in (17)–(20). According to the stable attractor behaviors, it makes sense to consider the dark energy as a scalar field defined by the q-deformed scalar field, due to the negative pressure of q-deformed boson field, as dark energy field.

Finally, we can investigate the relation between q-deformed and standard dark energy density, pressure, and scalar field equations in (24), (27), and (31). We illustrate the behavior of q-deformed energy density and pressure in terms of the standard ones with respect to the total number of particles and the deformation parameter q in Figures 6 and 7, respectively. We observe that for a large particle number the q-deformed energy density and pressure function decrease with the decrease in deformation parameter q. On the contrary, if the particle number is small, the deformed energy density and pressure increase with the decrease in deformation parameter. Note that when the deformation parameter decreases from 1, this increases the deformation of the model, since the deformation vanishes by approaching 1. The deformation parameter significantly affects the value of the deformed energy density and pressure. In the $q \to 1$ limit, deformed energy density and pressure function became identical to the standard values, as expected.

In Figure 8, we represent the q-deformed scalar field behavior in terms of the standard one. It is observed that while the deformation parameter $q \to 1$, q-deformed scalar field becomes identical to the standard one. However, it asymptotically approaches lower values, while q decreases with large number of particles. Since the square of a quantum mechanical field means the probability density, q-deformed probability density decreases when the deformation increases, and in the $q \to 0$ limit it approaches zero.

Also, since the dark matter pressure is taken to be zero, $\omega_m \approx 0$ and $\omega_{\text{tot}} \approx \omega_{\phi_q}$. For the stable accelerated expansion condition $\omega_{\text{tot}} \approx \omega_{\phi_q} < -1/3$, solutions require the scalar field dark energy pressure to be negative $p_{\phi_q} < 0$. From the relation $p_{\phi_q} = \Delta_q(n_k) p_\phi$ in (27), we finally represent the effect of q on the deformed dark energy pressure p_{ϕ_q}, namely, on the

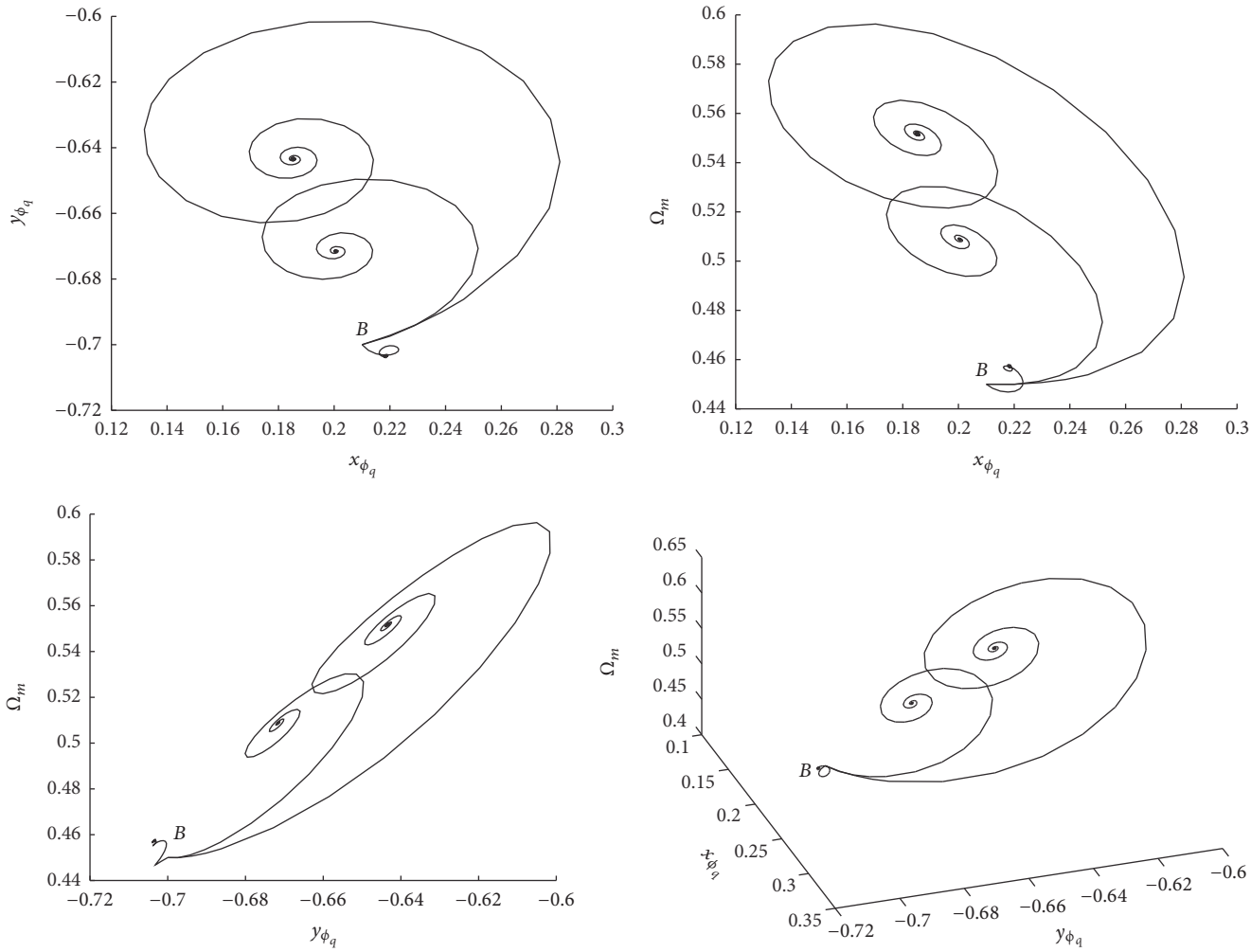

FIGURE 2: Two- and three-dimensional projections of the phase-space trajectories for $\beta = 2.51$, $\lambda = 3.1$, $\lambda = 3.6$, and $\lambda = 4.1$. All plots begin from the critical point $B = (0.21, -0.70, 0.45, 0)$ being a stable attractor.

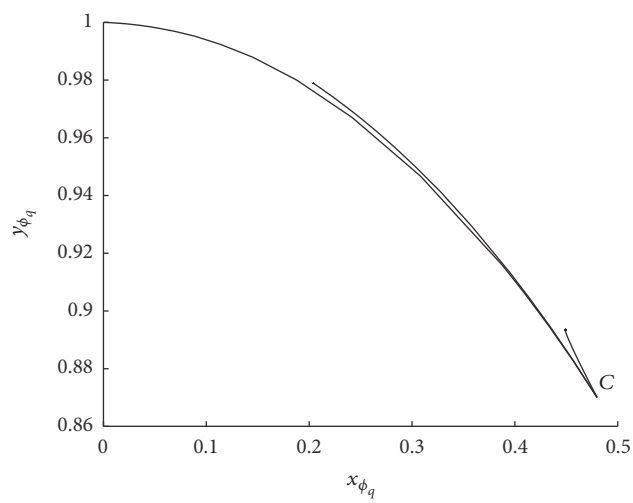

FIGURE 3: Two-dimensional projections of the phase-space trajectories for $\beta = 1.5$, $\lambda = 0.001$, $\lambda = 0.5$, and $\lambda = 1.1$. All plots begin from the critical point $C = (0.48, 0.87, 0, 0)$ being a stable attractor.

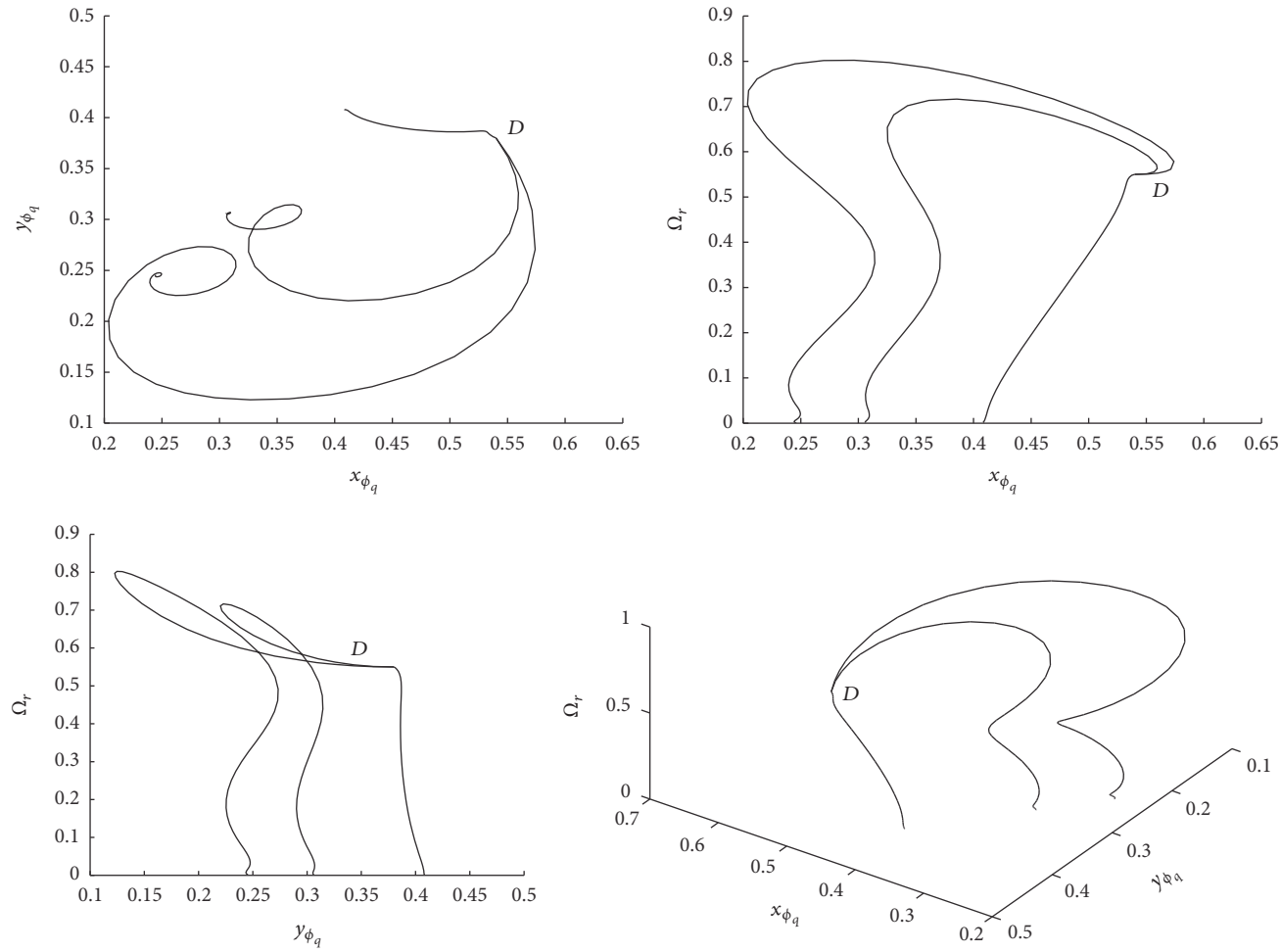

Figure 4: Two- and three-dimensional projections of the phase-space trajectories for $\beta = 1.5$, $\lambda = 3$, $\lambda = 4$, and $\lambda = 6$. All plots begin from the critical point $D = (0.54, 0.38, 0, 0.55)$ being an unstable solution.

accelerated expansion behavior in Figure 9. From the figure, we deduce that, for any values of q, the deformed dark energy shows the accelerated expansion behavior with the negative deformed dark energy pressure.

4. Conclusion

Since it is known that the dark energy has a negative pressure acting as gravitational repulsion to drive the accelerated expansion of the universe, we are motivated to propose that the dark energy consists of negative-pressure q-deformed scalar field whose field equation is defined by the q annihilation and creation operators satisfying the q-deformed boson algebra in (17)–(20). In order to confirm our proposal, we consider q-deformed dark energy coupling to the dark matter inhomogeneities and then investigate the dynamics of the model. Later on, we perform the phase-space analysis, whether it will give stable attractor solutions or not, which refers to the accelerating expansion phase of the universe. Therefore, the action integral of coupling q-deformed dark energy model is set up to study its dynamics, and the Hubble parameter and Friedmann equations of the model are obtained in spatially flat FRW geometry. Later on, we find the energy density and pressure values with the evolution equations for q-deformed dark energy, dark matter, and the radiation fields from the variation of the action and the Lagrangian of the model. After that, we translate these dynamical equations into the autonomous form by introducing suitable auxiliary variables, in order to perform the phase-space analysis of the model. Then, the critical points of the autonomous system are obtained by setting each autonomous equation to zero and four perturbation matrices can be written for each critical point by constructing the perturbation equations. We determine the eigenvalues of four perturbation matrices to examine the stability of critical points. There are also some important calculated cosmological parameters, such as the total equation of state parameter and the deceleration parameter to check whether the critical points satisfy an accelerating universe. We obtain four stable attractors for the model depending on the coupling parameter β. An accelerating universe exists for all stable solutions due to $w_{\text{tot}} < -1/3$. The critical points A and B are late-time stable attractors for the given λ and β values for the negative eigenvalues in the second column of Table 2.

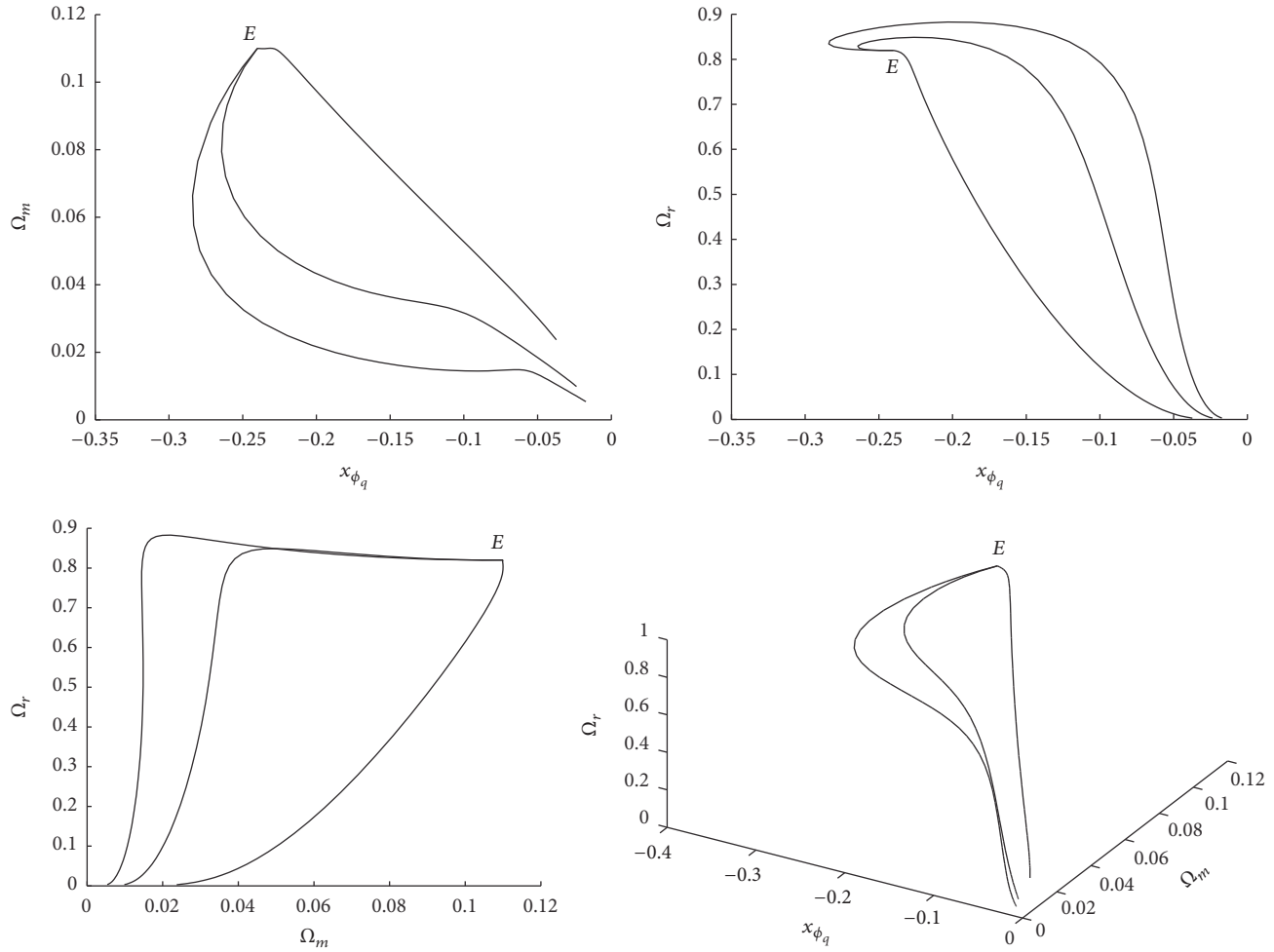

FIGURE 5: Two- and three-dimensional projections of the phase-space trajectories for $\lambda = 1$, $\beta = 1.7$, $\beta = 2.6$, and $\beta = 3.5$. All plots begin from the critical point $E = (-0.24, 0, 0.11, 0.82)$ being an unstable solution.

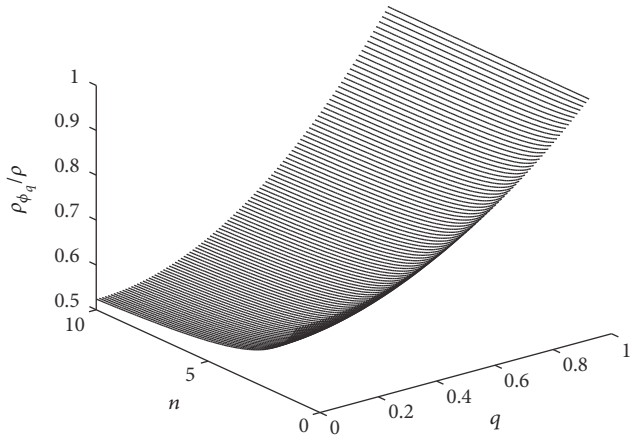

FIGURE 6: q-deformed energy density for various values of n and q, in terms of standard energy density.

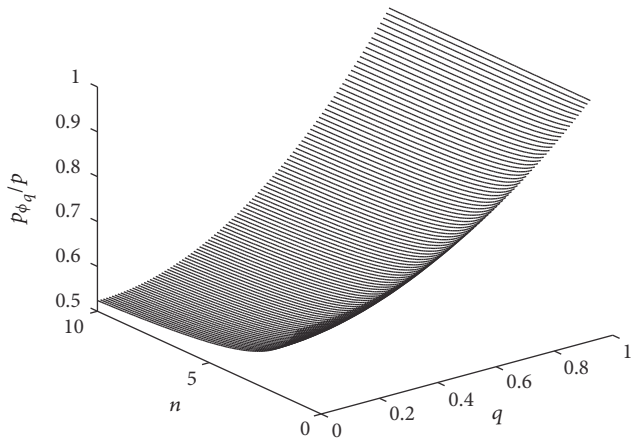

FIGURE 7: q-deformed pressure for various values of n and q, in terms of standard pressure.

The point A refers to expansion, while the point B refers to contraction with stable acceleration for $\lambda < 2\beta$. However, the critical point C is late-time stable attractor for $\beta < (3 - \lambda^2)/\lambda$ and $\lambda < \sqrt{3}$ with expansion. The stable attractor behavior of the model at each critical point is demonstrated in Figures 1–3. In order to solve the differential equation system (62)

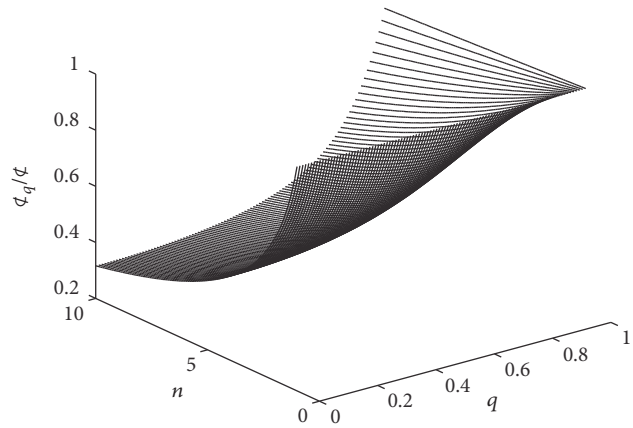

Figure 8: q-deformed scalar field for various values of n and q, in terms of standard scalar field.

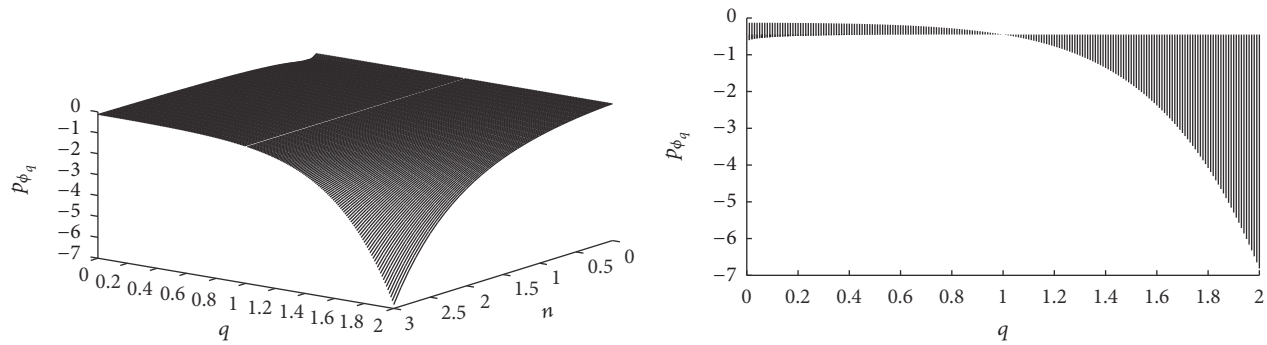

Figure 9: Effect of q on the accelerated expansion behavior with negative dark energy pressure.

with the critical points and plot the graphs in Figures 1–5, we use adaptive Runge-Kutta method of 4th and 5th order, in Matlab programming. Then, the solutions with the stability conditions of critical points are plotted for each pair of the solution sets being the auxiliary variables in (53), (55), and (56).

These figures represent the notion that, by choosing the suitable parameters of the model, we obtain the stable and unstable attractors as A, B, C, D, and E, depending on the existence conditions of critical points A, B, C, D, and E. Also, the suitable parameters with the stability conditions give the stable accelerated behavior for A, B, and C attractor models.

The q-deformed dark energy is a generalization of the standard scalar field dark energy. As seen from the behavior of the deformed energy density, pressure, and scalar field functions with respect to the standard functions, in the $q \to 1$ limit, they all approach the standard corresponding function values. However, in the $q \to 0$ limit, the deformed energy density and the pressure functions decrease to smaller values of the standard energy density and the pressure function values, respectively. This implies that the energy momentum of the scalar field decreases when the deformation becomes more apparent, since q reaches 1 which gives the nondeformed state. Also, when $q \to 0$ for large n values, the deformed scalar field approaches zero value meaning a decrease in the probability density of the scalar field. This state is expected to represent an energy-momentum decrease leading to a decrease in the probability of finding the particles of the field. Consequently, q deformation of the scalar field dark energy gives a self-consistent model due to the existence of standard case parameters of the dark energy in the $q \to 1$ limit and the existence of the stable attractor behavior of the accelerated expansion phase of the universe for the considered coupling dark energy and dark matter model.

The results confirm that the proposed q-deformed scalar field dark energy model is consistent since it gives the expected behavior of the universe. The idea to consider the dark energy as a q-deformed scalar field is a very recent approach. There are more deformed particle algebras in the literature which can be considered as other and maybe more suitable candidates for the dark energy. As a further study on the purpose of confirming whether the dark energy can be considered as a general deformed scalar field, the other couplings between dark energy and dark matter and also in the other framework of gravity, such as teleparallel or maybe $f(R)$ gravity, can be investigated.

Competing Interests

The author declares that they there are no competing interests regarding the publication of this paper.

References

[1] S. Perlmutter, G. Aldering, G. Goldhaber et al., "Measurements of Ω and Λ from 42 high-redshift supernovae," *The Astrophysical Journal*, vol. 517, no. 2, pp. 565–586, 1999.

[2] A. G. Riess, A. V. Filippenko, P. Challis et al., "Observational evidence from supernovae for an accelerating universe and a cosmological constant," *Astronomical Journal*, vol. 116, no. 3, pp. 1009–1038, 1998.

[3] U. Seljak, A. Makarov, P. McDonald et al., "Cosmological parameter analysis including SDSS Lyα forest and galaxy bias: constraints on the primordial spectrum of fluctuations, neutrino mass, and dark energy," *Physical Review D*, vol. 71, no. 10, Article ID 103515, 2005.

[4] M. Tegmark, M. A. Strauss, M. R. Blanton et al., "Cosmological parameters from SDSS andWMAP," *Physical Review D*, vol. 69, no. 10, Article ID 103501, 2004.

[5] D. J. Eisenstein, I. Zehavi, D. W. Hogg et al., "Detection of the baryon acoustic peak in the large-scale correlation function of SDSS luminous red galaxies," *Astrophysical Journal Letters*, vol. 633, no. 2, pp. 560–574, 2005.

[6] D. N. Spergel, L. Verde, H. V. Peiris et al., "First-year Wilkinson Microwave Anisotropy Probe (WMAP) observations: determination of cosmological parameters," *Astrophysical Journal, Supplement Series*, vol. 148, no. 1, pp. 175–194, 2003.

[7] E. Komatsu, K. M. Smith, J. Dunkley et al., "Seven-year Wilkinson microwave anisotropy probe (WMAP) observations: cosmological interpretation," *The Astrophysical Journal Supplement Series*, vol. 192, no. 2, article 18, 2011.

[8] G. Hinshaw, D. Larson, E. Komatsu et al., "Nine-year wilkinson microwave anisotropy probe (WMAP) observations: cosmological parameter results," *Astrophysical Journal, Supplement Series*, vol. 208, no. 2, article 19, 2013.

[9] P. A. R. Ade, N. Aghanim, C. Armitage-Caplan et al., "Planck 2013 results. XVI. Cosmological parameters," *Astronomy & Astrophysics*, vol. 571, p. A16, 2013.

[10] P. A. R. Ade, N. Aghanim, M. Arnaud et al., "Planck 2015 results. XIII. Cosmological parameters," https://arxiv.org/abs/1502.01589.

[11] C. Wetterich, "Cosmology and the fate of dilatation symmetry," *Nuclear Physics B*, vol. 302, no. 4, pp. 668–696, 1988.

[12] B. Ratra and P. J. E. Peebles, "Cosmological consequences of a rolling homogeneous scalar field," *Physical Review D*, vol. 37, no. 12, pp. 3406–3427, 1988.

[13] E. J. Copeland, M. Sami, and S. Tsujikawa, "Dynamics of dark energy," *International Journal of Modern Physics D*, vol. 15, no. 11, pp. 1753–1935, 2006.

[14] M. Li, X.-D. Li, S. Wang, and Y. Wang, "Dark energy," *Communications in Theoretical Physics*, vol. 56, no. 3, pp. 525–604, 2011.

[15] C. Wetterich, "The cosmon model for an asymptotically vanishing time dependent cosmological 'constant'," *Astronomy & Astrophysics (A&A)*, vol. 301, pp. 321–328, 1995.

[16] L. Amendola, "Coupled quintessence," *Physical Review D*, vol. 62, no. 4, Article ID 043511, 2000.

[17] N. Dalal, K. Abazajian, E. Jenkins, and A. V. Manohar, "Testing the cosmic coincidence problem and the nature of dark energy," *Physical Review Letters*, vol. 87, no. 14, Article ID 141302, 2001.

[18] W. Zimdahl, D. Pavón, and L. P. Chimento, "Interacting quintessence," *Physics Letters B*, vol. 521, no. 3-4, pp. 133–138, 2001.

[19] J.-Q. Xia, Y.-F. Cai, T.-T. Qiu, G.-B. Zhao, and X. Zhang, "Constraints on the sound speed of dynamical dark energy," *International Journal of Modern Physics D*, vol. 17, no. 8, pp. 1229–1243, 2008.

[20] A. Vikman, "Can dark energy evolve to the phantom?" *Physical Review D*, vol. 71, no. 2, Article ID 023515, 14 pages, 2005.

[21] W. Hu, "Crossing the phantom divide: dark energy internal degrees of freedom," *Physical Review D*, vol. 71, no. 4, Article ID 047301, 2005.

[22] R. R. Caldwell and M. Doran, "Dark-energy evolution across the cosmological-constant boundary," *Physical Review D*, vol. 72, no. 4, Article ID 043527, 2005.

[23] G.-B. Zhao, J.-Q. Xia, M. Li, B. Feng, and X. Zhang, "Perturbations of the quintom models of dark energy and the effects on observations," *Physical Review D—Particles, Fields, Gravitation and Cosmology*, vol. 72, no. 12, Article ID 123515, 2005.

[24] M. Kunz and D. Sapone, "Crossing the phantom divide," *Physical Review D*, vol. 74, no. 12, Article ID 123503, 2006.

[25] B. Gumjudpai, T. Naskar, M. Sami et al., "Coupled dark energy: towards a general description of the dynamics," *Journal of Cosmology and Astroparticle Physics*, vol. 2005, no. 6, p. 7, 2005.

[26] M. Jamil, D. Momeni, and R. Myrzakulov, "Stability of a non-minimally conformally coupled scalar field in F(T) cosmology," *European Physical Journal C*, vol. 72, no. 7, article 2075, 2012.

[27] M. Jamil, K. Yesmakhanova, D. Momeni, and R. Myrzakulov, "Phase space analysis of interacting dark energy in $f(T)$ cosmology," *Open Physics*, vol. 10, no. 5, pp. 1065–1071, 2012.

[28] M. Jamil, D. Momeni, and R. Myrzakulov, "Attractor solutions in $f(T)$ cosmology," *European Physical Journal C*, vol. 72, article 1959, 2012.

[29] M. Jamil, D. Momeni, and M. A. Rashid, "Notes on dark energy interacting with dark matter and unparticle in loop quantum cosmology," *The European Physical Journal C*, vol. 71, p. 1711, 2011.

[30] A. Banijamali and B. Fazlpour, "Tachyonic teleparallel dark energy," *Astrophysics and Space Science*, vol. 342, no. 1, pp. 229–235, 2012.

[31] C.-Q. Geng, C.-C. Lee, E. N. Saridakis, and Y.-P. Wu, "'Teleparallel' dark energy," *Physics Letters, Section B: Nuclear, Elementary Particle and High-Energy Physics*, vol. 704, no. 5, pp. 384–387, 2011.

[32] C.-Q. Geng, C.-C. Lee, and E. N. Saridakis, "Observational constraints on teleparallel dark energy," *Journal of Cosmology and Astroparticle Physics*, vol. 2012, no. 1, article 002, 2012.

[33] C. Xu, E. N. Saridakis, and G. Leon, "Phase-space analysis of teleparallel dark energy," *Journal of Cosmology and Astroparticle Physics*, vol. 2012, no. 7, p. 5, 2012.

[34] H. Wei, "Dynamics of teleparallel dark energy," *Physics Letters B*, vol. 712, no. 4-5, pp. 430–436, 2012.

[35] G. Otalora, "Scaling attractors in interacting teleparallel dark energy," *Journal of Cosmology and Astroparticle Physics*, vol. 2013, no. 7, article 44, 2013.

[36] A. Banijamali, "Dynamics of interacting tachyonic teleparallel dark energy," *Advances in High Energy Physics*, vol. 2014, Article ID 631630, 14 pages, 2014.

[37] B. Fazlpour and A. Banijamali, "Tachyonic teleparallel dark energy in phase space," *Advances in High Energy Physics*, vol. 2013, Article ID 279768, 9 pages, 2013.

[38] G. Otalora, "Cosmological dynamics of tachyonic teleparallel dark energy," *Physical Review D*, vol. 88, no. 6, Article ID 063505, 2013.

[39] E. Dil and E. Kolay, "Dynamics of mixed dark energy domination in teleparallel gravity and phase-space analysis," *Advances in High Energy Physics*, vol. 2015, Article ID 608252, 20 pages, 2015.

[40] A. E. Shalyt-Margolin, "Deformed quantum field theory, thermodynamics at low and high energies, and gravity. II. Deformation parameter," *International Journal of Theoretical and Mathematical Physics*, vol. 2, no. 3, pp. 41–50, 2012.

[41] A. E. Shalyt-Margolin and V. I. Strazhev, "Dark energy and deformed quantum theory in physics of the early universe," in *Non-Eucleden Geometry in Modern Physics. Proc. 5-th Intern. Conference of Bolyai-Gauss- Lobachevsky (BGL-5)*, Yu. Kurochkin and V. Red'kov, Eds., pp. 173–178, Minsk, 2007.

[42] Y. J. Ng, "Holographic foam, dark energy and infinite statistics," *Physics Letters B*, vol. 657, no. 1–3, pp. 10–14, 2007.

[43] Y. J. Ng, "Spacetime foam," *International Journal of Modern Physics D*, vol. 11, no. 10, pp. 1585–1590, 2002.

[44] M. R. Setare, D. Momeni, V. Kamali, and R. Myrzakulov, "Inflation driven by q-de sitter," *International Journal of Theoretical Physics*, vol. 55, no. 2, pp. 1003–1018, 2016.

[45] E. Dil and E. Kolay, "Interacting dark matter and q-deformed dark energy with particle creation and annihilation," https://arxiv.org/abs/1607.03928.

[46] A. Lavagno and P. N. Swamy, "Thermostatistics of a q-deformed boson gas," *Physical Review E. Statistical, Nonlinear, and Soft Matter Physics*, vol. 61, no. 2, pp. 1218–1226, 2000.

[47] A. Algin, A. S. Arikan, and E. Dil, "High temperature thermostatistics of fermionic Fibonacci oscillators with intermediate statistics," *Physica A: Statistical Mechanics and Its Applications*, vol. 416, pp. 499–517, 2014.

[48] A. Algin and M. Senay, "High-temperature behavior of a deformed Fermi gas obeying interpolating statistics," *Physical Review E—Statistical, Nonlinear, and Soft Matter Physics*, vol. 85, no. 4, Article ID 041123, 2012.

[49] A. M. Gavrilik and A. P. Rebesh, "Deformed gas of p, q-bosons: virial expansion and virial coefficients," *Modern Physics Letters B*, vol. 26, no. 5, Article ID 1150030, 2012.

[50] M. R. Ubriaco, "Anyonic behavior of quantum group gases," *Physical Review E*, vol. 55, no. 1, pp. 291–296, 1997.

[51] M. Arik and D. D. Coon, "Hilbert spaces of analytic functions and generalized coherent states," *Journal of Mathematical Physics*, vol. 17, no. 4, pp. 524–527, 1976.

[52] A. J. Macfarlane, "On q-analogues of the quantum harmonic oscillator and the quantum group $SU(2)_q$," *Journal of Physics. A. Mathematical and General*, vol. 22, no. 21, pp. 4581–4588, 1989.

[53] L. C. Biedenharn, "The quantum group SU_q (2) and a q-analogue of the boson operators," *Journal of Physics A: Mathematical and General*, vol. 22, no. 18, pp. L873–L878, 1989.

[54] M. Chaichian, R. G. Felipe, and C. Montonen, "Statistics of q-oscillators, quons and relations to fractional statistics," *Journal of Physics A: Mathematical and General A*, vol. 26, no. 16, pp. 4017–4034, 1993.

[55] J. Wess and B. Zumino, "Covariant differential calculus on the quantum hyperplane," *Nuclear Physics B-Proceedings Supplements*, vol. 18, no. 2, pp. 302–312, 1991.

[56] G. Vinod, *Studies in quantum oscillators and q-deformed quantum mechanics [Ph.D. thesis]*, Cochin University of Science and Technology, Department of Physics, Kochi, India, 1997.

[57] B. K. Berger, "Scalar particle creation in an anisotropic universe," *Physical Review D*, vol. 12, no. 2, pp. 368–375, 1975.

[58] S. W. Hawking, "Breakdown of predictability in gravitational collapse," *Physical Review D*, vol. 14, no. 10, pp. 2460–2473, 1976.

[59] B. K. Berger, "Classical analog of cosmological particle creation," *Physical Review D*, vol. 23, p. 1250, 1981.

[60] L. Parker, "Quantized fields and particle creation in expanding universes. I," *Physical Review*, vol. 183, no. 5, pp. 1057–1068, 1969.

[61] J. W. Goodison and D. J. Toms, "No generalized statistics from dynamics in curved spacetime," *Physical Review Letters*, vol. 71, no. 20, pp. 3240–3242, 1993.

[62] D. Bonatsos and C. Daskaloyannis, "Quantum groups and their applications in nuclear physics," *Progress in Particle and Nuclear Physics*, vol. 43, no. 1, pp. 537–618, 1999.

[63] S. Carroll, *Spacetime and Geometry: an Introduction to General Relativit*, Addison Wesley, San Francisco, Calif, USA, 2004.

[64] M. Jamil, E. N. Saridakis, and M. R. Setare, "Thermodynamics of dark energy interacting with dark matter and radiation," *Physical Review D*, vol. 81, no. 2, Article ID 023007, 2010.

[65] R. G. Leigh, "Dirac-born-infeld action from drichlet σ-model," *Modern Physics Letters A*, vol. 4, pp. 2767–2772, 1989.

[66] N. A. Chernikov and E. A. Tagirov, "Quantum theory of scalar field in de Sitter space-time," *Annales de l'I.H.P. Physique Théorique*, vol. 9, no. 2, pp. 109–141, 1968.

[67] C. G. Callan Jr., S. Coleman, and R. Jackiw, "A new improved energy-momentum tensor," *Annals of Physics*, vol. 59, no. 1, pp. 42–73, 1979.

[68] V. Faraoni, "Inflation and quintessence with nonminimal coupling," *Physical Review D—Particles, Fields, Gravitation and Cosmology*, vol. 62, no. 2, Article ID 023504, 2000.

[69] P. G. Ferreira and M. Joyce, "Structure formation with a self-tuning scalar field," *Physical Review Letters*, vol. 79, no. 24, pp. 4740–4743, 1997.

[70] E. J. Copeland, A. R. Liddle, and D. Wands, "Exponential potentials and cosmological scaling solutions," *Physical Review D*, vol. 57, no. 8, pp. 4686–4690, 1998.

[71] X.-M. Chen, Y. G. Gong, and E. N. Saridakis, "Phase-space analysis of interacting phantom cosmology," *Journal of Cosmology and Astroparticle Physics*, vol. 2009, no. 4, article 001, 2009.

[72] X.-M. Chen and Y. Gong, "Fixed points in interacting dark energy models," *Physics Letters, Section B: Nuclear, Elementary Particle and High-Energy Physics*, vol. 675, no. 1, pp. 9–13, 2009.

[73] A. de Felice and S. Tsujikawa, "f (R) theories," *Living Reviews in Relativity*, vol. 13, article 3, 2010.

[74] T. P. Sotiriou and V. Faraoni, "*f (R)* theories of gravity," *Reviews of Modern Physics*, vol. 82, no. 1, pp. 451–497, 2010.

[75] S. Tsujikawa, "Modified gravity models of dark energy," in *Lectures on Cosmology*, vol. 800 of *Lecture Notes in Physics*, pp. 99–145, Springer, Berlin, Germany, 2010.

[76] G. N. Remmen and S. M. Carroll, "Attractor solutions in scalar-field cosmology," *Physical Review D*, vol. 88, no. 8, Article ID 083518, 2013.

[77] A. R. Liddle, P. Parsons, and J. D. Barrow, "Formalizing the slow-roll approximation in inflation," *Physical Review D*, vol. 50, no. 12, pp. 7222–7232, 1994.

[78] P. G. Ferreira and M. Joyce, "Cosmology with a primordial scaling field," *Physical Review D*, vol. 58, no. 2, Article ID 023503, 1998.

[79] Y. Gong, A. Wang, and Y.-Z. Zhang, "Exact scaling solutions and fixed points for general scalar field," *Physics Letters. B*, vol. 636, no. 5, pp. 286–292, 2006.

[80] Z.-K. Guo, Y.-S. Piao, X. Zhang, and Y.-Z. Zhang, "Cosmological evolution of a quintom model of dark energy," *Physics Letters, Section B: Nuclear, Elementary Particle and High-Energy Physics*, vol. 608, no. 3-4, pp. 177–182, 2005.

[81] R. Lazkoz and G. León, "Quintom cosmologies admitting either tracking or phantom attractors," *Physics Letters B*, vol. 638, no. 4, pp. 303–309, 2006.

[82] Z.-K. Guo, Y.-S. Piao, X. Zhang, and Y.-Z. Zhang, "Two-field quintom models in the w-w' plane," *Physical Review D*, vol. 74, no. 12, Article ID 127304, 4 pages, 2006.

[83] R. Lazkoz, G. León, and I. Quiros, "Quintom cosmologies with arbitrary potentials," *Physics Letters, Section B: Nuclear, Elementary Particle and High-Energy Physics*, vol. 649, no. 2-3, pp. 103–110, 2007.

[84] M. Alimohammadi, "Asymptotic behavior of ω in general quintom model," *General Relativity and Gravitation*, vol. 40, no. 1, pp. 107–115, 2008.

[85] M. R. Setare and E. N. Saridakis, "Coupled oscillators as models of quintom dark energy," *Physics Letters B*, vol. 668, no. 3, pp. 177–181, 2008.

[86] M. R. Setare and E. N. Saridakis, "Quintom cosmology with general potentials," *International Journal of Modern Physics. D. Gravitation, Astrophysics, Cosmology*, vol. 18, no. 4, pp. 549–557, 2009.

[87] M. R. Setare and E. N. Saridakis, "The quintom model with O(N) symmetry," *Journal of Cosmology and Astroparticle Physics*, vol. 2008, no. 9, article 026, 2008.

[88] M. R. Setare and E. N. Saridakis, "Quintom dark energy models with nearly flat potentials," *Physical Review D—Particles, Fields, Gravitation and Cosmology*, vol. 79, no. 4, Article ID 043005, 2009.

[89] G. Leon, R. Cardenas, and J. L. Morales, "Equilibrium sets in quintom cosmologies: the past asymptotic dynamics," http://arxiv.org/abs/0812.0830.

[90] Z.-K. Guo, Y.-S. Piao, R.-G. Cai, and Y.-Z. Zhang, "Inflationary attractor from tachyonic matter," *Physical Review D*, vol. 68, no. 4, Article ID 043508, 2003.

[91] L. A. Ureña-López, M. J. Reyes-Ibarra, and A. A. Starobinsky, "On the dynamics of a quadratic scalar field potential," *International Journal of Modern Physics D*, vol. 18, no. 4, pp. 621–634, 2009.

[92] V. A. Belinsky, L. P. Grishchuk, I. M. Khalatnikov, and Y. B. Zeldovich, "Inflationary stages in cosmological models with a scalar field," *Physics Letters B*, vol. 155, no. 4, pp. 232–236, 1985.

[93] T. Piran and R. M. Williams, "Inflation in universes with a massive scalar field," *Physics Letters B*, vol. 163, no. 5-6, pp. 331–335, 1985.

[94] A. R. Liddle and D. H. Lyth, *Cosmological Inflation and Large-Scale Structure*, Cambridge University Press, Cambridge, UK, 2000.

[95] V. V. Kiselev and S. A. Timofeev, "Quasi-attractor dynamics of $\lambda\phi^4$-inflation," http://arxiv.org/abs/0801.2453.

[96] S. Downes, B. Dutta, and K. Sinha, "Attractors, universality, and inflation," *Physical Review D*, vol. 86, no. 10, Article ID 103509, 2012.

[97] J. Khoury and P. J. Steinhardt, "Generating scale-invariant perturbations from rapidly-evolving equation of state," *Physical Review D*, vol. 83, no. 12, Article ID 123502, 2011.

[98] S. Clesse, C. Ringeval, and J. Rocher, "Fractal initial conditions and natural parameter values in hybrid inflation," *Physical Review D—Particles, Fields, Gravitation and Cosmology*, vol. 80, no. 12, Article ID 123534, 2009.

[99] V. V. Kiselev and S. A. Timofeev, "Quasiattractor in models of new and chaotic inflation," *General Relativity and Gravitation*, vol. 42, no. 1, pp. 183–197, 2010.

[100] G. F. R. Ellis, R. Maartens, and M. A. H. MacCallum, *Relativistic Cosmology*, Cambridge University Press, Cambridge, UK, 2012.

[101] Y. Wang, J. M. Kratochvil, A. Linde, and M. Shmakova, "Current observational constraints on cosmic doomsday," *Journal of Cosmology and Astroparticle Physics*, vol. 2004, p. 006, 2004.